AMERICAN UNIVERSITY OF BEIRUT

KINETIC MODELING OF THE HYDROLYSIS AND FERMENTATION OF ARUNDO DONAX BIOMASS FOR THE PRODUCTION OF BIOETHANOL

by
CELINE SAMER AYOUB

A thesis
submitted in partial fulfillment of the requirements
for the degree of Master of Science
to the Baha and Walid Bassatne Department of Chemical Engineering
and Advanced Energy
of Maroun Semaan Faculty of Engineering and Architecture
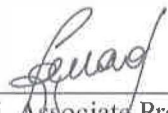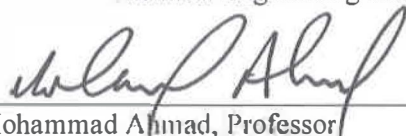at the American University of Beirut

Beirut, Lebanon
December 2022

AMERICAN UNIVERSITY OF BEIRUT

KINETIC MODELING OF THE HYDROLYSIS AND
FERMENTATION OF ARUNDO DONAX BIOMASS FOR
THE PRODUCTION OF BIOETHANOL

by
CELINE SAMER AYOUB

Approved by:

Signature

Dr. Joseph Zeaiter, Associate Professor   Advisor
Department of Chemical Engineering and Advanced Energy

Signature

Dr. Fouad Azizi, Associate Professor   Member of Committee
Department of Chemical Engineering and Advanced Energy

Signature

Dr. Mohammad Ahmad, Professor   Member of Committee
Department of Chemical Engineering and Advanced Energy

Date of thesis defense: December 14, 2022

AMERICAN UNIVERSITY OF BEIRUT

THESIS RELEASE FORM

Student Name: ___Ayoub_____Celine_____Samer_____
               Last   First   Middle

I authorize the American University of Beirut, to: (a) reproduce hard or electronic copies of my thesis; (b) include such copies in the archives and digital repositories of the University; and (c) make freely available such copies to third parties for research or educational purposes:

☒ As of the date of submission

☐ One year from the date of submission of my thesis.

☐ Two years from the date of submission of my thesis.

☐ Three years from the date of submission of my thesis.

_____   30 January 2023_____

Signature   Date

ACKNOWLEDGEMENTS

ABSTRACT

OF THE THESIS OF

Celine Samer Ayoub   for   Master of Science
                                                       Major: Chemical Engineering

Title: Kinetic Modeling of the Hydrolysis and Fermentation of Arundo Donax Biomass for the Production of Bioethanol

The importance of renewable energy applications is rising increasingly every day in a world dominated by pollution and climate change. Finding alternatives to the use of fossil fuels is vital for the decrease in greenhouse gases emissions. Hence, new research studies are continuously devising solutions that are less polluting, more eco-friendly and less expensive.

The conversion of biomass to biofuel represents an emerging alternative to fossil fuel. For instance, organic waste, crops and plants can be converted to produce bioethanol. Second generation bioethanol in particular is an alternative that has been studied for decades. Many feedstocks were tested, and the ethanol yields of each feed type were compared, in order to determine the most efficient, in terms of costs and ethanol production.

In this research, the use of Giant Reed is evaluated as a feedstock for the conversion to bioethanol, with a focus on the biomass ethanol yield, process configuration, operating conditions as well as reaction kinetic rates.

Kinetic models for the hydrolysis and fermentation of lignocellulosic biomass, more specifically Arundo donax, were assessed in this thesis. Data from literature was used to generate materials concentration data for Arundo donax feedstock for the production of bioethanol. The kinetic model was developed in MATLAB, where parameter estimation was employed. A simulation modeling the SHF of Arundo donax biomass was created, using the previously developed kinetic models. This simulation will model a semibatch hydrolysis followed by a batch fermentation. An ethanol concentration of 28 g/L was reached. The results obtained led to an estimation of the land area needed to plant Arundo donax to provide Lebanon with the necessary amount of ethanol, if 10% of the ethanol will be mixed with gasoline. A total area of 17,203,187 m^2 is required to cover 10,256,500 L of ethanol per year. Arundo donax can be planted on landfills and quarries, across Lebanon.

Further developments could include developing a model using Aspen PLUS for the production of ethanol from Arundo donax, balancing ethanol yield, economic and environmental costs.

TABLE OF CONTENTS

4

ILLUSTRATIONS

Figure

TABLES

ABBREVIATIONS

CO_2	Carbon dioxide
CPB	Consolidated Bioprocessing
FAME	Fatty acid methyl esters
GHG	Green House Gas
MSW	Municipal Solid Waste
PDCL	Partially delignified cellulignin
PEG	Polyethylene glycol
S. cerevisiae	Saccharomyces cerevisiae
SHF	Separate Hydrolysis and Fermentation
SSCF	Simultaneous Saccharification and Co-Fermentation
SSF	Simultaneous Saccharification and Fermentation
NaOH	Sodium hydroxide
NPMPLT	National Physical Master Plan of the Lebanese Territory
SO_2	Sulfur dioxide
H_2SO_4	Sulfuric acid
WIF	Water Insoluble Fraction
WSF	Water Soluble Fraction

CHAPTER 1

INTRODUCTION

It is widely known that the world's reliance on fossil fuels has resulted in negative environmental consequences such as diminishing crude oil reserves, poor air quality, increasing temperatures and irregular seasonal changes.

Bioethanol is currently used blended with petrol or even totally replacing it in an attempt to improve sustainability and decrease the dependence on fossil fuels. However, since the feed for first generation bioethanol is made from edible crops, its production is limited because of the food vs. energy conflict. Second generation bioethanol production is a preferred route since it uses non-edible feed generated from agricultural and forest waste, which contain lignocellulosic and starchy components that can be converted to fermentable sugars and bioethanol. The process of ethanol production involves the pretreatment of the biomass, followed by its hydrolysis, fermentation, and distillation for ethanol recovery. Kinetic models for the hydrolysis and fermentation were developed. The findings can be used to model a second generation bioethanol production plant, and possibly plan an actual plant in Lebanon to help reduce reliance on transportation fuel (gasoline) in the country [1].

1.1. Bioethanol, an alternative to gasoline

Biofuels are nowadays becoming more interesting as a renewable energy source because of their lower environmental impact and economic cost when compared to fossil fuels.

Biofuels are liquid or gas fuels that are generated from biodegradable products, agricultural, industrial and municipal waste [2].

Studies have shown that bioethanol is the most consumed biofuel: it is mainly used as fuel or as an additive to fuel. 84% of this produced biofuel is used for transportation purposes, thus decreasing the GHG emissions by 85% [3]. The figure below shows the production of bioethanol of different countries in 2020.
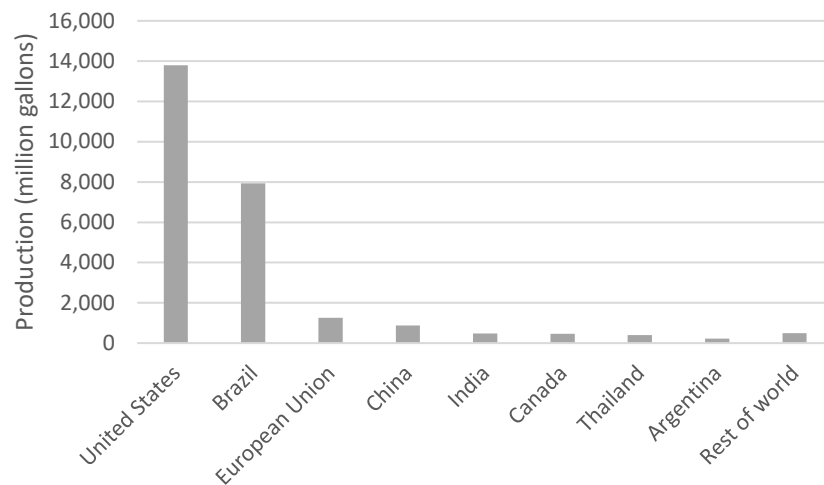
Figure 1 Bioethanol production in various countries in 2020 [4].

Ethanol can be produced from the hydration of ethylene, but it can also be manufactured from the fermentation of sugars present in plants containing starch. In other words, bioethanol can be made from biomass hydrolysis and fermentation (direct fermentation) or from the biomass gasification to syngas then fermentation to biofuel (indirect fermentation) [5].

Bioethanol is currently employed as a gasoline additive due to its high-octane number and its ability to enhance petrol. Adding ethanol to petrol oxygenates the mixture, which causes it to burn entirely thus lowering toxic emissions [2].

However, bioethanol has a smaller energy density when compared to gasoline. In other words, for the same amount of energy produced, more ethanol is needed than gasoline, i.e. 1.5 gallons of ethanol vs. 1 gallon of gasoline for a same produced quantity of energy [6]. Despite this fact, an engine using bioethanol has less energy waste than a gasoline-operated engine, and using bioethanol is a step towards reducing GHG emissions that can reach up to 86% [6].

Bioethanol, a renewable liquid biofuel and energy source, can be categorized into first, second and third generation bioethanol, depending on its origin, i.e. feedstock [7].

First generation bioethanol is generated from edible crops containing sucrose and starch. Examples as listed in the table below include sugar cane (Brazil), corn (USA), rapeseed (Germany), maize, sugar beet [7] etc.

Table 1. First generation bioethanol feedstock [8].

1st generation bioethanol feedstock	
Rich in sucrose	Rich in starch
Sugar cane	Corn
Sugar beet	Wheat
Sweet sorghum	Rice
Fruits	Potato and Sweet Potato
	Cassava
	Barley

On the other hand, second generation ethanol is produced from the lignocellulosic biomass of non-edible plants coming from forests and agriculture, like wood, straw and grass [8]. The production of ethanol from the latter is much preferred since it is a product from the waste of crops and plants, and not from edible plants that

could be consumed by people, thus no food vs. energy competition [3]. In other words, when the demand for food increases, the cost follows as well, which could lead to inflation. According to the World Food Program, around 821 million people go to sleep every night with an empty stomach [9], while people from the richer parts of the world are running their cars on fuel produced from food crops. Also, first generation bioethanol is not a sustainable product, since it indirectly leads to deforestation, and requires water for its irrigation, which is rare in some parts of the world. All these drawbacks justify the need of a cleaner way to produce bioethanol, thus the second generation bioethanol is the preferred alternative. This category has the possibility to reduce GHG emissions and reduce the risk of shifting lands or crops for the development of biofuels at the expense of food supply. This more sustainable and environmental-friendly product can be produced from various non-edible crops such as Arundo donax, Jatropha, etc. The potential ethanol yield from Arundo donax is 265 kg ethanol / ton raw material, which is equivalent to around 330 L of ethanol [10].

The majority of bioethanol generated now is made using the first-generation processes, which is expected to reach roughly 100 million m^3 by 2022 [3]. Third generation bioethanol is emerging nowadays. It is produced from algae biomass and includes macro and micro-algae [8].

1.2. Modeling

The lignocellulosic biomass, made of cellulose, hemicellulose, and lignin will undergo chemical or enzymatic hydrolysis, which leads to the production of pentose and hexose sugars that are used in a later stage as substrates for the production of bioethanol after fermentation [11]. The process is summarized in the figure below.
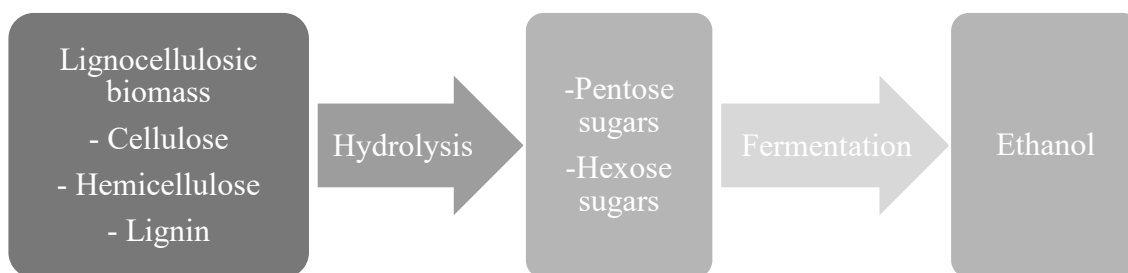
Figure 2. Process model

S. cerevisiae is the yeast that is mostly used in fermentation because of the several benefits that it offers, including high rates of sugar consumption, osmo-tolerance, resistance to environmental factors, and genetic versatility. However, a major disadvantage is its inability to ferment hemicellulose, like xylose. A possible solution is using more than one microorganism for the fermentation. Having a co-culture system helps in achieving simultaneous fermentation of the different sugars involved, which leads to high ethanol yields. Developing a strong co-culture system for the effective fermentation of sugars for the production of sustainable biofuel and other products is still a significant task. Studying the fermentation kinetics of strains is essential for achieving simultaneous usage of sugars in co-culture systems. Kinetic models may be employed to describe cell growth, substrate usage, and biofuel generation [11]. Several kinetic models were evaluated in this thesis, and a hydrolysis kinetic model, as well as a new modified kinetic model were developed, taking into consideration xylose and glucose fermentation in order to obtain high ethanol yield [11].

1.3. Thesis objectives

It was concluded from the literature that Arundo donax is a good candidate for second generation bioethanol production. Since it can quickly grow on any soil and under any conditions, it can be planted anywhere, even on landfills and arid land since

no other vegetation can grow there. In such case ample land space can be made available for energy crops without inducing competition with food crops. The plan is to plant Arundo donax on Lebanese non-cultivated lands (incl. landfills), to help reduce the dependability on gasoline through a 10% ethanol blend.

This thesis focuses on the production of bioethanol from Arundo donax, because of the high experimental yields found in the literature. Kinetic models for the hydrolysis and the fermentation steps were developed and enhanced, based on existing models. Parameter estimation for the kinetic models from data found on Arundo donax in the literature will be performed on MATLAB. The simulation uses a semibatch hydrolysis and a batch fermentation.

Chapter 1 introduces this thesis by identifying the different types of feedstocks for bioethanol production. It also offers a brief description about modeling bioethanol production. Chapter 2 presents a literature review about the different processes of bioethanol production, from various feedstocks, and the different yields achieved. Chapter 3 delves into the methodology, where the kinetic models used in the literature are listed, as well as the Arundo donax data developed, while highlighting major challenges that can be faced when producing bioethanol. Chapter 4 discusses the model development for the hydrolysis and fermentation, and the simulation of Arundo donax SHF. It also includes the determination of Arundo donax plantation land to satisfy Lebanon's gasoline consumption by introducing 10% ethanol blend. Finally, Chapter 5 summarizes the findings obtained with conclusion and recommendations.

CHAPTER 2

LITERATURE REVIEW

2.1. From biomass to second generation bioethanol

2.1.1. Process steps

The choice of manufacturing technique, together with the type of raw material used, are determining factors in the bioethanol cost and yield.

The main steps for converting lignocellulosic biomass to second generation bioethanol are summarized in the figures below:

Figure 3. Second generation bioethanol production steps [7].
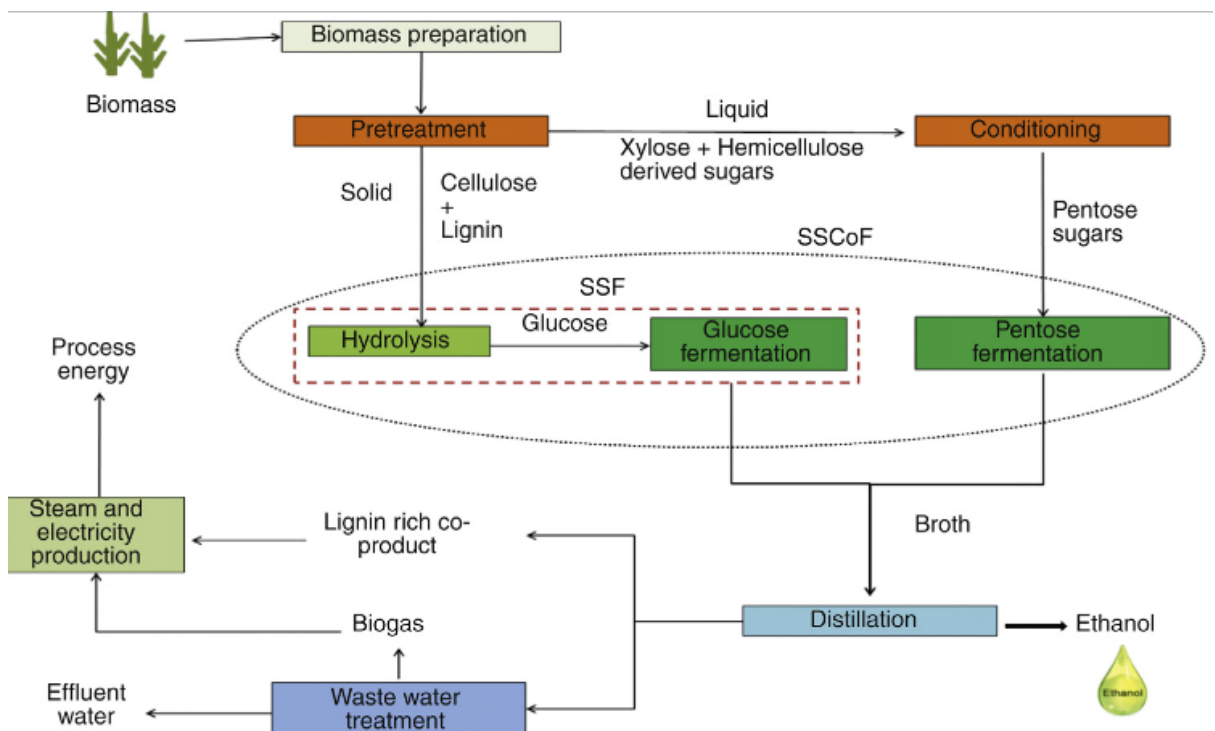
Figure 4. Production of cellulosic ethanol process [12].

The biomass is composed of cellulose, hemicellulose and lignin. Initially, the biomass should be pretreated for the delignification of the cellulosic and hemi-cellulosic components in order for the polysaccharides to be released which will later be de-polymerized by either acid treatment or enzymes, then transformed to monosaccharides that will finally be fermented to ethanol [7].

As opposed to first generation bioethanol, second generation bioethanol's process is more complex since lignocellulose is composed of cellulose, hemicellulose and lignin as seen in the figure below [13] and not simply glucose and fructose which is the case of first generation bioethanol from corn and sugarcane [7]. During the de-polymerization, two different treatments should be employed for the hydrolysis of cellulose and hemicellulose.
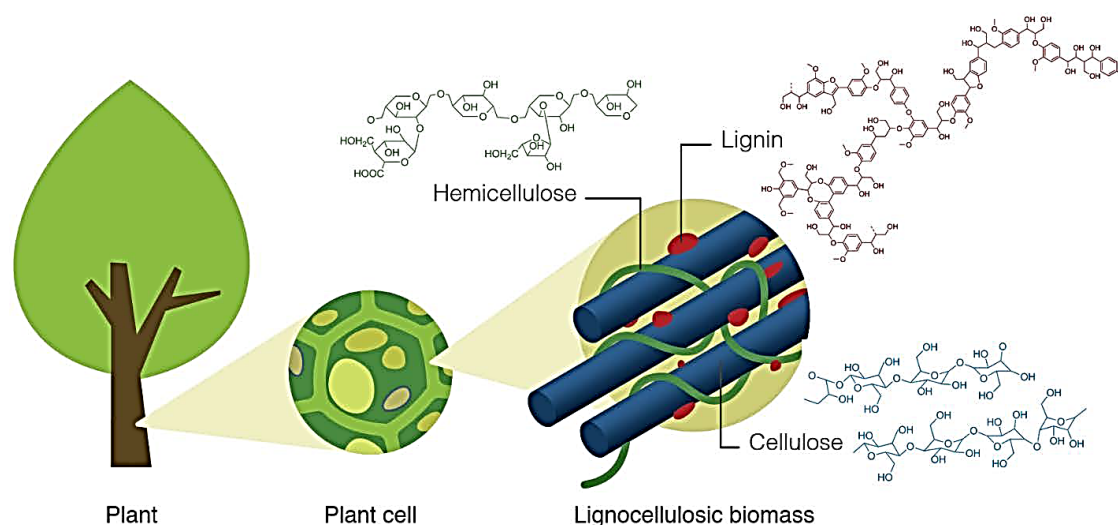
Figure 5. Components of lignocellulosic biomass [14].

2.1.1.1. Pretreatment

The first step in bioethanol production from lignocellulosic biomass is essential to facilitate the hydrolysis step by increasing the quantity of sugars that will be later fermented and to achieve high ethanol yields. Pretreatment processes employed can be

physical (e.g. mechanical milling for substrate grounding), chemical (e.g. ozonolysis, acid or alkaline hydrolysis, organosolv based method), biological (e.g. fungi) and physicochemical (e.g. ammonia fiber explosion, steam) [8].

The dehydration of hexose and pentose leads to the formation of toxic furane molecules which can inhibit cell development and reduce bioethanol productivity. Also, the presence of lignin inhibits yeast fermentation [8]. Therefore, the lignin should be completely removed, and the sugar polymers must be freed for the succeeding hydrolysis. Pretreatment of lignocellulosic materials demands more complicated and energy-intensive operations [1].

For the efficiency to be high, all the biomass should be saccharified and the enzymes participating in the process should be able to generate sugar monomers. The thermophilic bacteria, i.e., bacteria capable of developing at extreme conditions of temperature and pressure, can make cellulase and xylanase, which can entirely hydrolyze biomass at elevated temperatures and are not inhibited or will be little affected by the pretreatment lignin products which act as inhibitors of mesophilic enzymes; i.e. enzymes that develop best at temperatures ranging between 20°C and 45°C. Degrading lignocellulose will produce sugars of 5 and 6 carbons (xylose and glucose mostly) and their fermentation will involve the use of multiple steps and microorganisms because of the inexistence of a microorganism that can ferment both sugars [13]. Thus, the use of a thermophile will be able to ferment both kinds of sugars, yielding higher conversion of biomass to ethanol [7].

2.1.1.2. Hydrolysis

After the pretreatment, hydrolysis divides the biomass into sugars that will be fermented to produce ethanol. As mentioned before, acid hydrolysis and enzyme hydrolysis are commonly used [8].

2.1.1.2.1. Acid hydrolysis

There are 2 types of acid hydrolysis: dilute and concentrated. Dilute acid hydrolysis takes place under high temperatures and low acid concentrations whereas concentrated acid hydrolysis happens at low temperatures and high acid concentrations. Even though the dilute acid hydrolysis is the most used, it creates inhibitors that affect the ethanol yield.

Acid hydrolysis is a 2-step process: first, the hemicellulose hydrolysis with dilute acid takes place followed by the cellulose hydrolysis with concentrated acid. The concentrated acid hydrolysis has a higher sugar recovery (90%) achieved in less time. The main drawbacks of hydrolysis are the challenging acid recovery and recycling implementation which lead to higher costs [1].

2.1.1.2.2. Enzyme hydrolysis

As its name indicates, this type of hydrolysis involves enzymes where cellulose can be reduced under mild conditions (pH of 4.8-5 and temperatures between 45-50°C). Also, enzymatic hydrolysis is non corrosive to the reactors. Hydrolysis yield highly depends on temperature, pH, time, enzyme amount and concentration of substrate. Saccharification can improve by adding surfactants which act as a barrier for lignin. It was also determined that adding Polyethylene glycol (PEG) or Tween 20 can enhance

hydrolysis by increasing saccharification and lowering cellulase adsorption on lignin. The only drawback in using enzymes is their cost [8].

2.1.1.3. Fermentation

In this step, the released sugars will be fermented into ethanol. Fermentation can occur in batch or continuous mode. The most applied fermentation methods are Separate Hydrolysis and Fermentation (SHF), Simultaneous Saccharification and Fermentation (SSF) and Simultaneous Saccharification and Co-Fermentation (SSCF) [8].

2.1.1.3.1. Separate Hydrolysis and Fermentation

In this process, hydrolysis – where enzyme functions at high temperatures (better performance)- and fermentation –at moderate temperatures (sugar use optimization)- are separated [8].

2.1.1.3.2. Simultaneous Saccharification and Fermentation and Simultaneous Saccharification and Co-Fermentation

In both SHF and SSCF, hydrolysis and fermentation are simultaneous for low glucose concentration stability. In the former, glucose fermentation and pentose fermentation are separate whereas in the latter, the fermentation of both sugars occurs in the same reactor. It maintains a low concentration of hexose for better conversion of pentose and therefore improves the yield of ethanol produced. These two processes are favored because of their same tank use, low costs, fast and high bioethanol yield [8].

<u>2.1.1.3.3. Consolidated Bioprocessing</u>

CBP is a method where producing enzymes, hydrolysing the substrate, and fermentation are achieved in one step for the processing of cellulosic biomass. CBP requires less energy and therefore costs less when compared to the methods previously mentioned which use enzymes for the hydrolysis. Saccharification and fermentation in SHF and SSF use different operation temperatures, whereas in CBP the processes take place in the same vessel at one operating temperature. Also, minimal pretreatment is required, which leads to lower costs. However, finding a suitable microorganism, either a natural or an engineered one, is a hard task and still requires further research [15].

The table below lists the different process steps after the feed's pretreatment and compares the advantages and drawbacks of each technique.

Table 2. Main steps, advantages and drawbacks of lignocellulose conversion to bioethanol [7].

	Process steps after biomass pre-treatment	Advantages	Drawbacks
SHF	Hydrolytic enzymes production	Each step is carried out in the optimal conditions of pH and temperature	Glucose accumulated during saccharification inhibits cellulase
	Saccharification		Need of a cooling step after saccharification
	Fermentation		Need for separate vessel for saccharification and fermentation
SSF	Hydrolytic enzymes production	No cellulase inhibition	Hydrolysis and fermentation steps cannot be maintained at their optimal operational conditions
	Saccharification and hexoses fermentation		
	Pentoses fermentation		
SSCF	Hydrolytic enzymes production	No cellulase inhibition	
	Saccharification, hexoses and pentoses fermentation	Fermentation of all sugars produced during saccharification	
CBP	Simultaneous production of hydrolytic enzymes, saccharification, and fermentation of hexoses and pentoses	No additional cost for enzymes production	No microorganism already available
		No cellulase inhibition	
		Fermentation of all sugars produced during saccharification	

The figure below summarizes the different schemes of first (corn and sugarcane) and second (lignocellulosic biomass) generation bioethanol production.
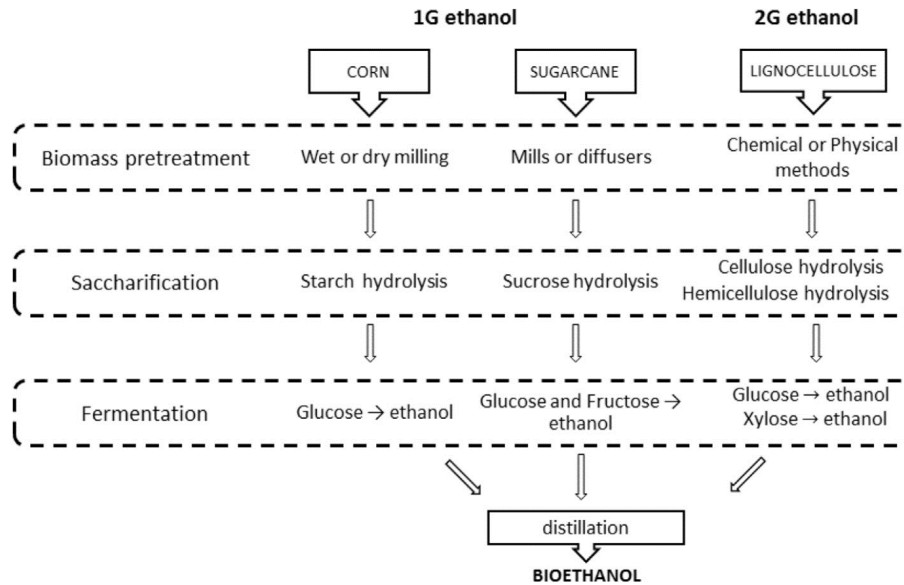
Figure 6. General schemes of first and second generation bioethanol production [7].

2.1.1.3.4. Yeast choice

A study examined different types of yeast and their influence on ethanol yield [8]. It is also known that ethanol yield will be higher if the yeast is immobilized. Bioethanol production depends on the yeasts' ability to reduce 6C molecules to 2C ones like ethanol, without oxidizing further to CO_2.

S. cerevisiae has been used for producing alcohol from a thousand years ago in a number of processes such as brewing and wine making, keeping the cost of distilling small since not only it has a high productivity and ethanol yield, but it can support the high alcohol concentrations.

These days, yeast is used for biofuel production like bioethanol from renewable energy sources. A good choice of yeast is one that can persist under high temperatures (35-45°C) and high ethanol concentrations (>20%). S. cerevisiae is capable of overcoming these conditions, but its only problem is its inability to ferment pentose to ethanol. This is why hybrid and genetically modified strains of yeast are created and

engineered so that all the parameters are fulfilled. Some strains from other yeasts (S. stipitis) able to reduce xylose were inserted in S. cerevisiae which led to a more rapid ethanol production. Co-culture, when a combination of yeasts are grown together, was also used. Pichia fermentans and stipites were put in culture with S. cerevisiae which resulted in a more efficient pentose conversion. The highest bioethanol yield of 96.9g/L with 3.46g/L/h productivity was obtained using a wild type yeast strain S. cerevisiae KL17 [8].

2.1.1.4. Purification and ethanol recovery

The ethanol solution obtained from the fermentation must be treated to separate it from water, resulting in anhydrous ethanol. Distillation can be used and is based on the different boiling points of the mixed components. The solution is heated until the ethanol's boiling point is reached (78.2 °C) which will cause the ethanol to evaporate and thus become isolated from the water [1].

Anhydrous ethanol can be obtained from adsorption, chemical dehydration, membrane processes, or either azeotropic, vacuum, diffusion, and extractive distillation [1].

2.1.2. Bioethanol process analysis

This section will discuss the production of bioethanol from different feedstocks.

2.1.2.1. Bioethanol from grass

Many researchers studied the simulation and techno-economic aspect of bioethanol synthesis using renewable energy sources. Various raw materials and

methods were employed. The following table shows the ethanol yield obtained when employing different feedstocks.

Table 3. Composition, yield and ethanol production from different feedstocks [16].

| Energy Crops | Composition (%) | | | Biomass yield (tons/ha) | Ethanol yield (g/L) | | Rate of ethanol production (L/ha/yr) |
	Cellulose	Hemicellulose	Lignin		Practical	Theoretical	
Coastal Bermuda grass	25	37.5	6.4	600,000			10,786
Elephant grass	22	24	24	18,000	23.4	36.4	23,700
Moroccan grass	33-38	27-32	17-19	10,805	17.62	23.11	6,762
Orchard grass	32	40	4.7	74,131.61			7,672
King grass	50	23	21	8,013	30.8	32.7	12,616
Switch grass	45	31	12	60,000	46.5	54.06	32,915

2.1.2.2. Newspaper and maize

One of the feedstocks that is used for bioethanol productions is organic waste. Organic waste represents 52% of municipal solid waste (MSW) in Lebanon [17].

In an experiment, 2 types of hydrolysis were evaluated. The acid hydrolysis of newspapers yielded 42% of fermentable sugar, whereas the microbe hydrolysis of maize yielded 63%. Fermentation was then performed using Saccharomyces cerevisiae. Both organic waste (newspaper) and food waste (maize) were used as feedstock. It was found that the latter is more economical due to the higher sugar yield in this type of biomass. They were able to produce 0.86 L of ethanol from 2.5 kg of food and organic waste [18], which is within the range predicted by literature that 70-100 gallons of ethanol can be produced from 1 ton of 40-60% fermentable sugar [19]. The process steps are summarized in the figure below.
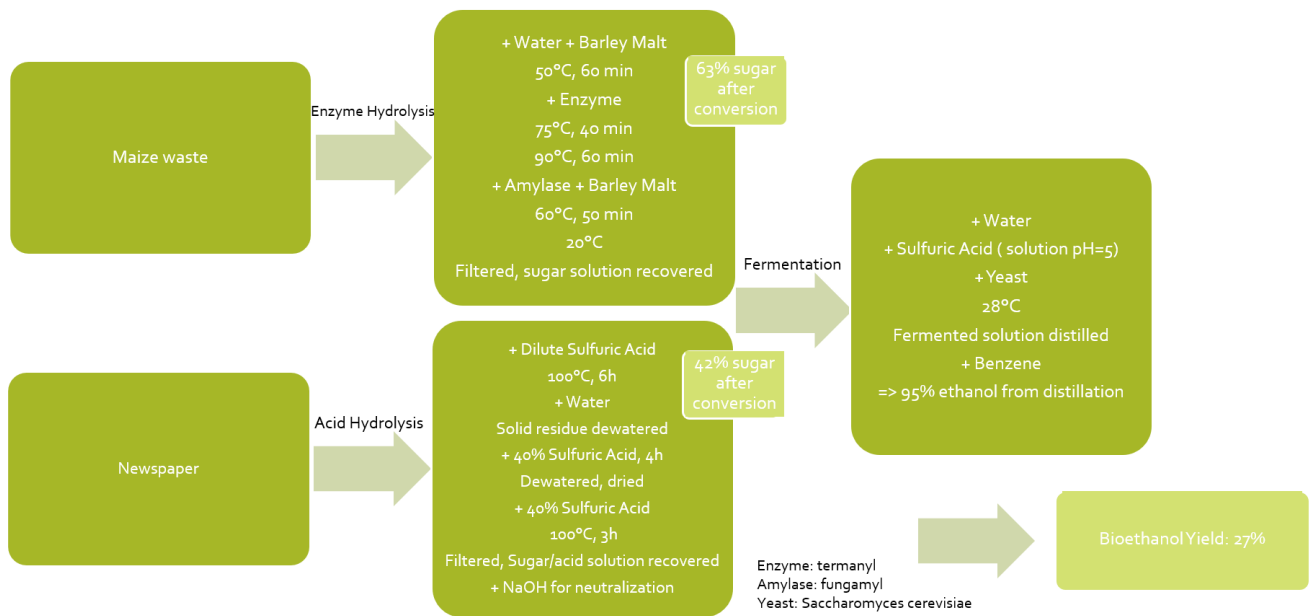
Figure 7. Process steps of bioethanol production from maize waste and

newspaper [18].

2.1.2.3. Food waste

A feasibility study of ethanol production from food waste was performed [20]. Pretreatment with different enzymes were tested for the hydrolysis. The highest glucose yield (0.63g ethanol/g total solid) was obtained with carbohydrase, as seen on the figure below.
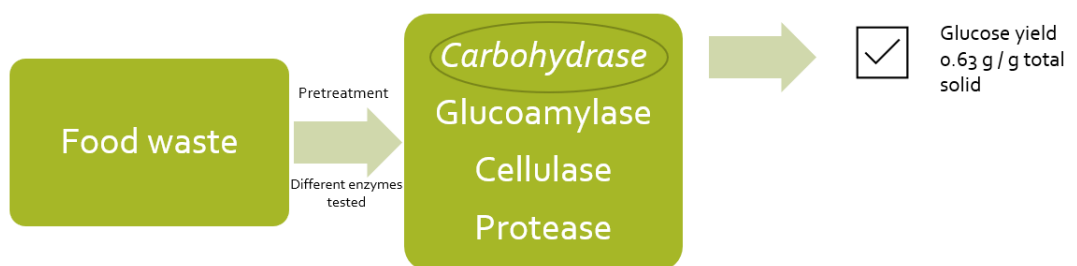
Figure 8. Glucose yield from pretreatment of food waste with carbohydrase [20].

Then enzymatic hydrolysis and fermentation by using the previously mentioned enzyme and S. cerevisiae were performed. The following results were obtained [20]:

Table 4. Ethanol yield in batch and continuous, SHF and SSF.

	Ethanol Yield (g ethanol/g total solids)	
Process	Batch	Continuous
SHF	0.43	0.3
SSF	0.31	0.2

2.1.2.4. Landfill organic waste

Another study focused on using landfill organic waste as feedstock for the

production of bioethanol [21].
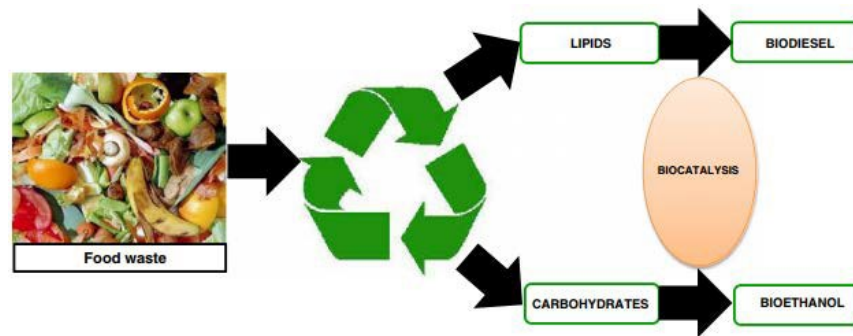
Figure 9. Conversion of municipal organic waste to biofuels [21].

The process steps are summarized in the figure below:
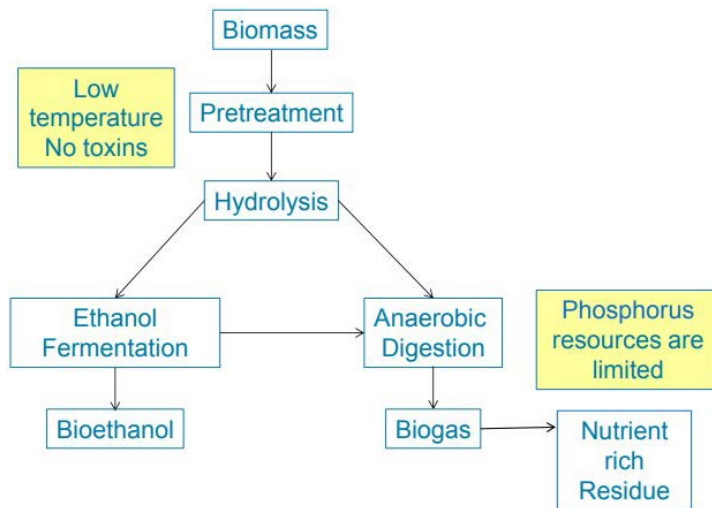
Figure 10. Biochemical pathways for biofuels from landfills organic fraction

[21].

First, the pretreatment of organic waste with diluted sulfuric acid took place at a temperature of 121°C for a period of 15 min. After that, it was subjected to 5 days of enzymatic hydrolysis with many enzymes at a temperature of 50°C to free the C6 sugars. After being cooled, the fermentation with yeast happened for 5 days at 30°C. Enzymatic hydrolysis and previous pretreatment led to a significant yield (60%) of C6 sugars. The amount of bioethanol generated from fermentable sugars was 40%.

Figure 11. Bio ethanol production process from organic waste fraction [21].
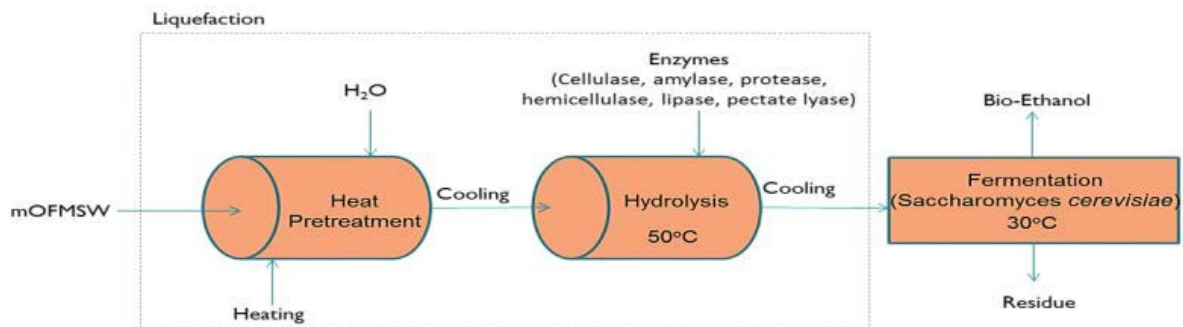
The landfill organic waste had the following composition:

Table 5. Feedstock composition [21].

Components	Composition
Glucose	42%
Soluble matter	33.6%
Cellulose	18.6%
Ash content	11.2%

Ash usually refers to compounds present in very small quantities like proteins, lipids, soluble sugars [14].

The low ash percentage indicates that the organic waste had a strong potential for being converted to bioethanol rather than residue upon fermentation.

2.1.2.5. Rape seed straw feedstock

Another paper focused on using the rape seed plant to produce many biofuels, like ethanol, methane and hydrogen [22]. Bioethanol was produced from the rape seed straw. The feed was mainly composed of glucose and xylose, monomers of cellulose and hemicellulose respectively. Lignin, on the other hand, acts as a physical obstacle that slows down the rate of carbohydrate hydrolysis. Pretreatment usually removes the non-cellulosic compounds and facilitates the enzyme's actions.

The feed was pretreated with hydrogen peroxide steam. The following procedure was followed:

Figure 12. Bioethanol from Rapeseed straw process steps [22].
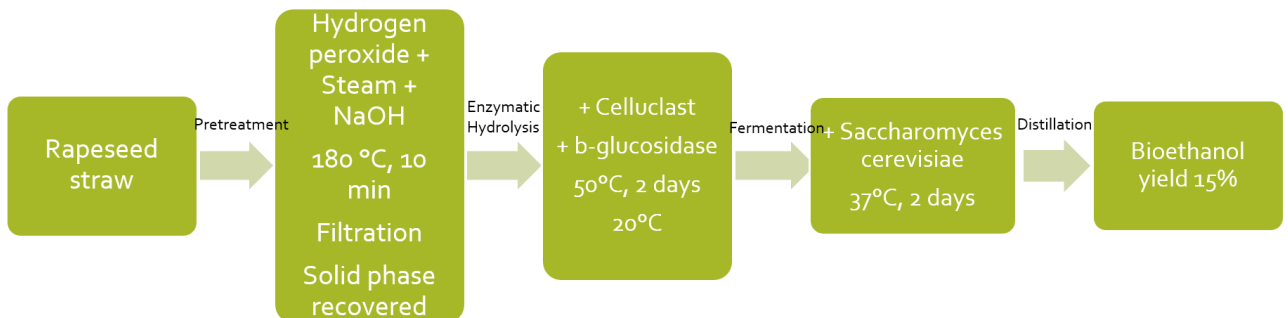
First, the slurry of straw with hydrogen peroxide in water using NaOH was mixed. After steam treatment at 180 °C for 10 min then filtration, the solid phase was dried then stored for the next step. Enzymatic hydrolysis was carried at 50°C for 2 days using celluclast and b- glucosidase. After cooling, yeast Saccharomyces cerevisiae was added, and fermentation was performed at 37°C for 2 days. Ethanol was obtained after

distillation and separation with stillage. They obtained an ethanol yield of 0.15g

ethanol/g dry straw, similar to their previous experiments where pretreatment with

hydrothermal sulfuric acid catalyst. 627 kg of ethanol was produced from 8,280 kg of

rape seed plant [22].

2.1.2.6. Woody biomass to bioethanol, Aspen simulation

In this study [23], a simulation was modeled for the production of bioethanol

from woody biomass as seen in the figure below. In this case, the yield obtained was

around 70%.
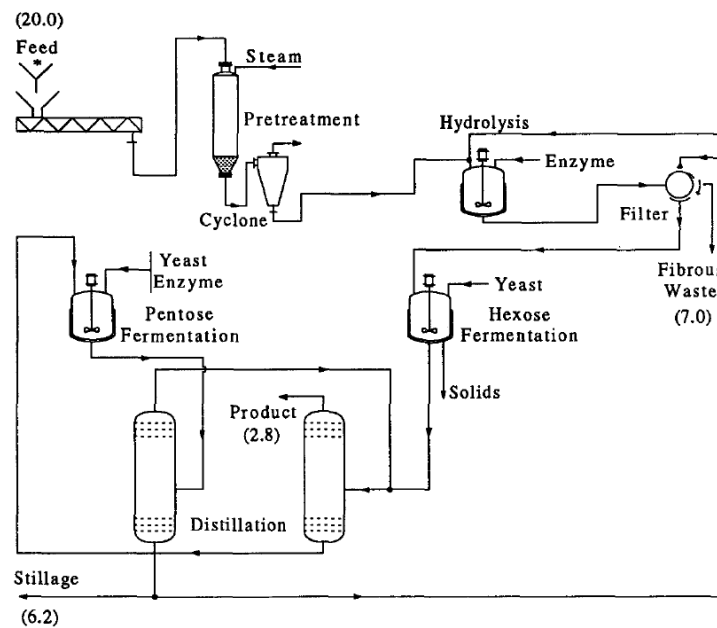
Figure 13. Simulation of bioethanol production from lignocellulosic material

[23].

2.1.2.7. Wheat meal to bioethanol, Aspen simulation

The following Aspen Plus simulation was developed to model bioethanol
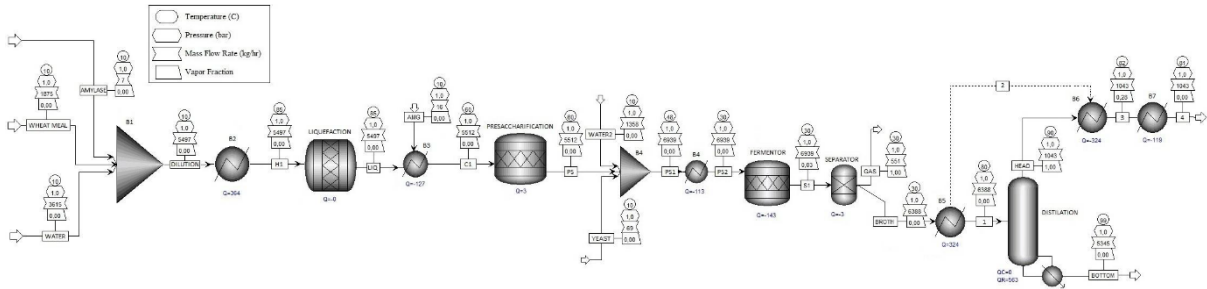
production from wheat meal [24].

Figure 14. Flowsheet for the technology of bioethanol production from wheat

meal [24].

The amount of feedstock (wheat meal) entering the system is 15,000 ton/year, with 8,000 h of operation yearly. The feed entering conditions and composition are listed in the following tables.

Table 6. Feed entering conditions.

Temperature (°C)	Pressure (bar)	ΔP (bar)
10	1	0

Table 7. Components' composition.

Components	Starch	Water	Solid
Composition	60%	15%	25%

The simulation was able to produce approximately 570.06 kg ethanol/h, or 4,560 ton/yr of bioethanol from 15,000 ton/yr. of wheat meal. The yield obtained is 30.4% [24].

2.1.2.8. Corn to bioethanol, Aspen simulation
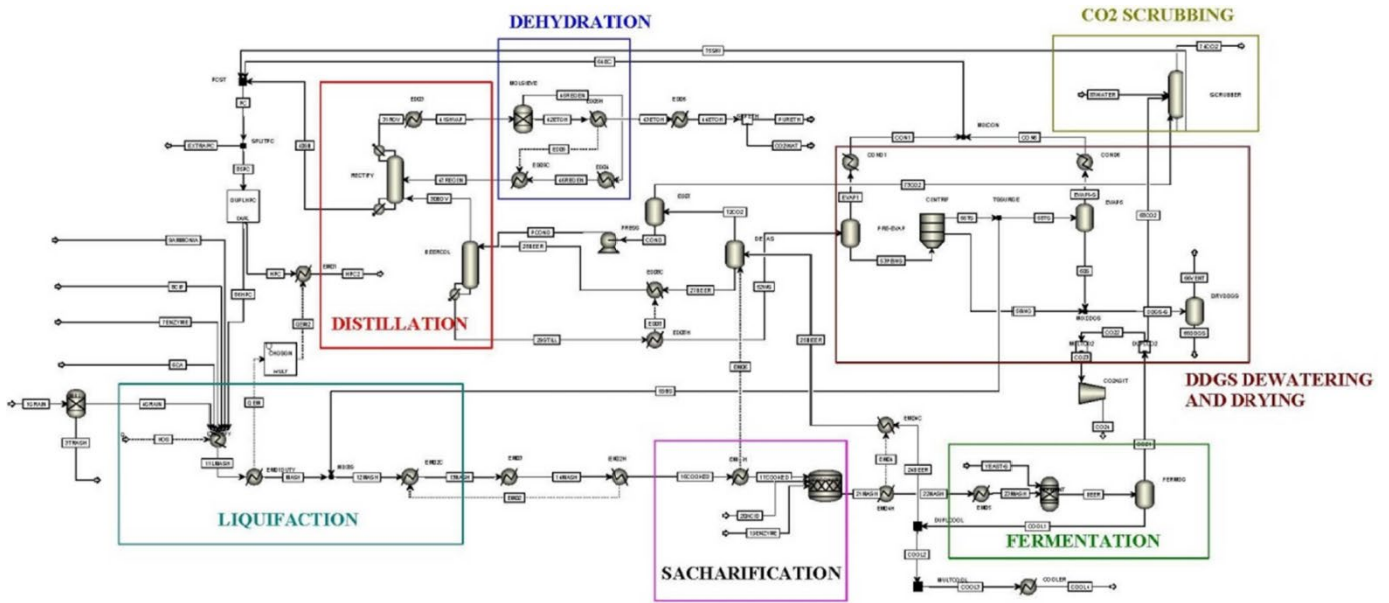
Corn was chosen as feedstock in this paper because it is the most agriculturally produced compared to other biomass. It was found that 630,000 barrels ethanol/yr. was produced from 113,071 kg corn/h [25].

Figure 15. Flowsheet for the technology of bioethanol production from corn [25].

2.1.2.9. Bioethanol production from Jatropha

Jatropha is a tropical plant that is used for production of bioethanol. The Jatropha plant can survive in various soil conditions including desert and non-arable locations. It doesn't compete with food crops for land. The oil present in the Jatropha seeds offers a potential for biodiesel production [26]. The main use of Jatropha is for the

production of biodiesel from esters and triglyceride conversion. The oils from the Jatropha seeds are converted to esters as seen in this figure:
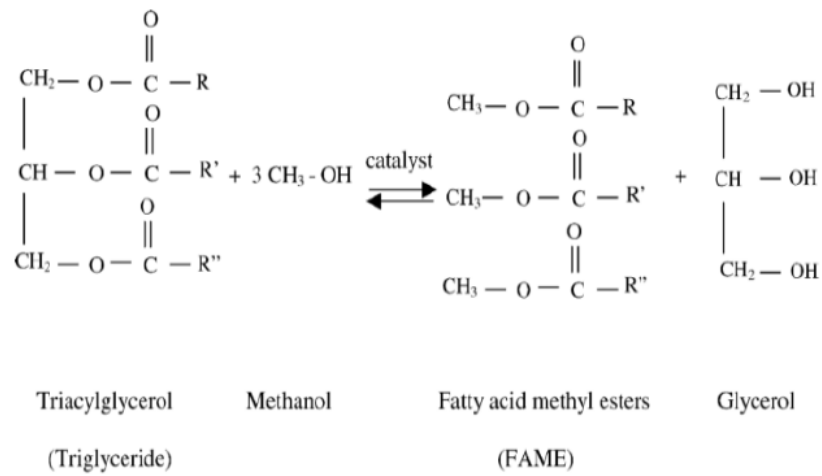
Figure 16. Biodiesel production from the catalytic transesterification of triglycerides found in Jatropha oil with methanol to produce biodiesel (FAME) [27].

Jatropha seed cake composition is shown in the figure below:
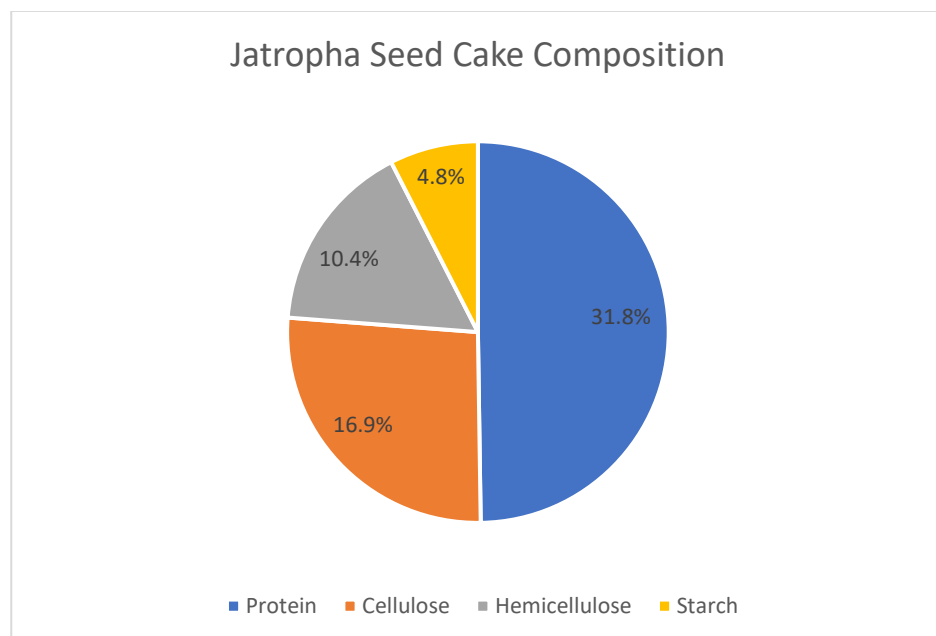
Figure 17. Jatropha seed cake composition [26].

The main steps employed when converting Jatropha plants to bioethanol are the oilseed cakes' pretreatment, followed by hydrolysis that releases the sugars and finally their fermentation to form ethanol [28].

Mishra et al. pretreated the oilseed cake with 0.5% H_2SO_4 at 125-130°C and 25 psi for an hour, in order to disrupt the crystalline lignocellulosic structure. This step is essential for the hydrolysis of cellulose with dilute acids. The mixture was later dried at around 30°C. The substrate was then hydrolyzed with 2, 3, and 5% sulphuric acid for 3 days which was then heated at high temperature (55°C). The hydrolysate was autoclaved and sterilized at 120°C, 15 psi and for 30 min. Finally, the anaerobic batch fermentation was done after adding NaOH to stimulate yeast development with Saccharomyces cerevisiae at 32°C for 9 days [28]. The process can be summarized in the figure below:
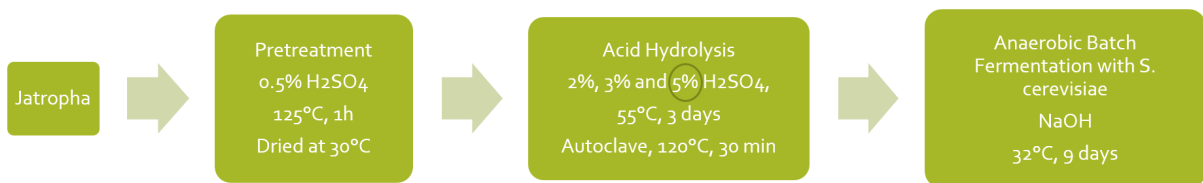
Figure 18. Bioethanol production from Jatropha [1].

Salviano et al. used a hydrolysis duration of 20 min, a 119°C temperature and a H_2SO_4 concentration of 3%. They found these conditions to be the most suitable for Jatropha seed cake hydrolysis. In order to account for the possible inhibition result of the hydrolysis by-products on the fermentation of the yeast, they experimented with diluted yeast which turned out to be more yielding than the undiluted hydrolysate. Anaerobic fermentation with 3% S. cerevisiae at 25°C yielded 88.5 L of ethanol from

1000 kg of cake oil [26]. The pretreatment was done with ethyl-ether, followed by

drying at 60°C for 2 days. The process is summarized below:
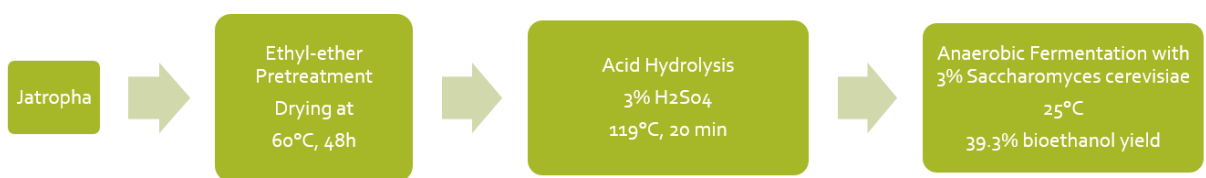
Figure 19. Bioethanol production from Jatropha [2].

The ability to produce bioethanol from seed cake might potentially supply the

ethanol needed by the biodiesel plant for the transesterification [26]. New research is

looking at using an anion exchange resin to trans-esterify Jatropha oil to biodiesel.

Laborde et al. discovered that using a heterogeneous catalyst for biodiesel synthesis is a

preferable alternative since it is not only simpler to recover and use the catalyst, but it is

also easier and less expensive to refine the product with less water and energy [29].

2.1.2.10. Bioethanol production from Giant Reed

Energy production plants use crops' biomass for energy which in its turn is a

step toward reducing CO_2 emissions. Arundo donax, commonly known as Giant reed, is

a crop that is used for the production of energy not only because of its quick growth rate

in soils of different characteristics and in various and extreme climates, but also because

of its strong yields and ability to resist a lengthy season of drought, just like Jatropha.

Another advantage for using Arundo donax for producing ethanol is that its crops are

cheap and do not compete with food crops since they can be planted in any soil. They

are also sustainable, reduce GHG emissions with photosynthesis and can be irrigated

with wastewater [10].

Using lignocellulosic biomass for producing ethanol is promising and very profitable. A case study where Giant reed is used for ethanol production was presented. The composition of Arundo donax can be seen in the figure below.

Arundo donax composition
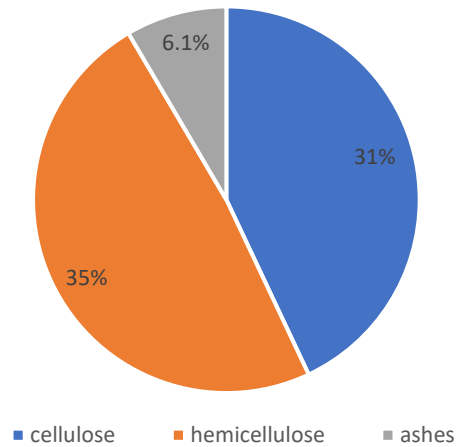
Figure 20. Arundo donax composition.

Arundo donax's ash composition is low compared to other plants, which is better especially since through the pretreatment the salts are solubilized in the hemicellulose and cellulose of the biomass. Thus, the ion concentration increases leading to the elevation in the osmotic pressure which can affect the ability of the formed hydrolysates to ferment.

The reduction in the hemicellulose composition is 85% following the alkaline pretreatment, with 75% reduction for the lignin. The removal of lignin is crucial for the enzymatic hydrolysis yield due to the better enzyme access to the cellulose.

It was found that ethanol yields produced from Arundo donax can reach up to 100 tonnes/hectare of biomass after a year or two of cultivation, or 37 tonnes of dry matter/hectare. Sugar cane can only reach up to 25 tonnes/hectare.

After studying the mass balances and taking into account the process stages, it was estimated that following the pretreatments (acid and alkaline), 1 kg of Giant reed produced 480 g of dry residue (acid cellulignin) including 72% cellulose. Expecting an efficiency of 52% for the enzymatic hydrolysis of partially delignified cellulignin (PDCL) Arundo, the efficiency of fermenting cellulose to ethanol was 40%, which could be improved with further process optimization. It can also be estimated that the ethanol yield can reach around 75 L/tonnes of biomass (60 kg). The fermentation of hemicellulose hydrosylate produced 8.2 g/L of ethanol in 2 days. As stated before, improving the hemicellulose conversion would increase the ethanol yield from the biomass. It was concluded that Giant reed for ethanol production is a good option [30].

Many studies proved that Arundo donax was a good feed crop for the production of ethanol because of its high yields and high carbohydrates constitution. The University of Washington did an assessment of the crop for its conversion to ethanol. They came up with the following results: Giant reed plant was chipped at 4°C. A factor that relates time and temperature of the pretreatment was measured. This severity factor (R_o) was found to vary between 3.4 and 4.2. Before the steam explosion pretreatment, SO_2 was added in plastic bags of 300 g of biomass until saturation. The biomass was then inserted in a reactor in samples of 50 g after weighing the plastic bags and leaving them overnight at room temperature. The table below lists the conditions of pretreatment for each sample.

Table 8. Steam pretreatment conditions for hybrid poplar and giant reed [31].

Feedstock (pre-treatment)	Severity log R_o	Conditions
Hybrid Poplar	3.6	200°C, 5 min, 3% SO_2
Giant reed (low severity)	3.4	190°C, 5 min, 3% SO_2
Giant reed (medium severity)	3.6	200°C, 5 min, 3% SO_2
Giant reed (high severity)	4.2	210°C, 5 min, 3% SO_2

The Giant reed samples were compared with the Hybrid Poplar crop in order to see which one is a better alternative for biorefineries.

Following the elapsed reaction time, the pretreatment slurry was separated into the water soluble and water insoluble fractions (WSF and WIF) applying vacuum filtration. The latter was then rinsed with a water volume 20 times the mass of the dry sample.

After the pretreatment, the enzymatic hydrolysis was conducted in 125 mL flasks in triples, the total volume of the solution was 50 mL. The water insoluble fraction washed solids were diluted to 2% with acetate buffer at 50°C and were agitated at 150 rpm. Cellulase (enzyme) was then added. The 500 μL samples were taken over 2 days, boiled for 5 min and stored at 20°C.

The next step is fermenting the liquid WSF. In flasks of 125 mL, 50 mL of medium (pH=6) were mixed with NaOH (0.5 M) and 5 g/L of Saccharomyces cerevisiae. Then, 2 g/L of ammonium phosphate and sodium nitrate and 0.2 g/L of sodium phosphate were inserted in every flask.

0.5 mL samples were taken with a syringe from the fermentation vessels-working at 30°C and agitating at 150 rpm-and were centrifuged for 5 min. Then the

supernatant liquid was removed with a 0.22 μm syringe filter and kept at 20°C. The glucose and ethanol concentrations of the samples were measured with respect to time.

Simultaneous saccharification and fermentation (SSF) were also done in 125 mL flasks where Saccharomyces cerevisiae was the sugar fermenting yeast. The washed WIF (8% concentration) were added with the WSF during the experiments. A temperature of 37°C was maintained in the fermentation vessels with constant agitation of 200 rpm. Each test was done 3 times. Hexose consumption and production of ethanol during SSF are shown in the figure below for different conditions.
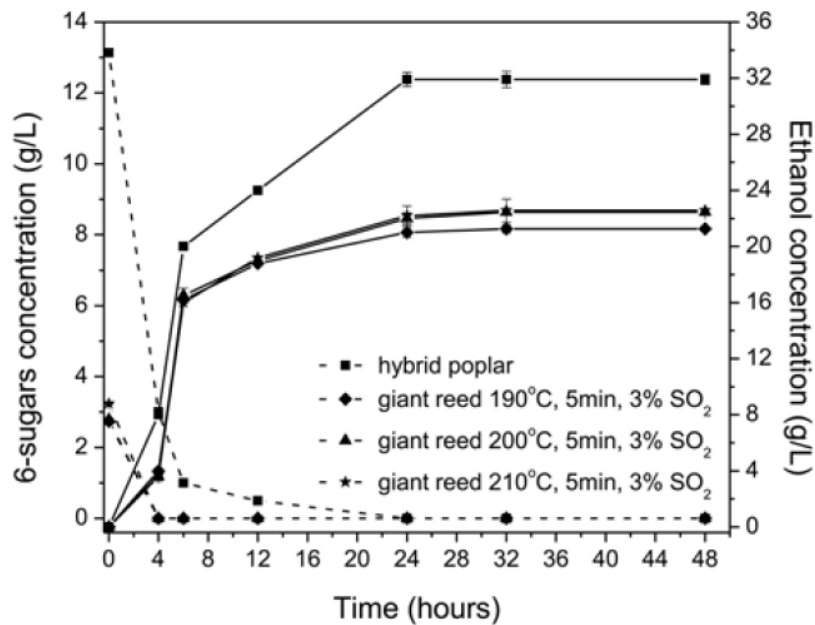
Figure 21. Hexose consumption and ethanol production during SSF [31]

As a result, the best ethanol yield (79%) -corresponding to 179 L/ton of raw material- was obtained from the SSF of the WIF and WSF from steam pretreatment of Arundo donax at the following conditions: 190°C, 5 min and 3% SO_2. This is the result obtained from laboratory experiments and not a full-scale reactor. It can be estimated that in the latter, around 315 L ethanol /ton of Arundo can be produced [31].

The previous process can be summarized in the figure below:

| Giant Reed | → | Steam explosion Pretreatment 190°C, 5 min and 3% SO_2 | → | Enzymatic Hydrolysis With cellulase | → | Simultaneous saccharification and fermentation (SSF) with Saccharomyces cerevisiae 79% bioethanol yield |
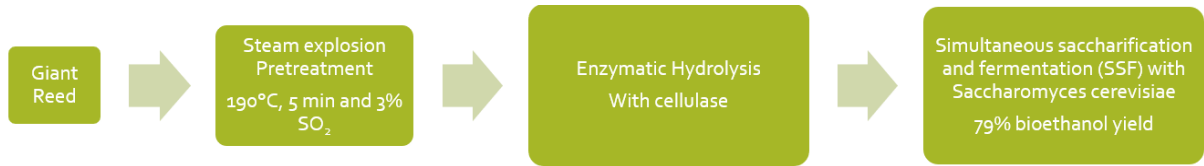
Figure 22. Process steps of bioethanol production from Giant Reed.

These high yields, as well as its high cellulose composition make the Arundo donax a good candidate for the production of ethanol [31].

Others found that after acid pretreatment of the Arundo donax, a recovery of 42 g/L of glucose was obtained from the enzymatic hydrolysis [32]. In addition, 39 g/L of ethanol was produced from SSF [30]. Others who also worked on the production of bioethanol from Arundo donax compared different methods of fermentation and came to the conclusion that in all the processes, a large concentration of enzyme is required to achieve a high cellulose conversion, which significantly raises manufacturing costs [33].

2.1.3. Feasibility in Lebanon: project and plan

The Naameh landfill in the Chouf caza, Lebanon occupies around 300,000 m^2 of land. This landfill has been welcoming municipal waste since 1997 and was forcefully shut by protestors in 2016 due to waste management conflicts and its toxicity being an uncontrolled dump site [34]. Even after the landfill was shut down, no attempts were undertaken to rehabilitate it or to develop an effective waste management strategy for the country, which resulted in the outbreak of the waste crisis [35]. The soil of the land is contaminated, with no current uses. Another landfill present in Burj Hamoud occupies 163,000 m^2.

As seen before, Arundo donax is a crop that could be planted on landfills, since it can grow on any soil and under any conditions. Making use of the landfill space in Lebanon with the plantation of Arundo donax could supply a biomass feedstock for the production of bioethanol, thus proving an alternative to fuel and maybe even replacing it.

Arundo donax crops can last up to 25 years. In addition, the crops can restore contaminated soils, restrict erosion and nutrient depletion [35].

It can be estimated that 330 L of bioethanol can be obtained per ton of Giant Reed per hectare [36]. Noting that 1 hectare = 10,000 m^2, by planting Arundo donax on the Naameh landfill soil of 300,000 m^2, 9900 L of bioethanol could be generated. Further directions could include planting the crop on other landfills including Burj Hammoud, which has an area of 163,000 m^2 and could provide an extra 5379 L of bioethanol.

These calculations could lead to an approximation of the amount of bioethanol that could be generated from planting Arundo donax on landfill soils. Landfills are the first target, but quarries and the east mountain range can also be places for Arundo donax plantation. These options will be evaluated in Chapter 4.

2.2. Modeling

2.2.1. Cellulose and hemicellulose degradation

Hemicellulose, mainly composed of xylan, degrades into xylose during hydrolysis. The table below summarizes the reactions taking place and their respective monomer sugar yields.

Table 9. Reactions and sugar monomer yields [37]

Reaction	Yield of Sugar Monomer
$Cellulose + 0.111H_2O \rightarrow 1.111Glucose$	5%
$Xylan + 0.136H_2O \rightarrow 1.136Xylose$	70%
$Lignin \rightarrow Soluble\ Lignin$	5%
$Xylose \rightarrow 0.64Furfural + 0.36H_2O$	15%
$Glucose \rightarrow 0.7HMF + 0.3H_2O$	15%

In the literature, the degradation of hemicellulose is mostly ignored when studying the hydrolysis kinetics of biomass. Studies focused on glucose, cellulose, and cellobiose [38]–[40]. However, the reaction above yields 70% of sugar monomer, and should be taken into account [37]. It can dramatically influence the yield of ethanol produced.

Mutturi et al. were able to obtain an ethanol yield of 16 g/L without taking into consideration xylose fermentation [41]. Another paper where xylose and glucose fermentation were included was able to achieve much higher ethanol concentrations, reaching up to 29 g/L.

2.2.2. Experimental results

A study (NEMO) performed Arundo donax hydrolysis followed by separate hydrolysis and fermentation (SHF) using engineered enzymes that yielded higher results than enzymes usually used. Ethanol concentrations of 45 g/L were reached. It was also deduced that SHF results were better than SSF for simulating bioethanol production as an enzyme for from Arundo donax [42].

Several processes are influenced by the SSF temperature, like the hydrolysis, fermentation, cell viability and death rates, as well as the by-products formed [41]. The inhibitors that could be present in the biomass after pretreatment, like HMF, furfural, and weak acids, affect the cell viability, which can heavily impact the process performance. It was found that the optimum temperatures for the hydrolysis and fermentation are, respectively, 45-50°C and 30-35°C [43]. Another important factor that affects the ethanol yield is the enzyme that is used in the process. A study performed a cost analysis on cellulase for ethanol production using Aspen Plus, and determined ways in how to minimize the process cost [44].

Many SSF experiments were performed on Arundo donax, and results ranged from 19.8 g/L of ethanol [33], 0.179 L ethanol/kg of raw material [31] and 39 g/L at 70 h [30].

A hybrid SSF approach using a pre-liquified Arundo donax biomass and where the temperature was risen during the process to increase the yields was performed. Ethanol concentrations of 30-40 g/L were obtained, depending on the pH, temperature and yeast dosage. The highest ethanol concentration of 42.9 g/L was obtained at a temperature of 37°C, a yeast dosage of 4 g/L and a pH of 5.5 after 144 hours. S. cerevisiae survived better in these conditions. It was also stated that when a higher enzymatic load was used, the ethanol concentration increased to 51 g/L [45]. This result was high compared to other results obtained in literature. Acetic acid steam pretreatment with co-fermentation on wheat straw led to 37.5 g/L ethanol [46]. A hybrid process where an enzymatic pre-liquefaction for 48 h was performed on Arundo donax with 21% slurry solids led to the production of 39 g/L ethanol [47]. 35 g/L ethanol was obtained after SO_2 steam pretreatment with 10% solids and SSF of wheat straw [48]. A

study performed liquefaction for 48 h on multiple feedstocks at 14% solids and obtained 50 g/L ethanol [49]. Enzymatic hydrolysis and SSF of Arundo donax as a function of severity factor and oxalic acid concentration led to a maximal ethanol concentration of 75 g/L [50].

Recently, studies are focusing on immobilizing cells, which was found to increase the fermentation productivity while decreasing the time, enhancing cell stability and recovery and biomass recycling [51].

A paper focused on the kinetics of alcohol fermentation in beer production, using immobilized and free cells, and employing different kinetic models. The results indicated that the immobilized cells began the process more gradually, but continued for 168 h, which is 24 h quicker than the fermentation using free cells. Immobilizing the cells protects them from possible inhibition. The ethanol concentration obtained reached 38 g/L [51].

An ethanol concentration of 100 g/L was obtained after 70 hours during the batch fermentation of sweet sorghum juice, using initial sugar concentrations ranging between 130 and 225 g/L, and an ethanol concentration of 63 g/L was reached during continuous fermentation after 100 h [52].

Another study evaluated the batch ethanol production applying a dual substrate model of xylose and cellobiose fermentation and using a co-culture versus a single strain system. Co-culture allows the simultaneous fermentation of cellobiose and xylose at variable substrate concentrations, whereas a single recombinant strain cannot handle changing substrate compositions. After trying different cellobiose concentrations, the highest ethanol concentration of 50 g/L was obtained with a cellobiose concentration of 120 g/L after 45 hours using S. cerevisiae EJ2. After trying different xylose

concentrations, the highest ethanol concentration of 23 g/L was obtained with a xylose

concentration of 80 g/L after 45 hours using S. cerevisiae SR8 [11]. The best results

obtained when using a co-culture system for the simultaneous fermentation of

cellobiose and xylose were an ethanol concentration of 47 g/L. The co-

culture technique employed multiple designed strains generated from the same host

organism (S. cerevisiae), allowing each specialized strain to reach optimum sugar

consumption without being limited by cultivation conditions (P_Pmax=200 g/L) [11].

Mutturi studied the hydrolysis and fermentation of Arundo biomass.

The concentrations of ethanol at the end of fiber-free fermentation range between 18,

19, 17, and 7 g/L, at temperatures of 35, 40, 45 and 50°C, respectively, after 50 hours.

The concentrations of ethanol after SSF range between 10.6, 13.7, 14.2, 12.5 g/L for

temperatures of 36, 39, 42, and 45°C, after 50 hours [41].

Chen (2010) obtained an ethanol concentration of around 38 g/L after 60 hours

of fermentation, using a fed-batch simultaneous saccharification and co-fermentation

process (SSCF) [43].

The table below summarizes the previous experiments that were done, with their

respective results. It is important to note that the experiments were done on Arundo

donax biomass and other types of biomass. The ethanol yields obtained depend on the

type of pretreatment, hydrolysis, fermentation, the feedstock, the operating conditions...

The results are solely here to put into perspective the yields that were obtained in the

literature.

Table 10. Experimental results

Study	Method	Ethanol concentration
NEMO [42]	Arundo Hydrolysis + SHF using engineered enzymes	45 g/L
[33],[31],[30]	Arundo SSF	19.8 g/L, 0.179 L/kg raw material, 39 g/L
[44]	Arundo Hybrid SSF using pre-liquified biomass	42.9 g/L
[45]	Acetic acid steam pretreatment + cofermentation on wheat straw	37.5 g/L
[46]	Arundo enzymatic pre-liquefaction + hybrid process	39 g/L
[47]	SO_2 steam pretreatment + SSF of wheat straw	35 g/L
[48]	Pre-liquefaction on multiple feedstocks	50 g/L
[49]	Enzymatic hydrolysis + Arundo SSF	75 g/L
[50]	Fermentation using immobilized cells in beer production	38 g/L
[51]	Batch fermentation of sweet sorghum juice / Continuous	100 g/L , 63 g/L
[11]	Xylose + cellobiose batch SF using co-culture system	47 g/L
[41]	Arundo fiber-free fermentation / Arundo SSF	19 g/L , 14.2 g/L
[43]	Fed-batch simultaneous saccharification and co-fermentation	38 g/L

2.2.3. Fermentation

2.2.3.1. Fermentation kinetic models

Microbial activity can be hindered in a variety of ways. The existence of inhibitors in the growing medium, such as phenolics, chlorides, benzenes, antibiotics, and so on, prevent growth and may alter microbial metabolism. In this case, substrate and product inhibitions could appear, in which substrate and product concentrations are permitted to rise to levels that cause growth to slow and eventually stop. Various mathematical equations for assessing the inhibition activity of substrate on growth

rate have been proposed, such as substrate inhibition of enzyme processes. Different

unstructured kinetic bacterial growth models are compared below [53].

2.2.3.1.1. The Monod model

This model portrays the relationship between specific growth rate and substrate

use in a reactor. Equation 1 below is based on substrate concentration, whereas

Equation 2 is also dependant on the biomass concentration [54].

$$\mu = \frac{\mu_{max}S}{K_s + S} \tag{1}$$

$$\mu = \frac{\mu_{max}XS}{K_s + S} \tag{2}$$

Where μ_{max} is the maximum bacteria growth rate (1/h)

S is the concentration of substrate (g/L)

K_s is the half saturation constant (g/L)

μ is the specific growth rate (1/h)

X is the concentration of biomass (g/L)

The Monod model implies that the bioreactor has just one growth limiting

substrate. There are five disadvantages to the Monod model.

At high substrate concentrations, the maximal specific growth rate is

independent of substrate concentration. At low substrate concentrations, growth

depends on the concentration of substrate. The Monod model cannot be used when a

substrate is inhibited. Another disadvantage of the model is that during the death

phase, it does not take into consideration the possible cell need of substrate for

maintenance. The Monod model also does not take into consideration the lag phase and

the death phase during growth. All these disadvantages were reported from experiments

done where poor kinetic fits were obtained when using this model, which was expected

because the substrate used has been reported as inhibiting cell growth. However, these limitations do not stop it from being the most widely used in experiments to model the specific growth rate and the substrate profile. Many experiments obtained promising results using the model, including experiments with ethanol production.

2.2.3.1.2. The Blackman model

This model is similar to the previous one where it uses similar assumptions. Growth is substrate-dependent at low substrate concentrations, but substrate-independent at higher concentrations. Some nutrients can be limiting at high substrate concentrations. The model has the ability to make a quick shift from first to zero order kinetics [55]. The Blackman model is portrayed in Equation 3.

$$\mu = \frac{\mu_{max}S}{K_s} \tag{3}$$

Where μ_{max} is the maximum specific growth rate (1/h)

S is the concentration of substrate (g/L)

K_s is the half saturation constant (g/L)

A similar disadvantage to the Monod model is that the Blackman model is not able to represent the lag phase and death phase, and hence overestimating the specific bacteria growth rate.

The Blackman model, like the Monod model, is unable to represent the lag and death phase, and hence overestimates the specific growth rate [56]. The Blackman model is not a common approach for modelling microbial growth, and it does not show promising results. A study compared different models (Blackman, Monod, Powell, Moser). It was found that the Blackman model was the only one that did

provide an accurate fit for the experimental data. Models such as the Monod model have cast a shadow on the Blackman model.

2.2.3.1.3. The Haldane model

This model is an extension to the Monod model, where K_i is added which takes into consideration the inhibition of specific growth rate at different substrate concentrations. It represents the greatest substrate concentration where the specific growth rate is one-half of the maximal growth rate without any inhibition present [57]. It was found that the existence of a hazardous substrate can reduce an organism's specific growth rate at elevated substrate concentrations [56]. Therefore, the addition of K_i will permit the model to take into account all kinds of substrates. The Haldane model is given by Equation 4.

$$\mu = \frac{\mu_{max}S}{K_s + S + \frac{S^2}{K_i}} \tag{4}$$

Where μ_{max} is the maximum bacteria growth rate (1/h)

S is the concentration of substrate (g/L)

K_S is the half saturation constant (g/L)

μ is the specific growth rate (1/h)

X is the concentration of biomass (g/L)

K_i is the inhibition constant (g/L)

The main advantage of this model is that it is able to account for all the phases of the cell growth (lag phase, exponential phase, stationary phase and death phase), and it is capable of representing growth rate at low and high substrate concentrations. The model was used in a number of experiments, and it represented a good fit.

2.2.3.1.4. The Teissier model (exponential)

This model is also close to the Monod and Blackman model. It relates the specific growth rate to the concentration of substrate. Experiments done using this model yielded results that fall between the previously mentioned models. However, just like the aforementioned models, a disadvantage is that it is unable to model the inhibition of cell growth, and therefore it is unable to comprehend the lag phase and the death phase. Equation 5 represents the Teissier model [58]:

$$\mu = \mu_{max}\left(1 - \exp\left(\frac{S}{K_T}\right)\right) \tag{5}$$

Where μ_{max} is the maximum specific growth rate (1/h)

μ is the specific growth rate (1/h)

S is the concentration of substrate (g/L)

K_T is a proportionality constant (g/L)

Something that distinguishes this model to the previously mentioned ones is the change from first to zeroth order kinetics. According to experiments done in the literature, it was found that the Teissier model can model specific growth rates in diverse substrate concentrations.

2.2.3.1.5. The Moser model

This model is a modification of the Monod model that depends only on the concentration of substrate and has an additional variable n which allows for greater flexibility in modelling experimental results. This term can be modified to suit the experimental results, which makes the model superior than the Monod model [56]. Equation 6 is used to portray the Moser model [59].

$$\mu = \frac{\mu_{max}S^n}{K_s + S^n} \qquad (6)$$

Where μ_{max} is the maximum specific growth rate (1/h)

μ is the specific growth rate (1/h)

S is the concentration of substrate (g/L)

K_S is the half saturation constant (g/L)

n is the adjustable variable

This model, along with the Blackman and Contois models, have not been frequently employed to define specific growth rates. The Moser model does not take into account substrate inhibition; however, experiments show that the variable n is employed to characterize substrate inhibition. In contrast to the Monod and Contois models, the Moser model can capture the lag phase for high substrate concentrations, however it is incapable of describing the dying phase.

2.2.3.1.6. The Contois model

This model is also a modification of the Monod model which is dependent on the substrate and biomass concentration as seen in Equation 7 [60].

$$\mu = \frac{\mu_{max}S}{K_s X + S} \qquad (7)$$

Where μ_{max} is the maximum specific growth rate (1/h)

μ is the specific growth rate (1/h)

X is the biomass concentration (g/L)

S is the concentration of substrate (g/L)

K_S is the half saturation constant (g/L)

This model assumes that X is inversely proportional to μ. Similar to the Monod, Blackman, and Teisser models, this model is unable to take into account the lag phase and death phase, as well as substrate inhibition. Although the Contois model is not the most employed, it shows promising results when used.

2.2.3.1.7. The Logarithmic model

The logarithmic model relates the specific growth rate to the logarithmic of the concentration of substrate. It was found that it is the least accurate model among all those discussed previously due to its inability to portray the lag phase, stationary phase and death phase. Another disadvantage is that the model over-estimates cell growth and can lead to negative growth rate results for low substrate concentrations [61]. The Logarithmic model is given in Equation 8.

$$\mu = a + b \ln(S) \tag{8}$$

Where a and b are constants

S is the concentration of substrate (g/L)

2.2.3.1.8. The Aiba-Edward model

This model is also a modification of the Monod model, where an inhibition constant with an exponential factor is added, as seen in the equation below [62]. The added variable takes into consideration the existence of a toxic substrate, thus taking into account the lag phase and death phase. The model is represented in Equation 9.

$$\mu = \frac{\mu_{max}S}{K_s + S} exp\left(-\frac{S}{K_i}\right) \tag{9}$$

Where μ_{max} is the maximum specific growth rate (1/h)

μ is the specific growth rate (1/h)

S is the concentration of substrate (g/L)

K_S is the half saturation constant (g/L)

K_i is the inhibition constant (g/L)

The use of this model was a good fit in many experiments.

2.2.3.1.9. The Yano and Koga model

The model can describe substrate inhibitory effects at elevated concentrations of substrate and is given in Equation 10 [63].

$$\mu = \frac{\mu_{max}}{K_s + S + \frac{S^2}{K_1} + \frac{S^3}{K_2^2}} \tag{10}$$

Where μ_{max} is the maximum specific growth rate (1/h)

μ is the specific growth rate (1/h)

S is the concentration of substrate (g/L)

K_S is the half saturation constant (g/L)

K_1 is a substrate inhibition constant (g/L)

K_2 is a substrate inhibition constant (g/L)

2.2.3.1.10. The Han and Levenspiel model

This is an extension of the Monod model which takes into account substrate inhibition effects, as seen in Equation 11 [64].

$$\mu = \frac{\mu_{max}S}{K_s \left(1 - \frac{S}{S_m}\right)^m + S}\left[1 - \left(\frac{S}{S_m}\right)\right]^n \tag{11}$$

Where μ_{max} is the maximum specific growth rate (1/h)

μ is the specific growth rate (1/h)

S is the concentration of substrate (g/L)

S_m is the critical inhibitor concentration (g/L)

K_I is the inhibition constant (g/L)

n is a constant (unitless)

m is a constant (unitless)

Adding the critical inhibitor concentration variable enhances the model's
accuracy in the prediction of the cell growth.

2.2.3.1.11. The Powell model

Another modification of the Monod model, the Powell model uses a variable m
named the maintenance parameter [65]. However, this model does not take into account
substrate inhibition, lag phase and death phase. Because of the lack of literature
using the Powell model, the addition of the maintenance parameter m could not be
investigated thoroughly. The model is portrayed in Equation 12.

$$\mu = \frac{(\mu_{max} + m)\, S}{K_s + S} - m \qquad (12)$$

Where μ_{max} is the maximum specific growth rate (1/h)

μ is the specific growth rate (1/h)

S is the concentration of substrate (g/L)

m is the maintenance parameter (1/h)

2.2.3.1.12. The Logistic model

Often named Verhulst model, the model assumes that an organism's growth rate
is related to its present population, and to the unused resources in a confined

environment [66]. It is not dependent on the concentration of substrate, only on the concentration of biomass and takes into consideration substrate inhibition, as seen in Equation 13.

$$\mu = \mu_{max} \left[1 - \frac{X}{X_m} \right] \tag{13}$$

Where μ_{max} is the maximum specific growth rate (1/h)

    X_m is the maximum biomass concentration (g/L)

    μ is the specific growth rate (1/h)

    X is the concentration of biomass (g/L)

    Even though the model demonstrated its capacity to deal with hazardous substrates, and because there is little research on the efficacy of this model, it is hard to make conclusions about its potential to represent kinetic growth.

2.2.3.1.13. The Luong model

    An extension to the Monod model, this model has an additional power term that helps in describing inhibition above a certain concentration of substrate [67]. S_m can estimate any limitation of substrate, no matter the substrate concentration, which solidified the model. This model, displayed in Equation 14, is able to predict the maximum possible substrate concentration.

$$\mu = \frac{\mu_{max} S}{K_s + S} \left(1 - \frac{S}{S_m} \right)^n \tag{14}$$

Where μ_{max} is the maximum specific growth rate (1/h)

    S_m is the critical inhibitor concentration (g/L)

    μ is the specific growth rate (1/h)

    S is the concentration of substrate (g/L)

K_S is the half saturation constant (g/L)

When this model was employed, it showed promising results because of its ability to model toxic and non toxic substrates.

2.2.3.1.14. The Webb model

Being a modification of the Haldane model, this model has an additional term $1 + \frac{S}{K_i}$ and is dependent on the concentration of substrate, as seen in Equation 15 [68]. However, literature has reported poor fits when using this model.

$$\mu = \frac{\mu_{max}\, S\left(1 + \frac{S}{K_i}\right)}{K_s + S + \frac{S^2}{K_i}} \tag{15}$$

Where μ_{max} is the maximum specific growth rate (1/h)

μ is the specific growth rate (1/h)

S is the concentration of substrate (g/L)

K_S is the half velocity saturation constant (g/L)

K_i is the inhibition constant (g/L)

2.2.3.2. Single substrate kinetic models

A modified kinetic model was developed in this thesis, based on an existing kinetic model for ethanol fermentation from sweet sorghum stalk pieces using genetically modified S. cerevisiae [52]. The existing model accounts for substrate limitation and inhibition, product inhibition and yeast death. The new model was modified in order to work for dual-substrate models.

To assess the quantitative relationship between environmental factors and bacterial kinetics, mathematical models were designed. As seen previously, the Monod

model (Equation 1) is a general formula for describing the connection between growth

rate and concentration of substrate, but it ignores inhibition produced by

high concentrations of substrate and product [52].

$$\mu = \frac{\mu_{max}S}{K_s + S} \tag{1}$$

The main inhibiting parameters in ethanol fermentation are large sugar and

ethanol concentrations, which have an inhibitory effect on yeast growth. The Andrew

and Levenspiel model takes this into account and is portrayed in Equation 16 [69].

$$\mu = \frac{\mu_{max}S}{K_{SX} + S + \frac{S^2}{K_{SXi}}}\left(1 - \frac{P}{P_{Xmax}}\right)^{\alpha} \tag{16}$$

Ethanol is a major metabolite produced by anaerobic yeast growth, and its

formation is linked to cell development. A product formation model was suggested in

Equation 17 based on the same principle as Equation 16.

$$q = \frac{q_{max}S}{K_{SP} + S + \frac{S^2}{K_{SPi}}}\left(1 - \frac{P}{P_{Pmax}}\right)^{\beta} \tag{17}$$

The following rates of cell growth (Equation 18) and ethanol generation

(Equation 19) are used to explain fermentation dynamics.

$$\frac{dX}{dt} = \mu X \tag{18}$$

$$\frac{dP}{dt} = qX \tag{19}$$

Substituting into the previous equations yields Equations 20 and 21.

$$\frac{dX}{dt} = \frac{\mu_{max}S}{K_{SX} + S + \frac{S^2}{K_{SXi}}}\left(1 - \frac{P}{P_{Xmax}}\right)^{\alpha} X \tag{20}$$

$$\frac{dP}{dt} = \frac{q_{max}S}{K_{SP} + S + \frac{S^2}{K_{SPi}}} \left(1 - \frac{P}{P_{Pmax}}\right)^{\beta} X \qquad (21)$$

Substrate is necessary in batch fermentation for cell growth, cell maintenance, and ethanol production. Equation 22 is used for substrate consumption [52].

$$-\frac{dS}{dt} = \frac{1}{Y_{X/S}}\left(\frac{dX}{dt}\right) + \frac{1}{Y_{P/S}}\left(\frac{dP}{dt}\right) + mX \qquad (22)$$

It was found that the model that fits best is the Monod model taking into account substrate and product inhibition [51]. The modified Monod kinetic model which accounts for product and substrate inhibition uses the following modified equations, Equations 23 and 24 [70].

$$\frac{dX}{dt} = \frac{\mu_{max}S}{K_{SX} + S + \frac{S^2}{K_{SXi}}} \left(1 - \frac{P}{P_{Xmax}}\right) X \qquad (23)$$

$$\frac{dP}{dt} = \frac{q_{max}S}{K_{SP} + S + \frac{S^2}{K_{SPi}}} \left(1 - \frac{P}{P_{Pmax}}\right) X \qquad (24)$$

Where μ is the specific growth rate (1/h)

μ_{max} is the maximum bacteria growth rate (1/h)

S is the concentration of substrate (g/L)

K_{sX} is the half saturation constant (g/L)

K_{sXi} is a substrate inhibition constant (g/L)

P is the concentration of product (g/L)

P_{xmax} is the maximum ethanol concentration for growth (g/L)

α is an ethanol inhibition constant (unitless)

q_{max} is the maximum specific ethanol production rate (1/h)

K_{sP} is an ethanol saturation constant (g/L)

K_{sPi} is a substrate inhibition constant (g/L)

P_{Pmax} is the maximum ethanol concentration (g/L)

β is an ethanol inhibition constant (unitless)

m is the cell maintenance coefficient (1/h)

X is the concentration of biomass (g/L)

It can be noticed that the differences between this model and the previous one are the absence of the power terms α and β, which are ethanol inhibition constants, as well as the absence of the maintenance coefficient m. Adding them solidifies the model further, and these constants will be used in the developed model.

Most papers only included glucose as a substrate for ethanol fermentation. However, xylose can be treated as an additional substrate along with glucose. The added terms will provide more accurate results, and in turn lead to higher ethanol yields.

2.2.3.3. Dual substrate kinetic models

The previous models were developed for single substrate models.

A study proposed a kinetic model for binary substrate fermentation for the fermentation of sucrose into glucose and fructose, with the latter having a slower rate of consumption [71]. This model takes into account substrate and product inhibition.

The suggested model is made up of three components: the first component denotes overall substrate inhibition, the second component covers inhibition by the second substrate, and the third component represents inhibition by the second substrate fraction.

$$S = S_G + S_F + S_{SC} \tag{25}$$

$$\mu = \frac{\mu_{max}S}{K_{S1} + S + \frac{S^2}{K_i}} \exp\left(-\frac{S_{SR}}{K_i'}\right)\left(1 - \frac{\eta}{\eta_{max}}\right)^n \tag{26}$$

$$\frac{dX}{dt} = \mu X \tag{18}$$

$$\frac{dS_{SC}}{dt} = -\alpha_s \left(\frac{S_{SC}}{K_{SC} + S_{SC}}\right) X \tag{27}$$

$$\frac{dS_{SG}}{dt} = \alpha_s \left(\frac{S_{SC}}{K_{SC} + S_{SC}}\right) X Y_{G/SC} - \frac{\mu X}{Y_{X/G}} \tag{28}$$

$$\frac{dS_F}{dt} = \alpha_s \left(\frac{S_{SC}}{K_{SC} + S_{SC}}\right) X Y_{F/FC} - \frac{\mu X}{Y_{X/F}} \tag{29}$$

Where S_G, S_F, S_{SC} are the concentrations of glucose, fructose and sucrose, respectively (g/L)

K_i, K_i' are inhibition rate constants for all substrates and fructose, respectively (g/L)

η_{max} is the maximum fraction of fructose at which cell growth is inhibited (unitless)

K_{S1}, K_{SC} are the growth saturation constant and sucrose uptake saturation constant, respectively (g/L)

μ_{max} is the maximum specific cell mass growth rate (1/h)

α_s is the specific sucrose uptake rate (unitless)

$Y_{G/SC}, Y_{F/FC}, Y_{X/G}, Y_{X/F}$ are the yield coefficients for glucose and fructose, and the yield coefficients of cell mass for glucose and fructose, respectively (unitless).

What is meant by second substrate is the substrate that is consumed at a slower pace than the other one, with a slower rate of consumption which might restrict growth.

The Haldane model is made of the first component only. The proposed model consists of adding into the equation the second component which takes into account the

possibility of substrate growth restriction, and third component which accounts for second substrate fraction in cell growth inhibition. At large starting substrate concentrations, the suggested model performed exceptionally well in estimating experimental results. As a result, it was found that the suggested model may be extended and used with any fermentation process with two substrates [71].

Another paper studied the fermentation kinetics of ethanol production from glucose and xylose with an engineered strain of S. cerevisiae 1400(pLNH33) and established a model incorporating substrate and product inhibition [72]. The following equations used in the model are valid for both substrates and yielded accurate results.

$$\mu = \frac{\mu_m S}{K_S + S + \frac{S^2}{K_i}} \left[1 - \left(\frac{P}{P_m} \right)^{\beta} \right] \tag{30}$$

$$q = \frac{q_m S}{K'_S + S + \frac{S^2}{K'_i}} \left[1 - \left(\frac{P}{P'_m} \right)^{\gamma} \right] \tag{31}$$

$$-\frac{dS}{dt} = \frac{1}{Y_{X/S}} \left(\frac{dX}{dt} \right) - \frac{1}{Y_{P/S}} \left(\frac{dP}{dt} \right) + mX \tag{22}$$

$$\mu_{mixture} = \frac{S_1}{S_1 + S_2} \mu_{S_1} + \frac{S_2}{S_1 + S_2} \mu_{S_2} \tag{32}$$

$$\frac{dP}{dt} = \left(q_{S_1} + q_{S_2} \right) X \tag{33}$$

$$\frac{dX}{dt} = \mu_{mixture} X \tag{34}$$

Where μ_{S_1}, μ_{S_2} are, respectively, the specific growth rates on glucose and xylose (1/h).

q_{S_1}, q_{S_2} are, respectively, the specific productivities on glucose and xylose (1/h).

CHAPTER 3

METHODOLOGY

This chapter assesses the kinetic modeling of the hydrolysis and fermentation for the production of bioethanol from Giant Reed feedstock.

3.1. Hydrolysis

The hydrolysis kinetics were examined in this section. Both cellulose and hemicellulose hydrolysis were studied.

3.1.1. Kinetic model

3.1.1.1. Kinetic modelling of cellulose and hemicellulose hydrolysis

The enzymatic hydrolysis of cellulose is a heterogeneous reaction because of the insolubility of cellulose. For the hydrolysis to occur, the enzymes introduced as liquid must adhere to the surface of the solid substrate. Equation 35 calculates the number of enzymes linked to the substrate and follows the Langmuir type adsorption isotherm [39].

$$E_{iB} = \frac{E_{imax}K_{iad}E_{iF}S_1}{1 + K_{iad}E_{iF}} \tag{35}$$

Where E_{iB} ($i = 1; 2$) is the bound concentration of enzyme on substrate (kg/m^3)

E_{imax} ($i = 1; 2$) is the maximum enzyme mass that can absorb onto a substrate unit mass (kg protein/kg cellulose)

K_{iad} ($i = 1; 2$) is the dissociation constant for the enzyme adsorption (m^3/kg protein)

E_{iF} ($i = 1; 2$) is the free enzymes concentration in solution (in kg/ m^3)

The substrate reactivity parameter, as seen in Equation 36, describes the \\

reduction in reactivity of the substrate as the reaction progresses, to fit the fed-

batch process [39]. It is included in the rate equations of cellulose and cellobiose,

Equations 51 and 52.

$$R_S = \frac{\alpha S_1 V}{S_{1F} V + S_{1,0} V_0} \tag{36}$$

$$S_{iF} = \lambda_i S_F \tag{37}$$

Where α is a substrate reactivity constant linked to hydrolysis degree (unitless)

S_1 is the concentration of cellulose (g/L)

V is the volume (m^3)

S_{iF} ($i = 1; 2$) is the feed concentration of cellulose and hemicellulose,

respectively (g/L)

λ_i ($i = 1; 2$) is the proportion of cellulose and hemicellulose in the

lignocellulose feed concentration, S_F (unitless)

$S_{1,0}$ is the initial concentration of cellulose (g/L)

V_0 is the fed-batch process initial volume (m^3)

Which give Equation 38:

$$R_S = \frac{\alpha S_1 V}{\lambda_1 S_F V + S_{1,0} V_0} \tag{38}$$

Pretreatment is required before the enzymatic hydrolysis step where

lignocellulosic biomass which is mostly made of cellulose, hemicellulose, and lignin, is

converted into fermentable sugars. It was assumed that the pretreatment was done

to remove lignin, which is not fermentable. After that, a thoroughly mixed solution of

cellulose, hemicellulose, lignin, nutrients, and enzymes is supplied to a bioreactor,

where both saccharification and co-fermentation take place at the same time. The

product is then converted into ethanol after it is purified. Cellulose is converted to cellobiose and glucose, while hemicellulose is hydrolysed into xylose during the saccharification stage. After that, a genetically engineered yeast uses both monosaccharides as carbon sources to make ethanol. The material balance equations for the enzyme hydrolysis and co-fermentation can be written this way [43].

$$\frac{dS_1}{dt} = -r_1 - r_2 + \frac{F}{V}(\lambda_1 S_F - S_1) \tag{39}$$

$$\frac{dS_2}{dt} = 1.056r_1 - r_3 - \frac{F}{V}S_2 \tag{40}$$

$$\frac{dS_3}{dt} = 1.111r_2 + 1.053r_3 - \frac{v_G X}{Y_{P/S_3}} - \frac{F}{V}S_3 \tag{41}$$

$$\frac{dS_4}{dt} = -r_4 + \frac{F}{V}(\lambda_2 S_F - S_4) \tag{42}$$

$$\frac{dS_5}{dt} = 1.136r_4 - r_5 - \frac{v_x X}{Y_{P/S_5}} - \frac{F}{V}S_5 \tag{43}$$

$$\frac{dX}{dt} = \mu_{mix}X - \frac{F}{V}X \tag{44}$$

$$\mu_{mix} = \frac{S_3}{S_3 + S_5}\mu_G + \frac{S_5}{S_3 + S_5}\mu_X \tag{45}$$

$$\mu_G = \frac{\mu_{m_G}S_3}{K_G + S_3 + \frac{S_3^2}{K_{iG}}} * \left[1 - \left(\frac{p_G}{p_{mG}}\right)^{\varphi_G}\right] \tag{46}$$

$$\mu_X = \frac{\mu_{m_X}S_5}{K_X + S_5 + \frac{S_5^2}{K_{iX}}} * \left[1 - \left(\frac{p_X}{p_{mX}}\right)^{\varphi_X}\right] \tag{47}$$

$$v_G = \frac{v_{m_G}S_3}{K'_G + S_3 + \frac{S_3^2}{K'_{iG}}} * \left[1 - \left(\frac{p_G}{p'_{mG}}\right)^{\varphi'_G}\right] \tag{48}$$

$$v_X = \frac{v_{mX}S_5}{K'_X + S_5 + \frac{S_5^2}{K'_{iX}}} * [1 - \left(\frac{p_X}{p'_{mX}}\right)^{\varphi'_X}] \qquad (49)$$

$$E_{iT} = E_{iF} + E_{iB} \qquad (50)$$

Where S_1, S_2, S_3, S_4, S_5 and X are the concentrations of cellulose, cellobiose, glucose, hemicellulose, xylose, and biomass respectively (g/L)

r_1, r_2, r_3, r_4, r_5 are their respective kinetic rates (kg/m³h)

μ_{mix} is the specific growth rate of yeast (1/h)

E_{iT} (i=1;2) is the total concentration of enzyme (g/kg)

E_{iF} (i=1;2) is the free concentration of enzyme (g/kg)

E_{iB} (i=1;2) is the bound concentration of enzyme (g/kg)

v_G and v_X are the specific yeast production rates on glucose and xylose, respectively (1/h)

μ_G and μ_X are the specific yeast cell growth rates on glucose and xylose, respectively (1/h)

μ_{mix} is the specific yeast cell growth rates on glucose and xylose mixtures (1/h)

F is the inlet lignocellulose flow rate (g/L)

V is the working volume (L)

S_F is the lignocellulosic feed concentration (g/L)

λ_1 and λ_2 are the proportions of cellulose and hemicellulose, respectively (unitless)

Y_{P/S_3} and Y_{P/S_5} are the ethanol yield coefficient from glucose and xylose, respectively (unitless)

v_{mG} and v_{mX} are the maximum specific ethanol production rate for yeast on glucose and xylose (1/h)

μ_{m_G} and μ_{m_X} are the maximum specific growth rate coefficient for yeast

on glucose and xylose (1/h)

K_G and K_X are the saturation coefficient for cell growth on glucose and

xylose (kg/m^3)

K_{iG} and K_{iX} are the inhibition coefficient for cell growth on glucose and

xylose (kg/ m^3)

p_{mG} and p_{mX} are the maximum ethanol concentration for cell growth on

glucose and xylose (kg/m^3)

p_G and p_X are the concentration of glucose and xylose (kg/m^3)

φ_G and φ_X are the power of ethanol inhibition for cell growth on glucose

and xylose (unitless)

λ_1 and λ_2 are the proportions of cellulose and hemicellulose in the feed

(unitless)

The coefficients used in the rate equations above were based on values from

literature due to adding water throughout the hydrolysis of cellulose and hemicellulose.

In other words, the coefficients were added to balance the reactions.

Three reactions were used to describe the hydrolysis of cellulose: r₁ for cellulose

to cellobiose, r₂ for cellulose to glucose, and r₃ for cellobiose to glucose. r₁ and r₂ follow

first order kinetics, whereas r₃ follows Michaelis–Menten kinetics with competitive

substrate inhibition. Cellobiose, glucose, and xylose are inhibitory for r₁, r₂ and r₃ [39].

Therefore, the equations below account for competitive inhibition of glucose, cellobiose

and xylose [40]. The kinetic rate equations are listed below [43].

$$r_1 = \frac{k_1 E_{1B} R_S S_1}{1 + \frac{S_2}{K_{1iG_2}} + \frac{S_3}{K_{1iG}} + \frac{S_5}{K_{1iX}}} \tag{51}$$

Where r_1 is the cellulose to cellobiose reaction rate (kg/m³h)

k_1 is the reaction rate constant (kg/g.h)

S_1, S_2, S_3, S_5 are the concentrations of cellulose, cellobiose, glucose and xylose respectively (g/L)

K_{1iG2} is the inhibition constant of cellobiose on enzymes (kg/m³)

K_{1iG} is the inhibition constant of glucose on enzymes (kg/m³)

K_{1iX} is the inhibition constant of xylose on enzyme (kg/m³)

$$r_2 = \frac{k_2(E_{1B} + E_{2B})R_S S_1}{1 + \frac{S_2}{K_{2iG_2}} + \frac{S_3}{K_{2iG}} + \frac{S_5}{K_{2iX}}} \tag{52}$$

Where r_2 is the cellulose to glucose reaction rate (kg/m³h)

k_2 is the reaction rate constant (kg/g.h)

K_{2iG2} is the inhibition constant of cellobiose on enzymes (kg/m³)

K_{2iG} is the inhibition constant of glucose on enzymes (kg/m³)

K_{2iX} is the inhibition constant of xylose on enzyme (kg/m³)

$$r_3 = \frac{k_3 E_{2F} S_2}{K_{3M}\left[1 + \frac{S_3}{K_{3iG}} + \frac{S_5}{K_{3iX}}\right] + S_2} \tag{53}$$

Where r_3 is the cellobiose to glucose reaction rate (kg/m³h)

k_3 is the reaction rate constant (1/h)

E_{2F} is concentration of free enzymes in solution (kg/m³)

K_{3M} is the cellobiose saturation constant (kg/m³)

K_{3iG} is the inhibition constant of glucose on enzymes (kg/m³)

K_{3iX} is the inhibition constant of xylose on enzyme (kg/m³)

Many distinct sugar monomers are found in hemicellulose. However, xylose is the most abundant one. As a result, it can be assumed that in the beginning, hemicellulose is hydrolysed to xylose that is later converted to furfural after it is freed from the solid matrix and in contact with the solution. Below are listed the degradation rate of hemicellulose to xylose (r_4) followed by furfural formation from xylose (r_5) [43].

$$r_4 = k_4 S_4 \tag{54}$$

Where r_4 is the hemicellulose to glucose reaction rate (kg/m^{3}h)

k_4 is the reaction rate constant (1/h)

S_4 is the concentration of hemicellulose (g/L)

$$r_5 = k_5 S_5 \tag{55}$$

Where r_5 is the xylose to furfural reaction rate (kg/m^{3}h)

k_5 is the reaction rate constant (1/h)

S_5 is the concentration of xylose (g/L)

All the previous equations were modeled in MATLAB in order to simulate the kinetic model for the hydrolysis of Arundo donax, solving the differential equations and obtaining a graph of the concentrations of the different components with respect to time, and comparing them to existing experimental data.

It was previously found that at temperatures above 50°C, the model predictions are greater than the actual yield because the hydrolysis enzymes become deactivated due to mixing rate (considered negligible in this model) and temperature [39]. To take into consideration the temperature effect on the rate constants, an Arrhenius relationship was used for each rate constant. The rate constants increase first with respect to temperature, to reach a certain maximum, which is then followed by a decrease because

of enzyme denaturation. The increasing part, which is also called temperature activation, is described by Equation 56 [43]:

$$k_i(T) = k_{i,max} e^{-\frac{E_i}{R}\left(\frac{1}{T} - \frac{1}{T_{S,max}}\right)} \tag{56}$$

Where k_i is the reaction rate constant (1/h)

$k_{i,max}$ is the maximal reaction rate constant (1/h)

E_i is the activation energy (kJ/mol)

R is the gas constant (kJ/mol K)

T is the temperature (K)

$T_{S,max}$ is the maximum temperature before enzyme denaturation (K)

On the other hand, the decreasing part, or thermal denaturation, follows Equation 57.

$$k_i(T) = k_{i,max} e^{-\frac{E_i}{R}\left(\frac{1}{T_{S,max}} - \frac{1}{T}\right)} \tag{57}$$

3.1.2. Data collection
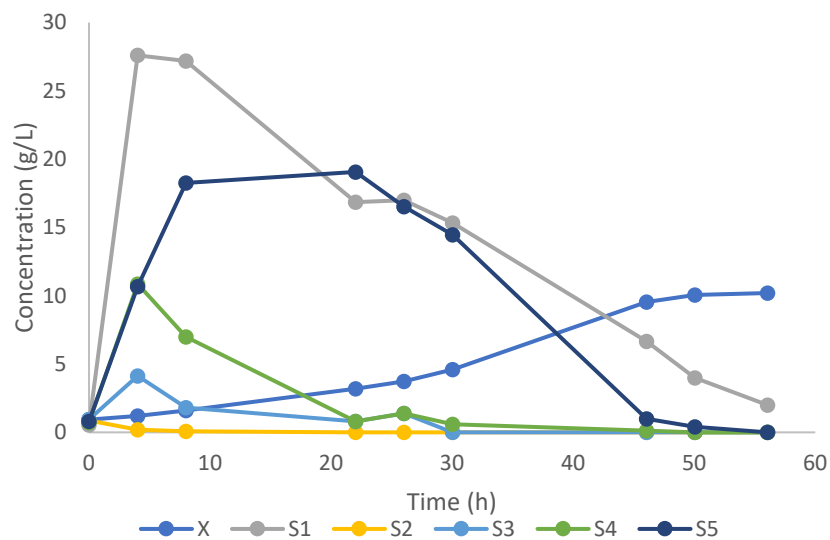
The hydrolysis data was obtained from [43].

69

Figure 23. Arundo donax hydrolysis data [43]

The curves represent, respectively, the concentrations of biomass (X), cellulose (S_1), cellobiose (S_2), glucose (S_3), hemicellulose (S_4) and xylose (S_5).

The previously plotted concentrations will be used in MATLAB for the hydrolysis model simulation.

3.1.3. Challenges

Enzymatic hydrolysis is affected by many factors, such as the enzyme concentration and activity, the substrate properties and loading, the sugar inhibition, and many more. The table below lists some challenges faced during cellulose hydrolysis and some proposed solutions.

Table 11. Challenges and potential solutions in cellulose hydrolysis [39]

Challenge	Solution	Drawback
Cellobiose accumulation and inhibition	Add β-glucosidase during hydrolysis	Higher cost due to additional supplementation
	Use yeast capable of making β-glucosidase for SSF	
Glucose inhibition	SSF	Ethanol inhibition
	Glucose tolerant enzymes	Temperature difference between hydrolysis and fermentation
Lignin adsorption	Add proteins or surfactants	Higher cost due to addition of protein or surfactant
Pretreatment degradation products	Detoxification	Higher cost due to additional process steps
	Less calcitrant feed and mild pretreatment conditions	Poor pretreatment sugar yield
Low solid loading	Feed continuously substrate or enzyme in fed-batch reactor	Glucose inhibition due to substrate addition
Enzyme cost	Recycle by readsorption	Readsorption not suitable for β-glucosidase
	Use engineered enzymes with high efficiency	
	Optimize process efficiency	

Experiments showed that cellulose hydrolysis follows a two-step mechanism: a high hydrolysis rate followed by a decreased hydrolysis rate. During the first step considered as the rate limiting step, large chains are broken down into smaller chains, soluble oligomers (<7 glucose molecules), which will later be reduced further into sugar monomers during the second hydrolysis step. The main factors affecting the rate of the second step can be grouped into three categories:

- biomass composition (% of cellulose, hemicellulose, lignin),

- structural properties, enzyme characteristics and interaction,

- substrate.

Physical factors also play a role, such as the crystallinity, polymerization, and surface area, which affect the enzyme access to cellulose, as well as enzyme adsorption, oligomers and glucose inhibition. Studies also prove that the hydrolysis rate can be affected by enzyme jamming and mass transfer challenges [12].

3.2. Fermentation

3.2.1. Kinetic model development

Taking all the models discussed in the previous chapter as a base for the new model development for dual-substrates systems, the biomass, product, and substrates equations become, respectively, Equations 58, 59, 60 and 61.

$$
\frac{dX}{dt} = \left[\frac{\mu_{max1}S_1}{K_{S_1X} + S_1 + \frac{S_1^2}{K_{S_1Xi}}} \left(1 - \frac{P}{P_{Xmax}}\right)^{\alpha} \right.
$$

$$
\left. + \frac{\mu_{max2}S_2}{K_{S_2X} + S_2 + \frac{S_2^2}{K_{S_2Xi}}} \left(1 - \frac{P}{P_{Xmax_2}}\right)^{\alpha_2} \left(1 - \frac{S_1}{S_{1max}}\right)^{\gamma} \right] X
$$

(58)

Where μ_{max1}, μ_{max2} are the maximum specific growth rate of the cell (g/g h)

S_1, S_2, P, X are the concentrations of glucose, xylose, ethanol, and biomass respectively (g/L)

K_{S_1X}, K_{S_2X} are Monod constants (g/L)

K_{S_1Xi}, K_{S_2Xi} are inhibition constants for growth (L)

P_{Xmax} is the maximum ethanol concentration for growth (g/L)

P_{Xmax_2} is the maximum ethanol concentration for growth with respect to xylose (g/L)

α is the ethanol inhibition constant (g/L)

α_2 is the ethanol inhibition constant with respect to xylose (g/L)

γ is the glucose inhibition constant (unitless)

$$\frac{dP}{dt} = \left[\frac{q_{max1}S_1}{K_{S_1P} + S_1 + \frac{S_1^2}{K_{S_1Pi}}} \left(1 - \frac{P}{P_{Pmax}}\right)^{\beta} \right.$$

$$\left. + \frac{q_{max2}S_2}{K_{S_2P} + S_2 + \frac{S_2^2}{K_{S_2Pi}}} \left(1 - \frac{P}{P_{Pmax_2}}\right)^{\beta_2} \left(1 - \frac{S_1}{S_{1max}}\right)^{\gamma} \right] X \tag{59}$$

Where q_{max1}, q_{max2} are the specific ethanol production rate (g/g h)

K_{S_1P}, K_{S_2P} are ethanol saturation constants (g/L)

K_{S_1Pi}, K_{S_2Pi} are substrate inhibition constants for ethanol formation (L)

P_{Pmax} is the maximum ethanol concentration for ethanol fermentation (g/L)

P_{Pmax_2} is the maximum ethanol concentration for ethanol fermentation with respect to xylose (g/L)

β is the ethanol inhibition constant (g/L)

β_2 is the ethanol inhibition constant with respect to xylose (g/L)

$$\frac{dS_1}{dt} = \left[-\frac{1}{Y_{X/S_1}} \frac{\mu_{max1}S_1}{K_{S_1x} + S_1 + \frac{S_1^2}{K_{S_1Xi}}} \left(1 - \frac{P}{P_{Xmax}}\right)^{\alpha} \right.$$

$$\left. - \frac{1}{Y_{P/S_1}} \frac{q_{max1}S_1}{K_{S_1p} + S_1 + \frac{S_1^2}{K_{S_1Pi}}} \left(1 - \frac{P}{P_{Pmax}}\right)^{\beta} \right] X + mX \tag{60}$$

$$\frac{dS_2}{dt} = \left[-\frac{1}{Y_{X/S_2}} \frac{\mu_{max2}S_2}{K_{S_2x} + S_2 + \frac{S_2^2}{K_{S_2Xi}}} \left(1 - \frac{P}{P_{Xmax_2}}\right)^{\alpha_2} \right.$$

$$\left. -\frac{1}{Y_{P/S_2}} \frac{q_{max2}S_2}{K_{S_2p} + S_2 + \frac{S_2^2}{K_{S_2Pi}}} \left(1 - \frac{P}{P_{Pmax_2}}\right)^{\beta_2} \right] \left(1 - \frac{S_1}{S_{1max}}\right)^{\gamma} X \qquad (61)$$

$$+ mX$$

Where $Y_{X/S_1}, Y_{X/S_2}$ are biomass yields (g/g)

$Y_{P/S_1}, Y_{P/S_2}$ are ethanol yields (g/g)

m is the cell maintenance coefficient (1/h)

S_{1max} is the critical inhibitor concentration (g/L)

A glucose substrate inhibition term $\left(1 - \frac{S_1}{S_{1max}}\right)^{\gamma}$ was added to Equations 58, 59 and 61 to take into account the glucose inhibition on xylose. The results obtained will be discussed in the next chapter to prove the accuracy of the model.

3.2.2. Experimental data

It is essential to include xylose in the fermentation step for the production of ethanol because of the higher yields obtained. Figure 24 shows the concentration profiles of glucose, xylose, ethanol and cells during oil palm hydrolysate fermentation by STXQ recombinant strain [73].
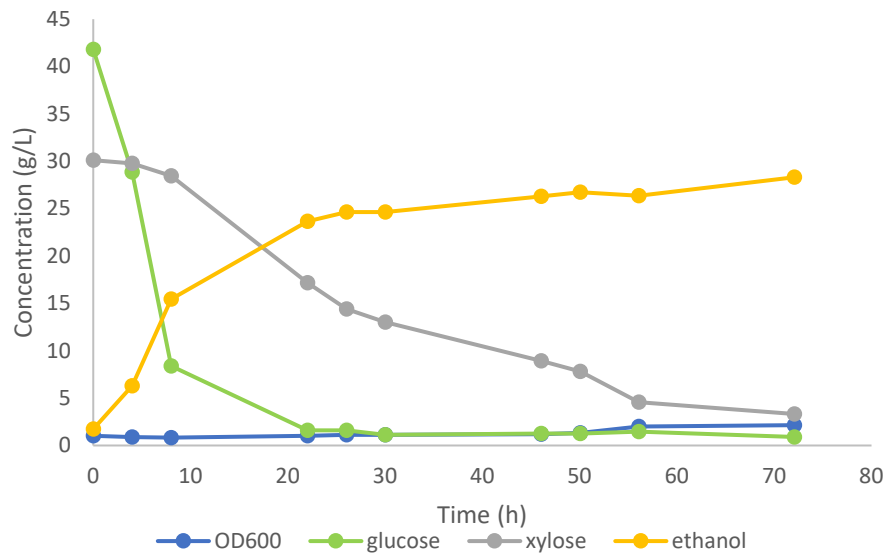
Figure 24. Fermentation experimental data [73]

Figure 25 represents the concentration profiles of glucose, ethanol and cells during fermentation of Arundo donax hydrolysate. Xylose was not considered for fermentation in this case [41].
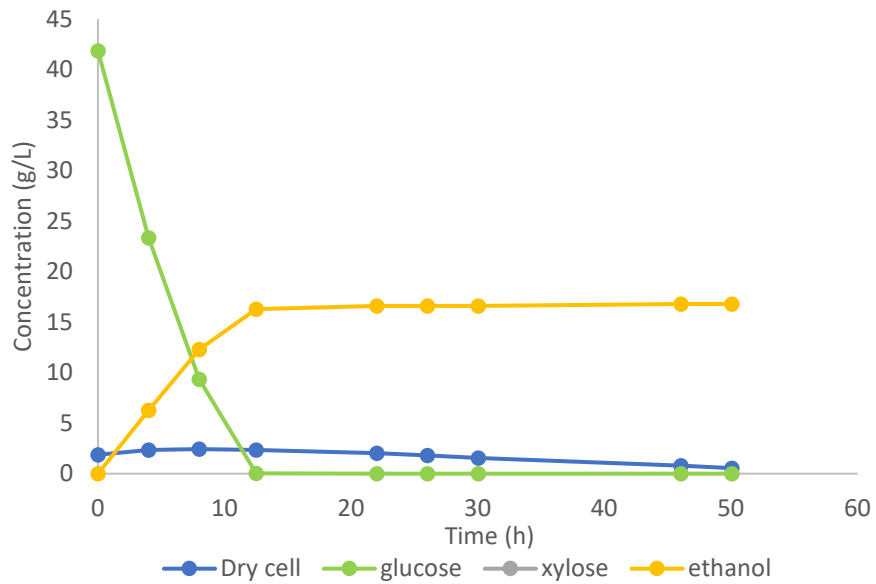
Figure 25. Arundo donax fermentation data [41]

When comparing the previous figures, it can be clearly seen how ignoring the xylose fermentation into ethanol can impact the ethanol yields. In the second figure, the curves of ethanol, glucose and dry cell weight remain constant after a time of 10 hours.

In the first figure, glucose is consumed at a faster rate than xylose, which leads to a high yield of ethanol production when xylose starts being consumed and much more accurate results.

Since no complete experimental data on Arundo donax containing all the compounds participating in the fermentation was found in the literature, fermentation graphs of oil palm (Figure 24) and Arundo donax (Figure 25) were superimposed (Figure 26), and many similarities have been found. The results are shown below.

Figure 26. Superimposed fermentation data

It can be seen that the glucose concentrations of both experiments are very similar, they start to vary when the time becomes 10 hours, where the glucose concentration curve of Figure25 experiment becomes constant and 0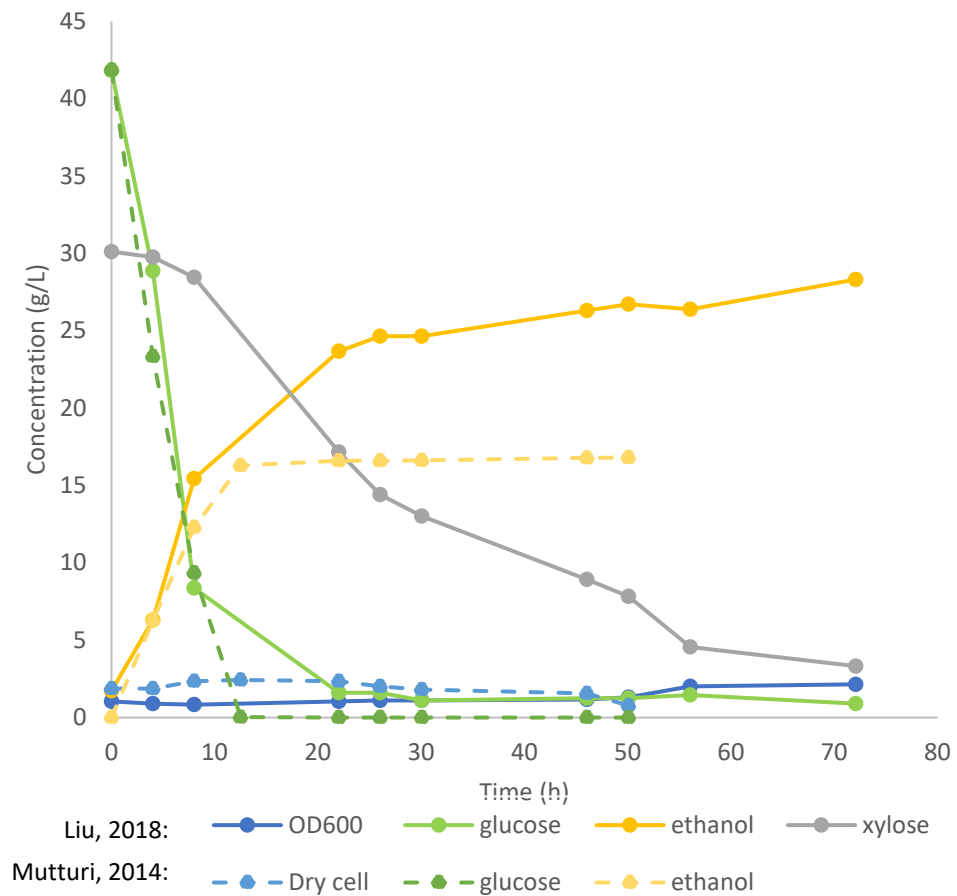, whereas Liu's glucose concentration curve decreases slowly until a time of 22 hours before becoming constant with a concentration value of 1.5 g/L.

For the ethanol concentration, both experiments are also very similar. The curve in both experiments increases at a similar rate, however, in Figure25, the ethanol concentration curve becomes constant (16 g/L) at a time of 12 hours, whereas in Figure 24, the ethanol curve increases more and reaches around 29 g/L. The reason of this increase is because the experiment shown in Figure 24 takes into account the concentration of xylose, which is an additional source of sugar that turns into ethanol when fermented.

Because of the similarities of fermentation data between the two feedstocks, and due to the lack of xylose fermentation data for Arundo donax, the fermentation experimental data used will be from Figure24.

3.2.3. Challenges

Before the fermentation process, biomass pretreatment using severe physicochemical properties and enzymatic hydrolysis should be done in order for the monosaccharides to be free. These treatments also release compounds that hinder yeast growth like organic acids (acetic acid from hemicellulose deacetylation), furaldehydes (furfural from pentose dehydration and 5-hydroxymethyl-furfural from hexose dehydration), and phenolics (from lignin degradation) [74]. The concentrations of these chemicals depend on the type of biomass that is used, as well as the type of

pretreatment and hydrolysis performed. When present in low concentrations, they can affect yeast growth, extending the lag phase, disrupting cell membranes and acidifying cytoplasms which results in low ethanol yields.

Choosing a resistant yeast strain is not enough to avoid yeast metabolism inhibition. The type of sugar also plays an important role. Yeast consumes xylose at a considerably slower pace than other sugars, which might lead to a reduction of essential metabolites that can be significant in the harsh circumstances caused by lignocellulosic hydrolysates. This is why designing strains with detoxifying properties and improved tolerance, transcriptive factors, mutagenesis and cultures have all been developed to enhance xylose fermentation while decreasing the impact of lignocellulosic hydrolysate inhibitors on yeast strains. Despite the effectiveness of these techniques, few advances in lignocellulosic hydrolysate inhibitors have been made in commercial strains. As a result, additional research is needed to understand xylose's tolerance on inhibitors, which is especially crucial for developing novel and strong engineered strains [74].

Saccharomyces cerevisiae and Zymomonas mobilis are the usual microorganisms used for the production of ethanol because of their strong ethanol resistance and yield. However, neither can ferment xylose. Pichia stipitis and Kluyveromyces marxianus, on the other hand, can ferment both xylose and glucose, but with reduced ethanol yields. They are also affected by the presence of small amounts of inhibitors in hydrolysates, such as acetate. In addition, they cannot develop in the absence of oxygen. Because of the absence of an ideal microorganism that is able to convert both xylose and glucose to ethanol, co-culturing and culturing in sequence have been investigated, as well as the development of genetically modified organisms [75].

However, the lack of strain kinetic data in a co-culture system can also cause complications in developing an accurate fermentation kinetic model. performance of each strain in co-culture systems differs from that seen in single culture systems because of possible strain interactions, and thus they will have different kinetic parameters. A strong kinetic model is an effective guide that can aid in obtaining optimal operating conditions with satisfactory results, and simplify assessments by removing extreme scenarios, by modeling the dynamic features of systems. This is why developing a co-culture system kinetic model for ethanol production might be beneficial [76].

New studies are trying to create engineered strains of yeast that are able to ferment both C5 and C6 sugars at the same time, thus achieving higher yields of sugars. Liu et al. experimented with many strains of yeast. It was found that the strain STXQ was able to ferment most sugars and yielded the highest ethanol yield [73]. Another study (NEMO) used engineered enzymes for the hydrolysis and SHF of Arundo donax biomass and obtained promising results [42].

3.3. SHF simulation

A simulation combining the saccharification reactions that produce sugars from lignocellulose with the sugar fermentation equations that produce ethanol was performed. A MATLAB file will call the hydrolysis codes to obtain the sugars, then it will call the fermentation file with the initial sugar concentrations given from the previous call. This simulation will model a semibatch hydrolysis followed by a batch fermentation. The parts of the hydrolysis equations that account for the conversion of glucose and xylose to produce ethanol were removed since the model simulates SHF

and not SSF, and the biomass equation was also removed from the hydrolysis model since it is already present in the fermentation model. The hydrolysis equations for glucose and xylose become Equations 62 and 63.

$$\frac{dS_3}{dt} = 1.111r_2 + 1.053r_3 - \frac{F}{V}S_3 \tag{62}$$

$$\frac{dS_5}{dt} = 1.136r_4 - r_5 - \frac{F}{V}S_5 \tag{63}$$

The equations will be called by the fermentation code in order to determine the ethanol yield from the process.

3.4. MATLAB and parameter estimation

MATLAB was used in order to solve the systems of differential equations of the hydrolysis and fermentation models and obtain the concentrations of biomass, ethanol, glucose and xylose with respect to time, while comparing the results to existing experimental data to determine the model's accuracy. Parameter estimation was performed to produce the best values for each parameter used in the differential equations, resulting in the best fit. The residual sum of squares between the model simulated data and the experimental data is minimized during parameter estimation.

The optimization toolbox feature in MATLAB makes it possible to find parameters which maximize or minimize objective functions under any constraints. It can be used to solve linear, mixed integer linear, quadratic, second order cone, and non linear programming problems, as well as constrained linear least squares, non linear least squares, and non linear equations [77].

In some cases, problem-based techniques are used. In this case, the problem is being solved with a solver-based technique.

The MATLAB optimization function lsqcurvefit - which solves nonlinear curve fitting problems using least squares - is used to estimate the kinetic parameters. It is a special case of lsqnonlin which is used to solve nonlinear data fitting problems using least-squares. The stiff solver's performance depends on the given problem's structure and options. In this case, the differential equations were solved using ode23s, to minimize the time of execution.

3.5. Mass balance

The overall reaction that describes glucose fermentation into ethanol is shown in Equation (64). It is based on the fermentation of glucose and ammonia by yeast to produce ethanol, glycerol, carbon dioxide and water [78].

$$C_6H_{12}O_6 + 0.0138\ NH_3$$
$$\rightarrow 0.069\ CH_{1.74}N_{0.2}O_{0.45} + 1.751\ C_2H_5OH + 0.21\ C_3H_8O_3 \quad (64)$$
$$+ 1.785\ CO_2 + 0.0168\ H_2O$$
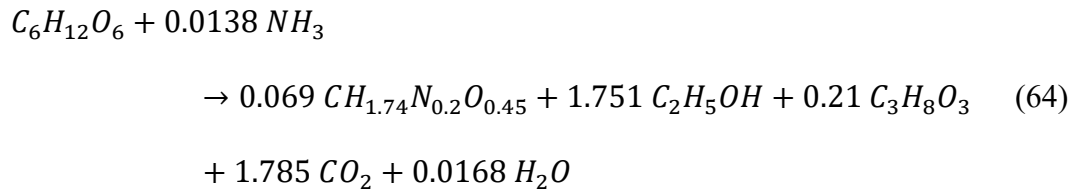
The ethanol yield from glucose was used to determine the stoichiometric coefficients.and to estimate CO_2, H_2O and glycerol. The amount of ethanol produced from xylose was used to estimate CO_2 from xylose, according to the following equation.

$$3\ C_5H_{10}O_5 \rightarrow 5\ C_2H_5OH + 5\ CO_2 \quad (65)$$
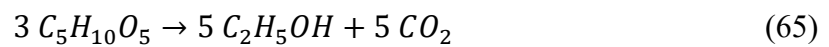
The mass balance summarized in Table 12 was generated using data from the fermentation simulation with the results illustrated in Figure 37.

Table 12. Mass balance

Concentrations (kg/m^3)	Fermentation (batch)	
	in	out
cellulose	-	-
cellobiose	-	-
glucose	41.81	1.02
hemicellulose	-	-
xylose	30.11	5.20
biomass	1.04	1.45
ethanol	1.73	27.08
carbon dioxide	-	35.6
water	-	0.1
glycerol	-	4.4
ammonia	0.10	0.0
Total	74.8	74.9
Error	-0.1	

A mass balance error of (0.1) was obtained and this could be due to the chemical formula adopted for the cells (yeast), and the fact that a simple xylose to ethanol reaction was used (Eq. 65) without accounting for the formation of other by-products.

CHAPTER 4

RESULTS AND DISCUSSION

4.1. Model development

4.1.1. Hydrolysis kinetic model

A MATLAB code was developed in order to simulate the hydrolysis of Arundo donax. Parameter estimation was employed to determine the parameter values based on the optimal feed rate and hydrolysis temperature profiles obtained in [43].

4.1.1.1. Parameter estimation

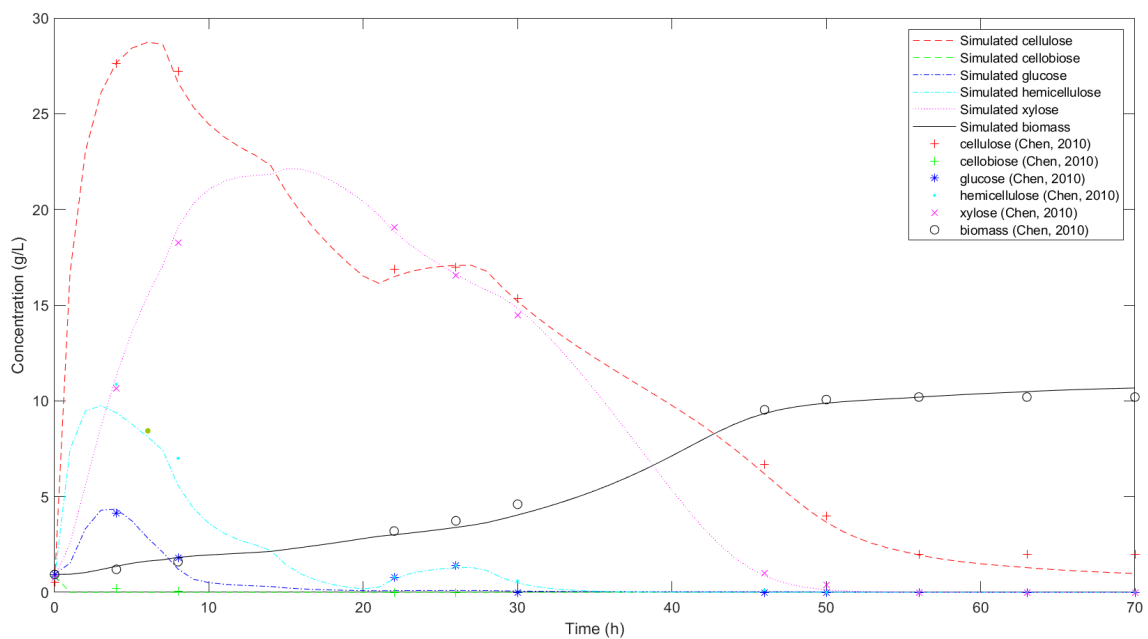The results obtained can be seen in the figure below.

Figure 27. Hydrolysis simulation

The previously mentioned work optimized and determined the optimal inlet rate, temperature, feed concentration, and fermentation time that correspond to the highest

amount of ethanol produced. The optimal feed concentration was found to be 178.52 g/L and the fermentation time t* around 70 h. The feed rate and the temperature were varied as seen in Figure 28 and Figure 29, respectively. The normalized time is equal to the time divided by t*. The optimal temperature started at 30°C then was increased to 48°C in the last couple of stages due to the concentration of cellulose remaining higher than 1 g/L (constraint) in order to quicken cellulose hydrolysis to glucose [43].
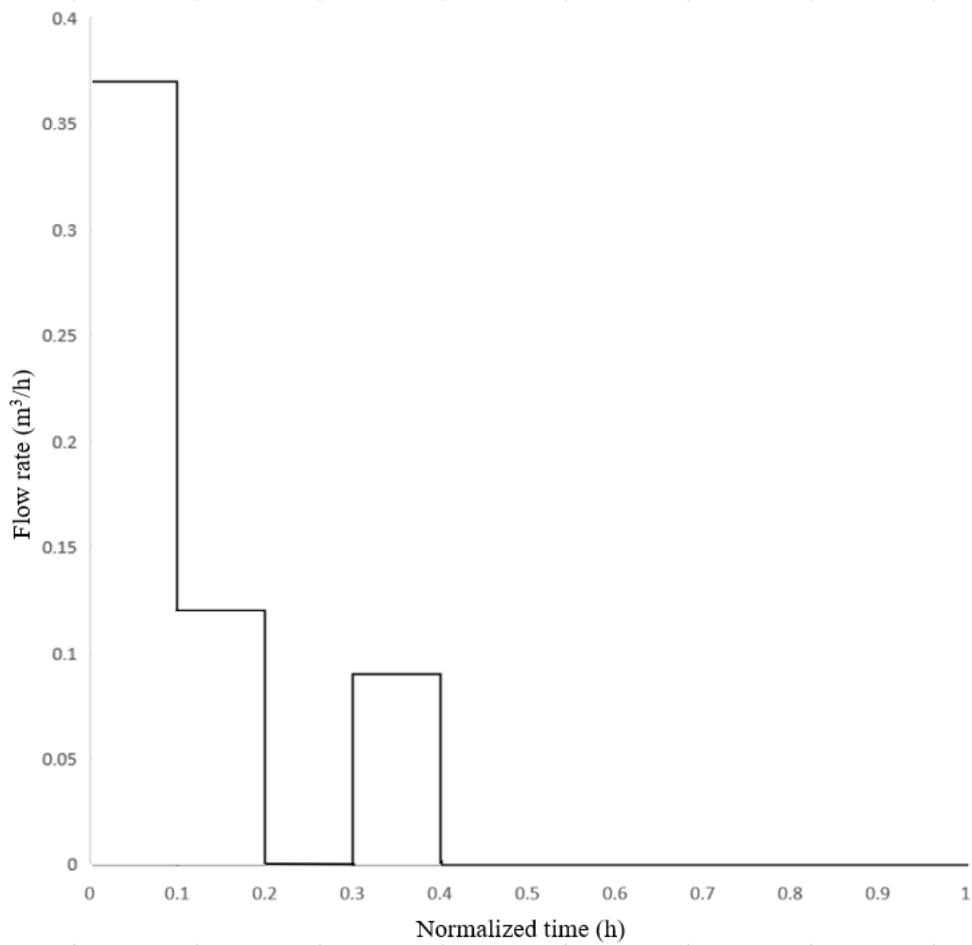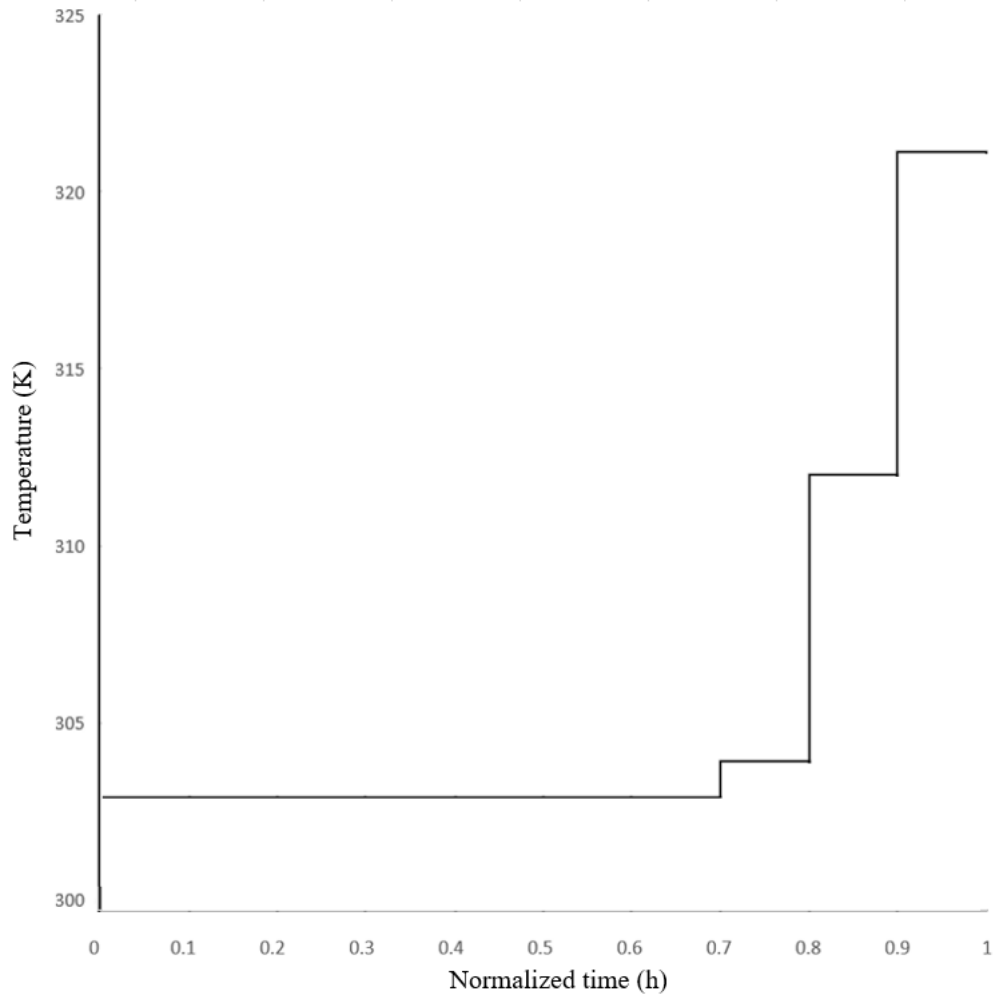

Figure 28. Feed rate vs. time

Figure 29. Temperature vs. time

The small increase in the concentration profiles of cellulose and hemicellulose at a time of 20 hours as seen in Figure 27 can be explained by the feed rate fluctuation that happens at the same time as seen in Figure 28. The flow rate slightly increases, which led to a slight increase in the concentrations of cellulose and hemicellulose.

The simulation obtained and the concentration profiles from [43] are very similar. Resnorm is the sum of squared errors and is already calculated in the simulation (resnorm=11.6323). It can be seen that the cellulose, glucose, hemicellulose, and xylose concentration profiles increase then decline. On the other hand, the biomass curve

increases slowly. Fermentation of the released sugars will cause the production of ethanol.

Parameter estimation was performed on all the parameters. The table below lists the values of the parameters estimated in this study, as well as the values found in the literature.

Table 13. Hydrolysis parameter values

Variables	Units	Kadam, 2004	Zheng, 2008	Chen, 2010	Mutturi, 2014	This study, 2022
K_{1ad}	m^3/kg protein	0.4	0.51	0.4	-	0.3307
K_{2ad}	m^3/kg protein	0.1	0.75	0.1	-	0.0844
$E_{1,max}$	kg protein/kg cellulose	0.06	0.08607	0.06	-	0.0231
$E_{2,max}$	kg protein/kg cellulose	0.01	0.1735	0.01	-	0.0100
E_{1F}	kg/m^3	-	-	54	-	55.0963
E_{2F}	kg/m^3	-	-	65	-	67.3984
α	-	1	1.007	1	-	0.0800
k_1	kg/g.h	22.3	16.5	14	20.54	24.6399
k_2	kg/g.h	7.18	7.1	5	299.04	6.6338
k_3	1/h	285.5	267.6	190		307.9984
k_4	1/h	-	-	0.34	-	0.5801
k_5	1/h	-	-	0.005	-	0.0077
K_{1iG2}	kg/m^3	0.015	0.04	0.015	1.04	0.0741
K_{2iG2}	kg/m^3	132	132.5	132	-	130.1909
K_{1iG}	kg/m^3	0.1	0.1	0.1	0.12	0.0949
K_{2iG}	kg/m^3	0.04	0.01	0.04	-	0.3760
K_{3iG}	kg/m^3	3.9	2.1	3.9	2.49	3.8922
K_{1iX}	kg/m^3	0.1	-	0.1	1.03	0.1000
K_{2iX}	kg/m^3	0.2	-	0.2	-	0.1645
K_{3iX}	kg/m^3	201	-	201	220.7	186.3843
K_{3M}	kg/m^3	24.3	25.5	24.3	13.03	25.6648
u_{mG}	1/h	-	-	0.662		0.9614
K_G	kg/m^3	-	-	0.565		0.5229
K_{iG}	kg/m^3	-	-	283.7	-	267.1443
p_G	kg/m^3	-	-	1	-	1.0000
p_{mG}	kg/m^3	-	-	95.4	-	100.1994
ϕ_G	-	-	-	1.29	-	1.1347
u_{mX}	1/h	-	-	0.19	-	0.1198
K_X	kg/m^3	-	-	3.4	-	3.4000
K_{iX}	kg/m^3	-	-	18.1	-	14.2085
p_X	kg/m^3	-	-	1	-	1.6252
p_{mX}	kg/m^3	-	-	59.04	-	60.9116
ϕ_X	-	-	-	1.036	-	1.2321
v_{mG}	1/h	-	-	2.005	-	2.2281
K_G'	kg/m^3	-	-	1.342	-	1.5476
K_{iG}'	kg/m^3	-	-	4890	-	4788.7187
p_{mG}'	kg/m^3	-	-	103	-	98.5379
ϕ_G'	-	-	-	1.42	-	2.6097
v_{mX}	1/h	-	-	0.25	-	0.2317
K_X'	kg/m^3	-	-	3.4	-	6.2008
K_{iX}'	kg/m^3	-	-	81.3	-	81.3000
p_{mX}'	kg/m^3	-	-	60.2	-	55.2332
ϕ_X'	-	-	-	0.608	-	0.2511
$Y_{P/S3}$	-	-	-	0.47	-	0.4499
$Y_{P/S5}$	-	-	-	0.4	-	0.4341
λ_1	-	-	-	0.356	-	0.3741
λ_2	-	-	-	0.189	-	0.1808

4.1.1.2. Sensitivity analysis

Because of the wide range of some parameters found in the literature, a sensitivity analysis was performed in order to see how the results would change if another value was used for a certain parameter. Parameter values found in the literature listed in Table 12 were tested on the developed model, if there is a noticeable range between the value obtained from parameter estimation and the value from literature.

K_{2ad}=0.7 instead of 0.084355 yields results close to the original case (resnorm = 13.5218). This parameter does not have a high influence on the differential equations.
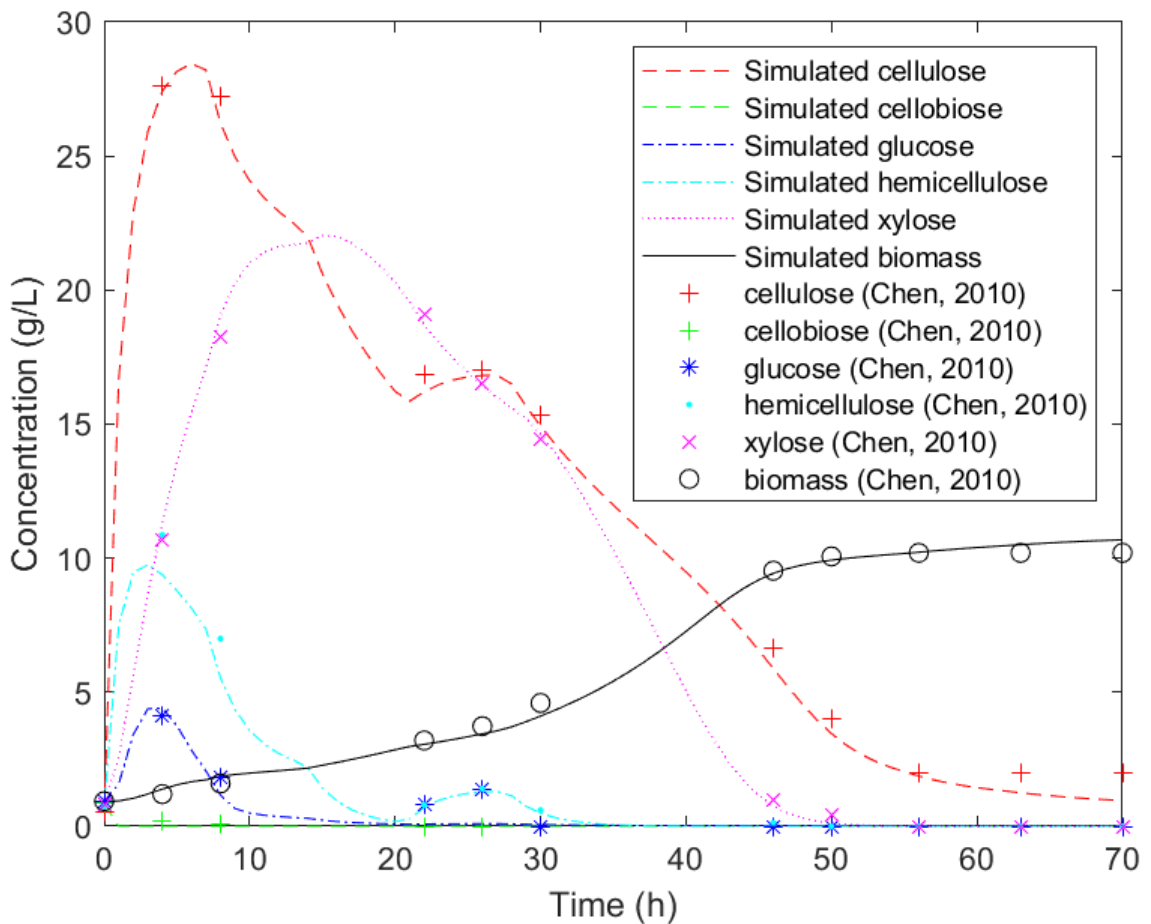

Figure 30. Sensitivity analysis of K_{2ad}

$E_{1,max}$=0.08 instead of 0.023083 causes the cellulose curve to shift downwards when compared to the original case, and glucose shifts higher. The xylose curve

decreases a little faster, the biomass curve reaches higher concentrations towards the end, whereas cellobiose and hemicellulose curves remain unchanged (resnorm = 292.2854).
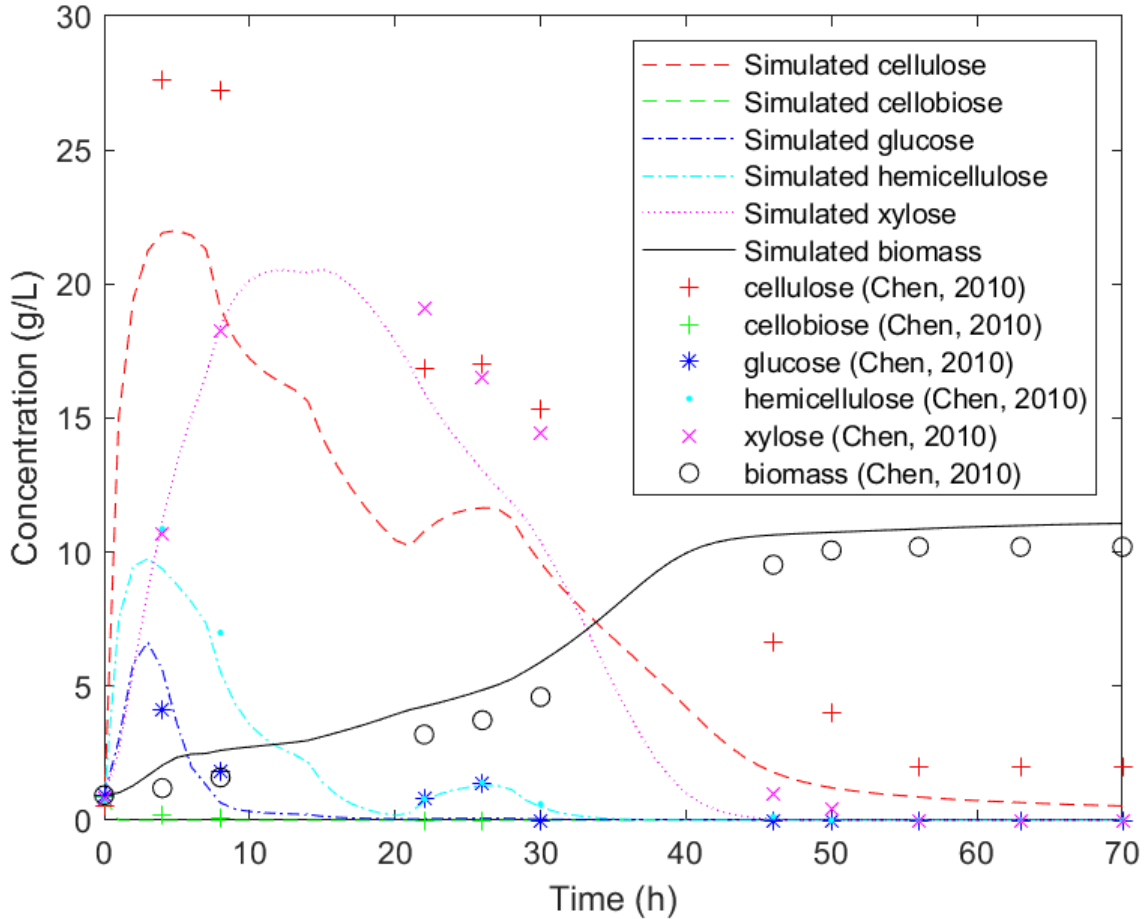

Figure 31. Sensitivity analysis of $E_{1,max}$

$E_{2,max}$=0.2 instead of 0.01 makes the cellulose curve shift even more downwards than the previous example, and the glucose shifts even more upwards. The xylose curve decreases a little faster, similarly to previously, and the biomass curve increases towards the end. Cellobiose and hemicellulose stay the same (resnorm = 708.1740).
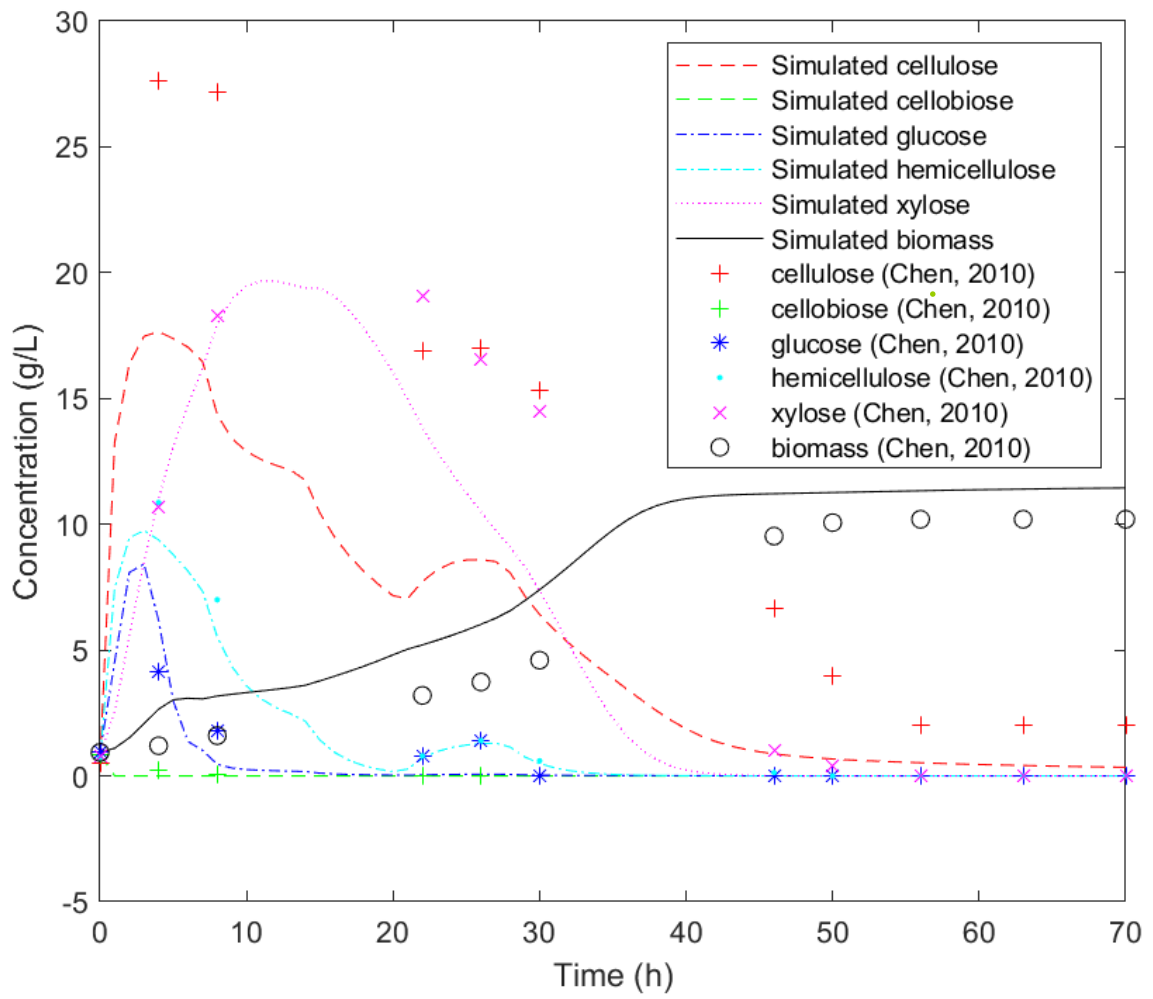
Figure 32. Sensitivity analysis of $E_{2,max}$

$\alpha=1$ instead of 0.07997 has effects similar to the previous example (resnorm = 1.0970e+03).
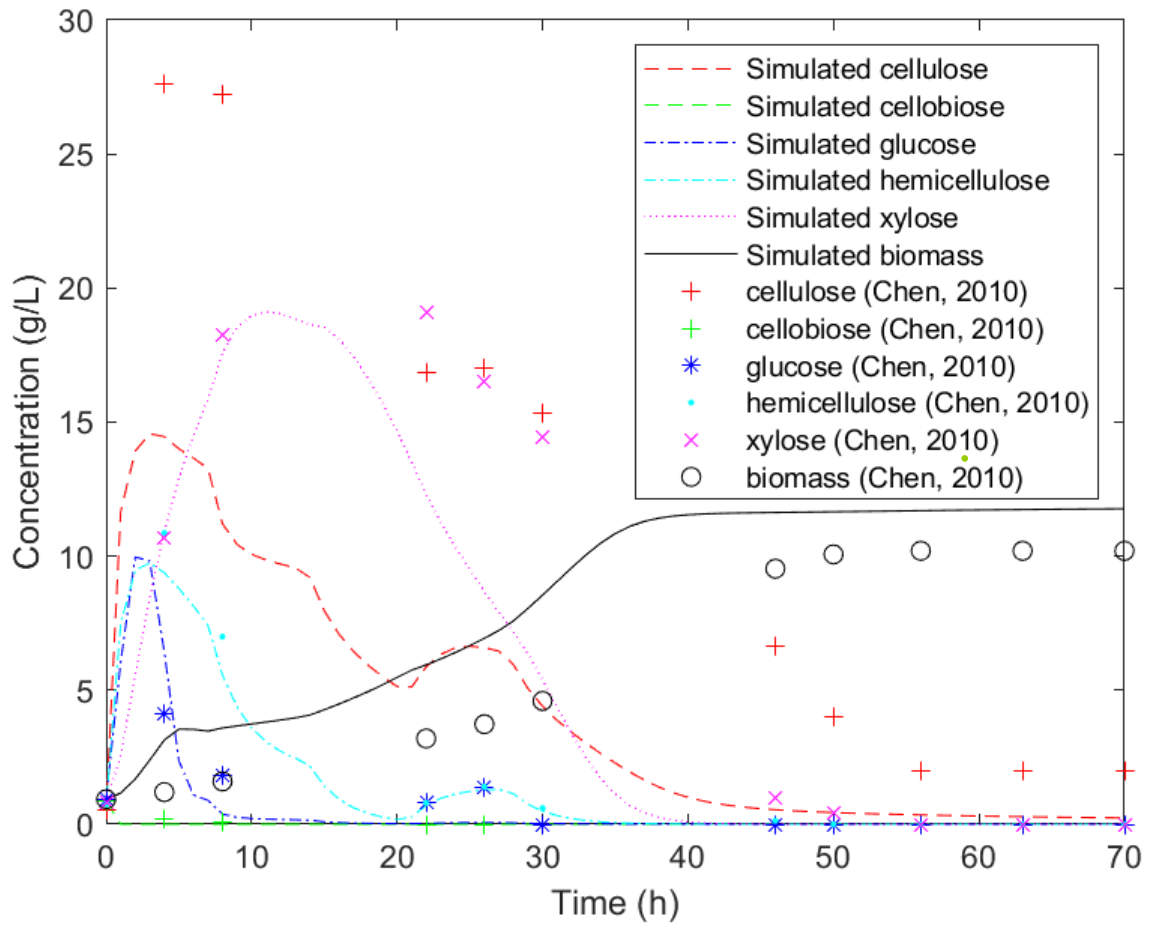
Figure 33. Sensitivity analysis of α

Setting K_{1iG2}= 0.01 then 1 instead of 0.07406 yield the same results as the original case (resnorm = 11.6324 vs. 11.6323 initially).
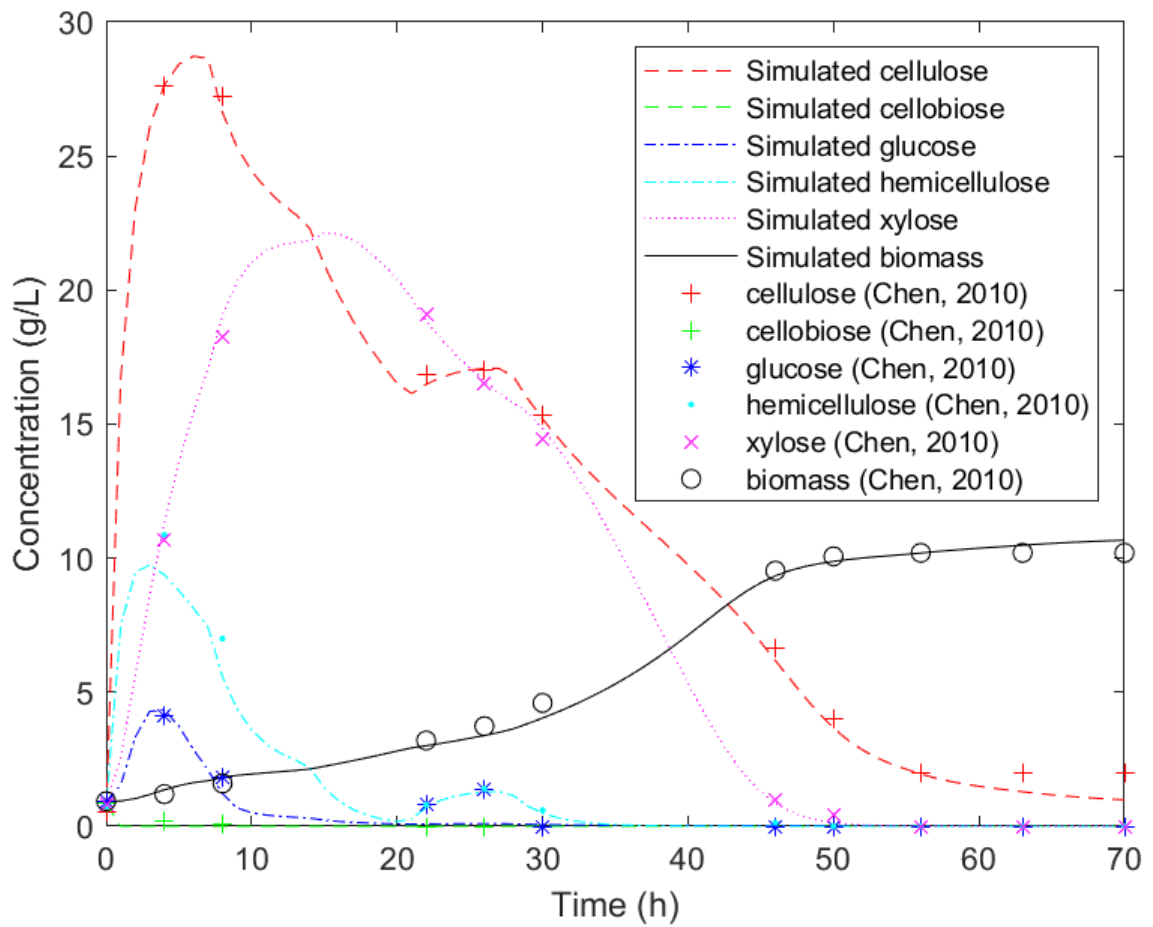
Figure 34. Sensitivity analysis of K_{1iG2} and K_{2iG2}

K_{1iX}=1 instead of 0.1 does not seem to heavily affect the results (resnorm = 14.1607).
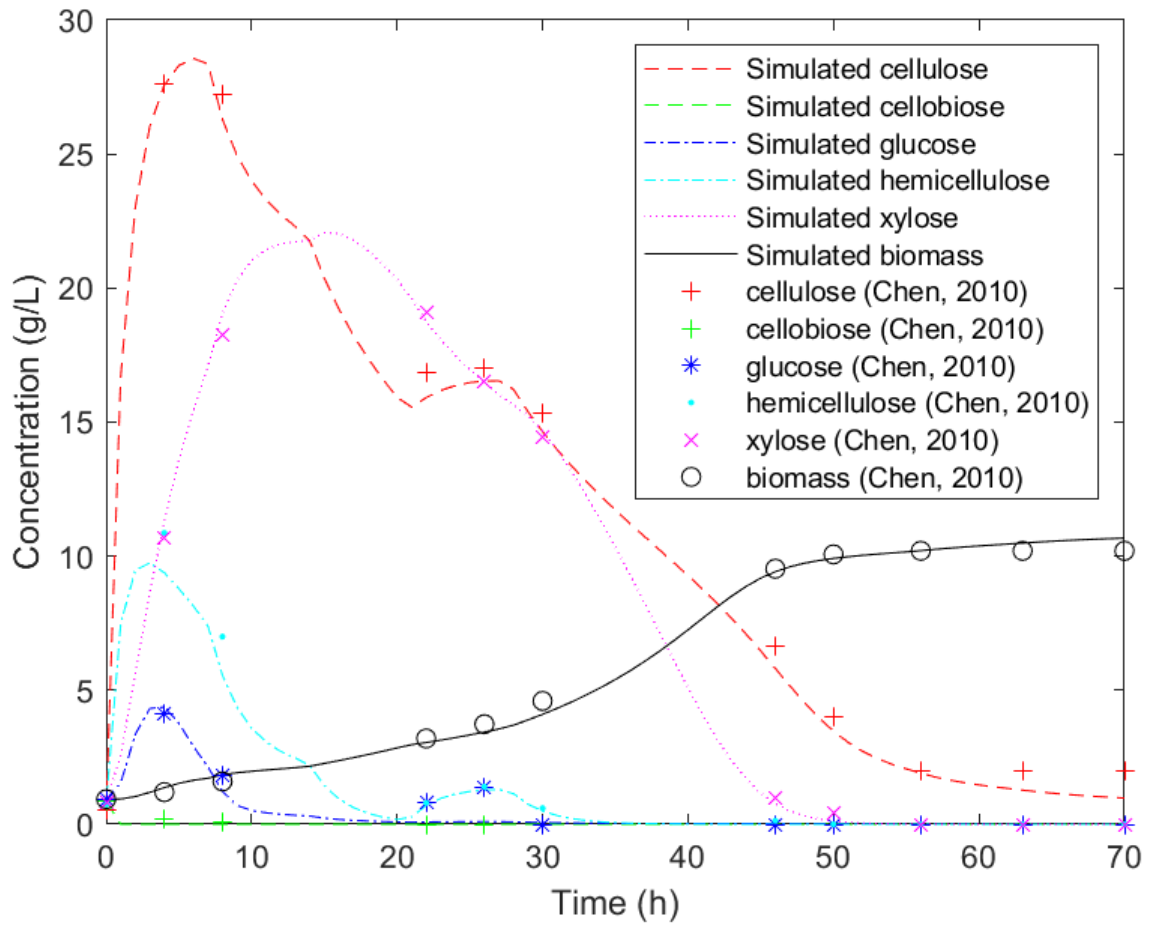
Figure 35. Sensitivity analysis of K_{1iX}

$K_{2iX}=0.2$ instead 0.164458 only affects cellulose and glucose concentration profiles. The cellulose curve slightly shifts down, whereas the glucose curve slightly shifts up (resnorm = 25.8565).
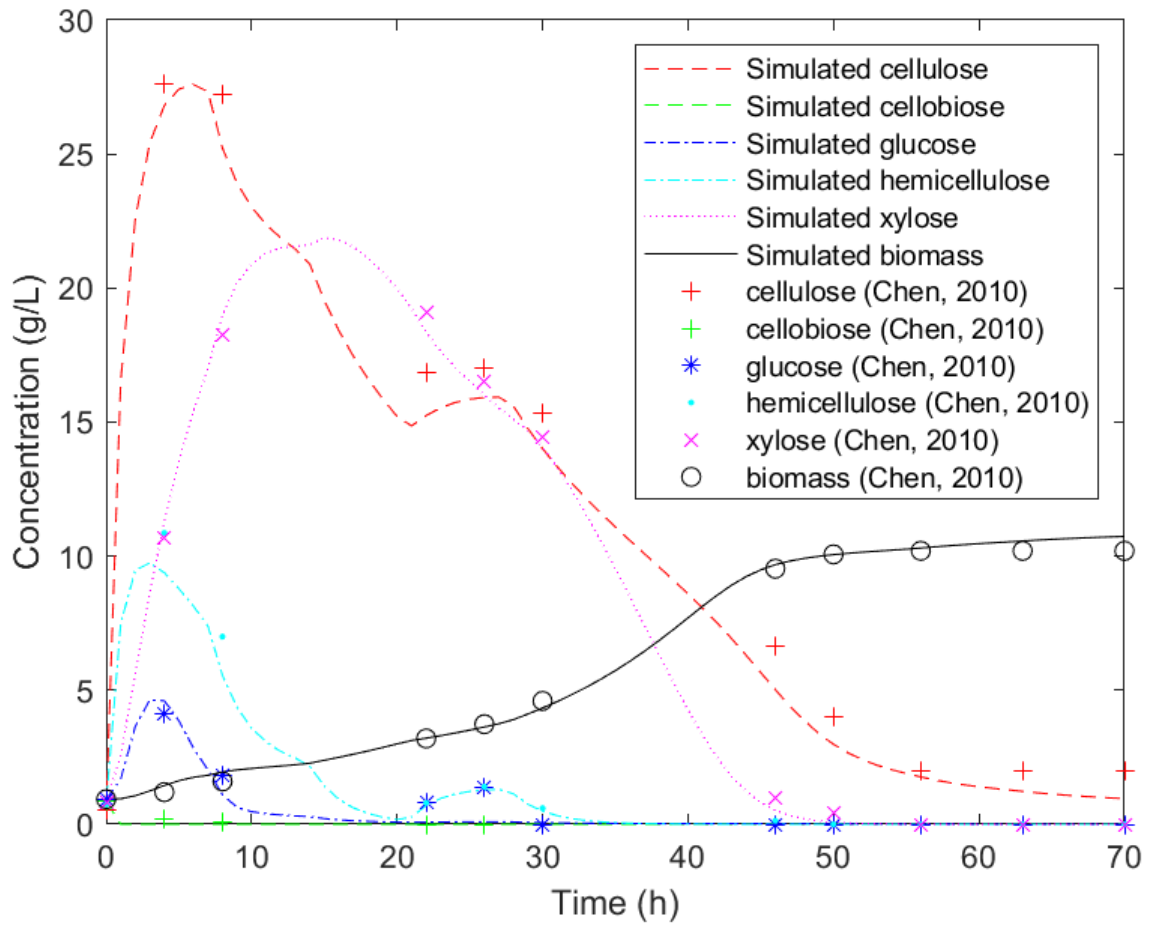
Figure 36. Sensitivity analysis of K_{2iX}

It can be deduced from the sensitivity analysis of variables that have a large range in the literature that K_{2iX} only influences cellulose and glucose, whereas $E_{1,max}$ affects xylose as well. In addition, modifying $E_{2,max}$ and α has the same effect as previously, but the changes are more visible.

4.1.2. Fermentation kinetic model

A MATLAB code was also built for the fermentation of Arundo biomass, where the equations developed in the previous chapter were inserted, and similarly to the hydrolysis model, parameter estimation was performed.

<u>4.1.2.1. Parameter estimation</u>

The results obtained from the simulation can be seen in the following figure.
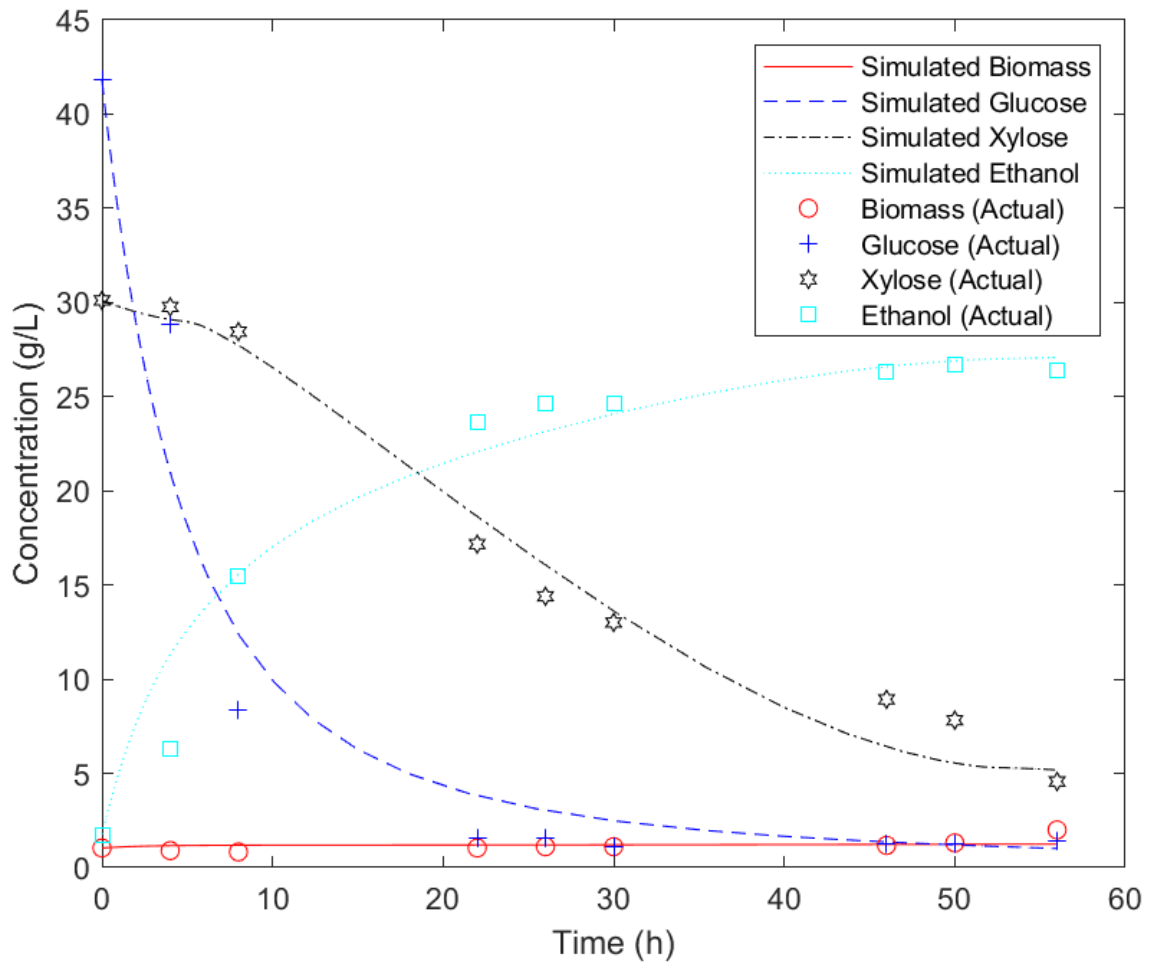
Figure 37. Fermentation simulation

The small difference between the simulated and experimental data given in the figure above proves the accuracy of the model. As expected, glucose and xylose concentrations decrease, in order to produce ethanol. The concentration of ethanol obtained is around 27 g/L, which is close to what is found in the literature. This model takes into account substrate and product inhibition and was developed for dual substrates.

The table below lists the parameters values obtained from the parameter estimation, compared with parameters used in literature.

Table 14. Fermentation parameter values

Variables	Units	Haldane, 1965	Andrews, 1968	Luong, 1987	Aiba, 1968	Krishnan, 1999	Mutturi, 2014		Ariya, 2016	Petelkov, 2016		Putra, 2018	This study, 2022
							fiber-free	SSF		Free cells	Immobilized cells		
μmax1	1/h	0.42	0.78	0.27	0.32	0.662	0.101	0.423	0.313	0.15	0.204	0.29	0.1483
KS1X	g/L	2.17	2.93	1.37	1.88	0.565	49.332	6.241	47.51	79	30.006	1.38	30
KS1Xi	g/L	5.42	2.93	-	19.47	283.7	-	-	308.13	28	1.53	29.91	100
PX,max	g/L	-	-	-	-	95.4-129.9	-	-	83.35	33.1	197.25	-	20
α	-	-	-	-	-	0.25-1.29	-	-	1.53	-	-	-	2
μmax2	1/h	-	-	-	-	0.19	-	-	-	-	-	-	0.0028
KS2X	g/L	-	-	-	-	3.4	-	-	-	-	-	-	2.5315
KS2Xi	g/L	-	-	-	-	18.1	-	-	-	-	-	-	18
PX,max2	g/L	-	-	-	-	59.04	-	-	-	-	-	-	60
α2	-	-	-	-	-	1.036	-	-	-	-	-	-	2
S1max	g/L	-	-	62.45	-	-	-	-	30	-	-	-	18
γ	-	-	-	2.2	-	-	-	-	0.5	-	-	-	0.4
qmax1	g/g.h	-	-	-	-	2.005	0.793	1.052	3.69	3.16	2.674	-	10
KS1P	g/L	-	-	-	-	1.342	0.052	0.032	28.39	19	53.698	-	60
KS1Pi	g/L	-	-	-	-	4890	-	-	299.67	99.6	131.21	-	300
PP,max	g/L	-	-	-	-	103-136.4	-	-	107.79	33.2	59.34	-	35
β	-	-	-	-	-	1.42	-	-	1.53	-	-	-	1.9
qmax2	g/g.h	-	-	-	-	0.25	-	-	-	-	-	-	0.6
KS2P	g/L	-	-	-	-	3.4	-	-	-	-	-	-	3.487
KS2Pi	g/L	-	-	-	-	81.3	-	-	-	-	-	-	30
PP,max2	g/L	-	-	-	-	60.2	-	-	-	-	-	-	27
β2	-	-	-	-	-	0.608	-	-	-	-	-	-	0.4
m	1/h	-	-	-	-	0.097	-	-	0.001	-	-	-	0.001
YX/S1	g/g	-	-	-	-	0.115	-	-	0.48	0.576	0.0056	-	0.2
YP/S1	g/g	-	-	-	-	0.47	-	-	0.5	0.53	0.0846	-	0.46
YX/S2	g/g	-	-	-	-	0.162	-	-	-	-	-	-	0.2
YP/S2	g/g	-	-	-	-	0.4	-	-	-	-	-	-	0.28

4.1.2.2. Sensitivity analysis

Sensitivity analysis was made on several parameters with a broad range in the literature, as seen in the previous table. The results are listed and discussed below.

Increasing μ_{max1} from 0.1483 to 0.8 yields the following graph. The xylose curve decreases more abruptly, as well as glucose. The biomass curve reaches higher concentrations when compared to the original case.
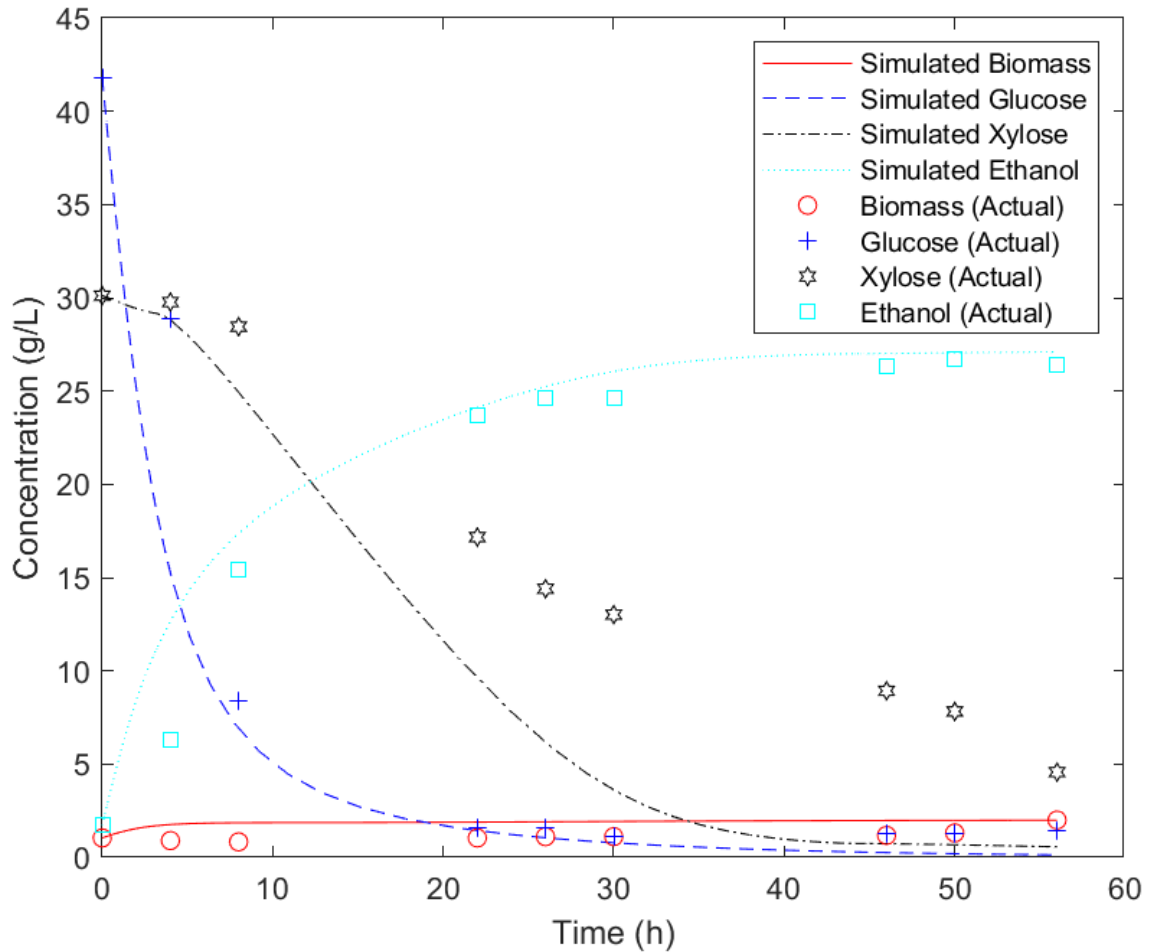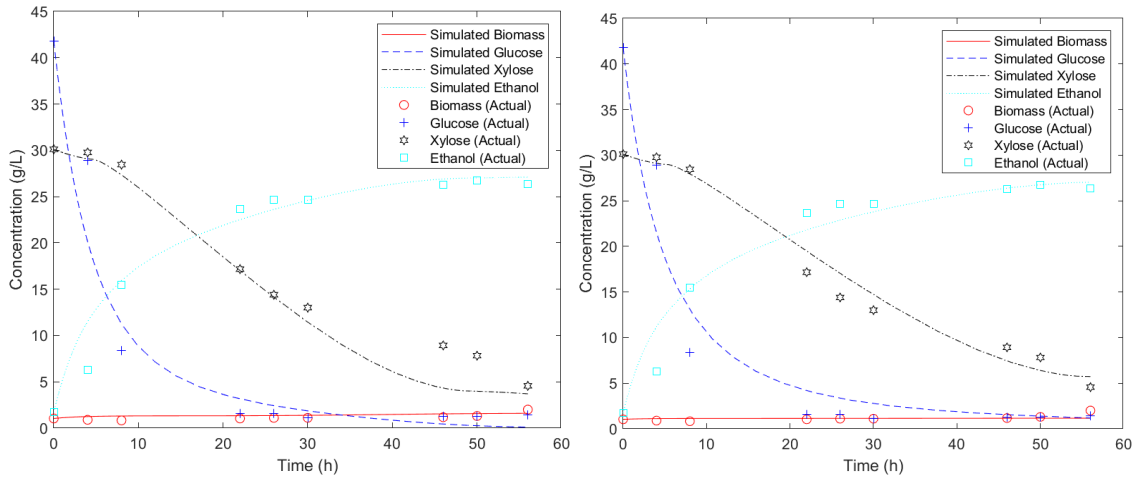
Figure 38. Sensitivity analysis on μ_{max1}

Decreasing K_{S1X} from 30 to 1 influences the xylose concentration profile

minimally, as seen in Figure 37. a). The xylose concentration is almost the same as the

original case, slightly lower. The glucose concentration reaches zero over the end of

fermentation time. On the other hand, increasing K_{S1X} to 80 also influences the xylose

concentration minimally, slightly higher this time, as seen in Figure 37. b). However,

the glucose concentration is almost the same as the original case.

a) $K_{S1X} = 1$ b) $K_{S1X} = 80$

Figure 39. Sensitivity analysis on K_{S1X}

When decreasing K_{S1Xi} to 1 instead of its initial value of 100, the ethanol,

xylose, and glucose concentrations reached are slightly higher (Figure 38. a)). When

giving the parameter a value of 300, the results are the same as the original case where

$K_{S1Xi} = 100$ (Figure 38. b)).
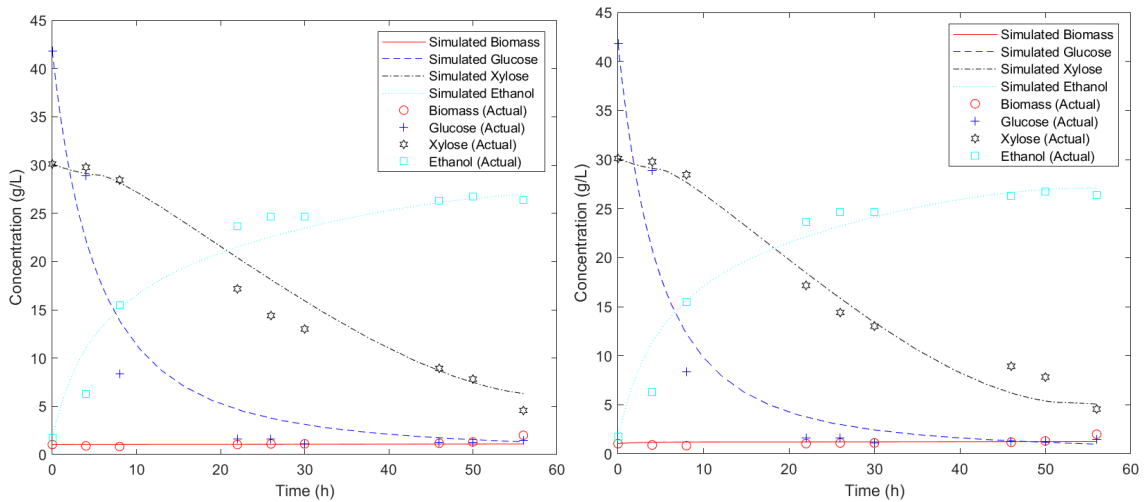
a) $K_{S1Xi} = 1$ b) $K_{S1Xi} = 300$

Figure 40. Sensitivity analysis on K_{S1Xi}

When $P_{X,max}$ =200 instead of 20, the xylose curve decreases faster with time and reaches 1 g/L, compared to 5 g/L in the original case. The glucose concentration becomes 0 towards the end of fermentation and the biomass concentration becomes slightly higher. The ethanol concentration curve increases slightly.
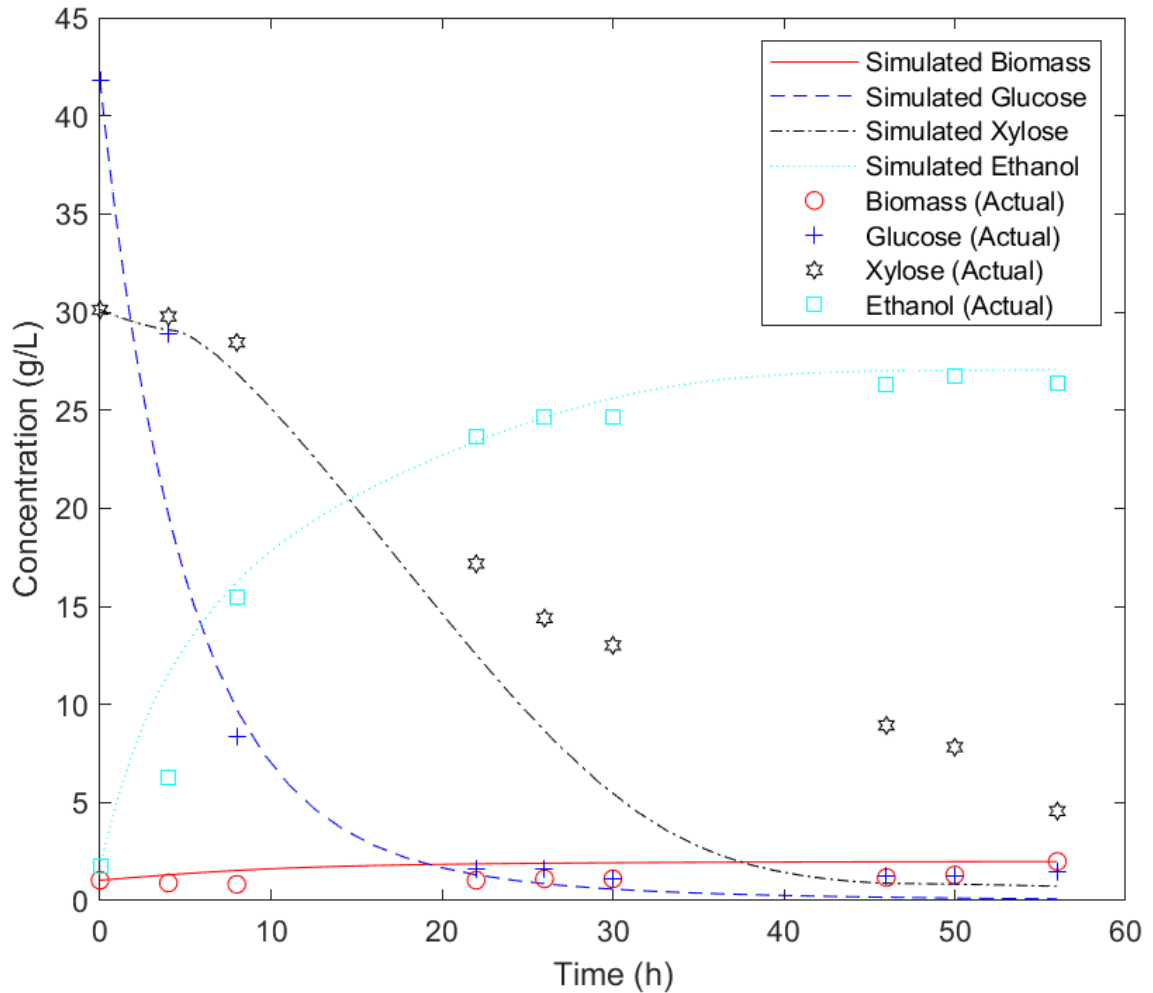

Figure 41. Sensitivity analysis on $P_{X,max}$

Increasing μ_{max2} from 0.0028 to 0.2 seems to yield inaccurate results, with xylose reaching negative concentrations. Ethanol and glucose concentrations are higher.
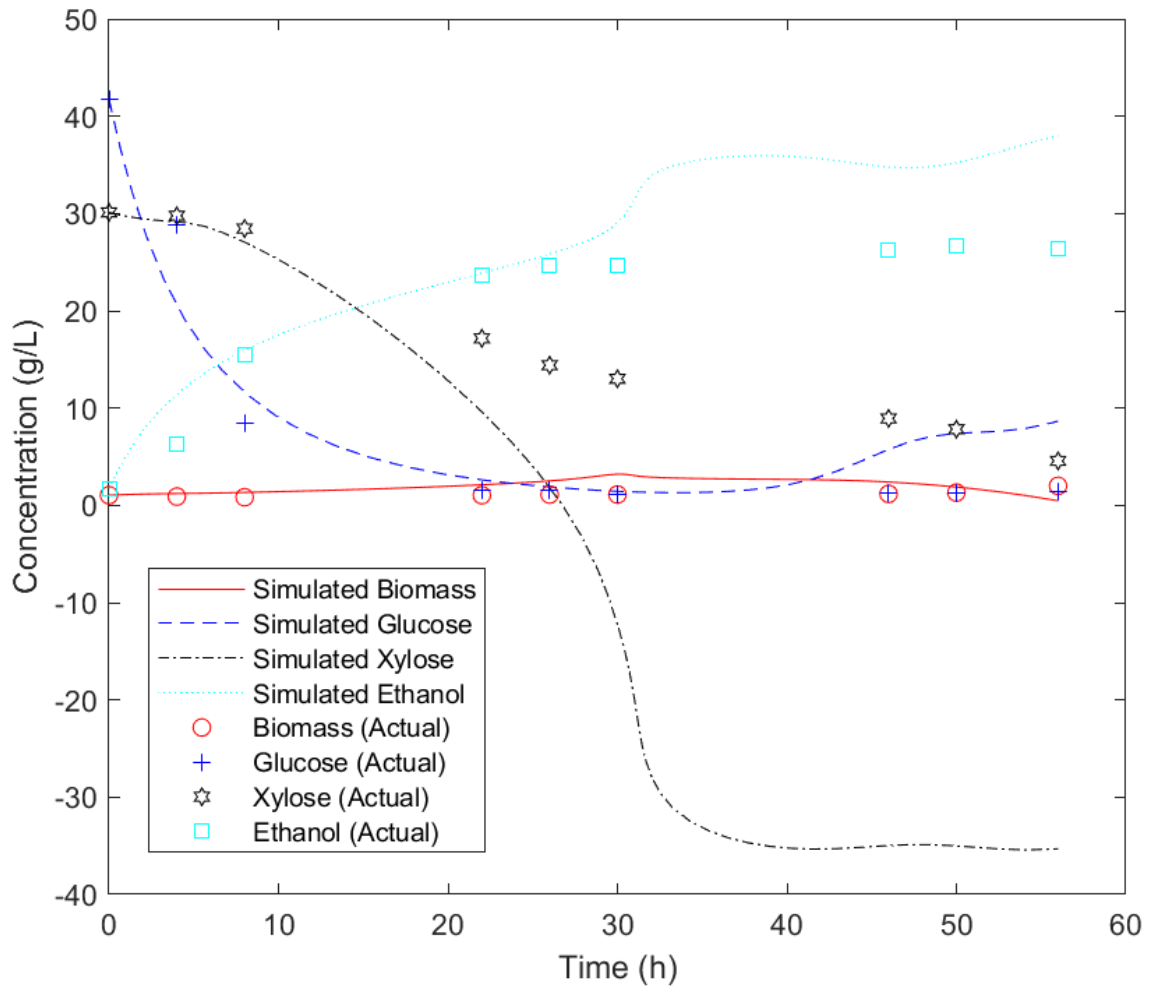
Figure 42. Sensitivity analysis on μ_{max2}

$S_{1,max}$=60 instead of 18 causes the ethanol concentration to become slightly higher, as well as the glucose concentration profile. On the other hand, the xylose curve decreases at a faster pace than the original case and reaches lower concentrations.
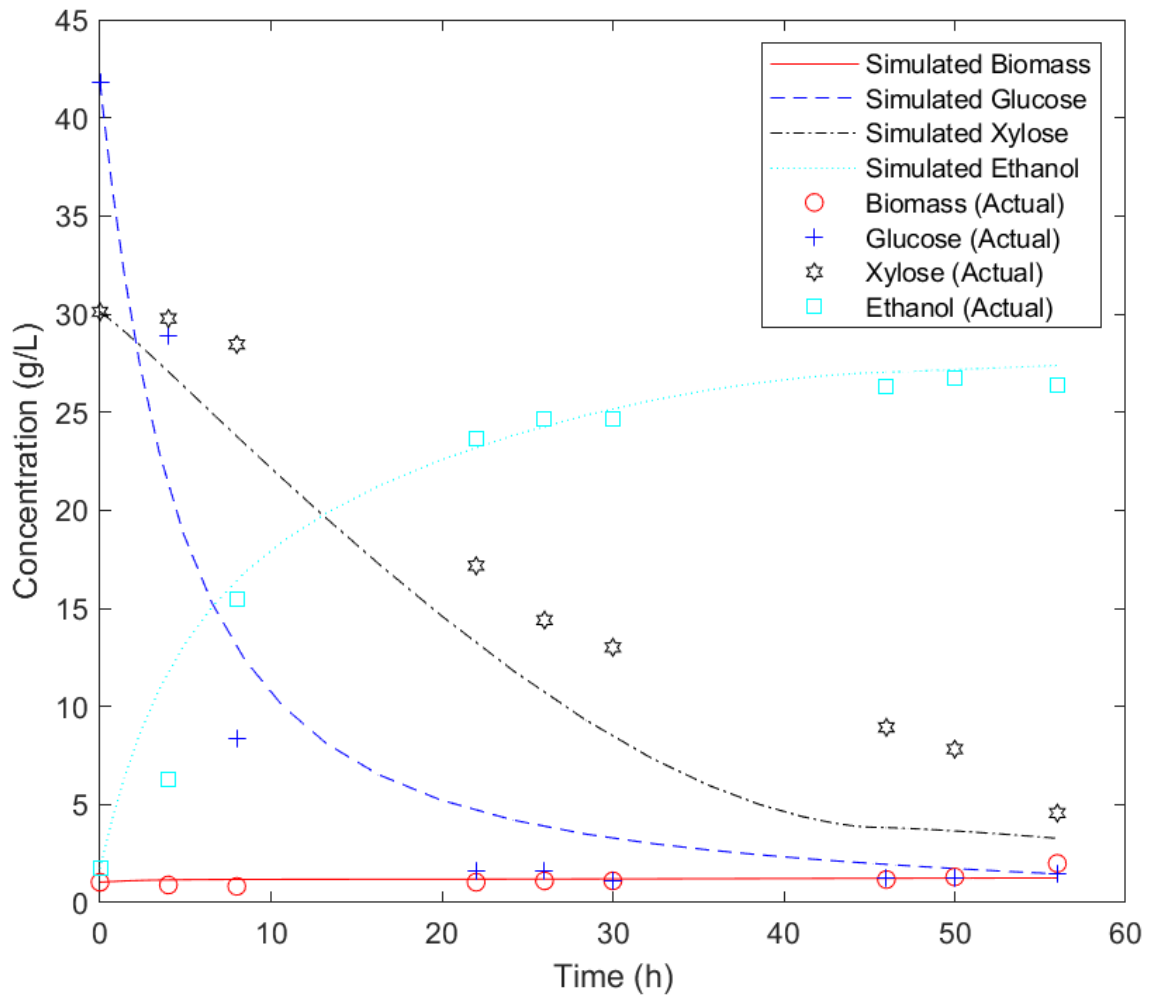
Figure 43. Sensitivity analysis on $S_{1,max}$

γ=2.2 instead of 0.4 yields the following results. The ethanol concentration increases at a slightly slower rate but it reaches almost the same ethanol concentration as the original case. On the other hand, xylose concentrations decrease at a slower rate. The final xylose concentration obtained is higher, whereas the final glucose concentration is slightly lower.
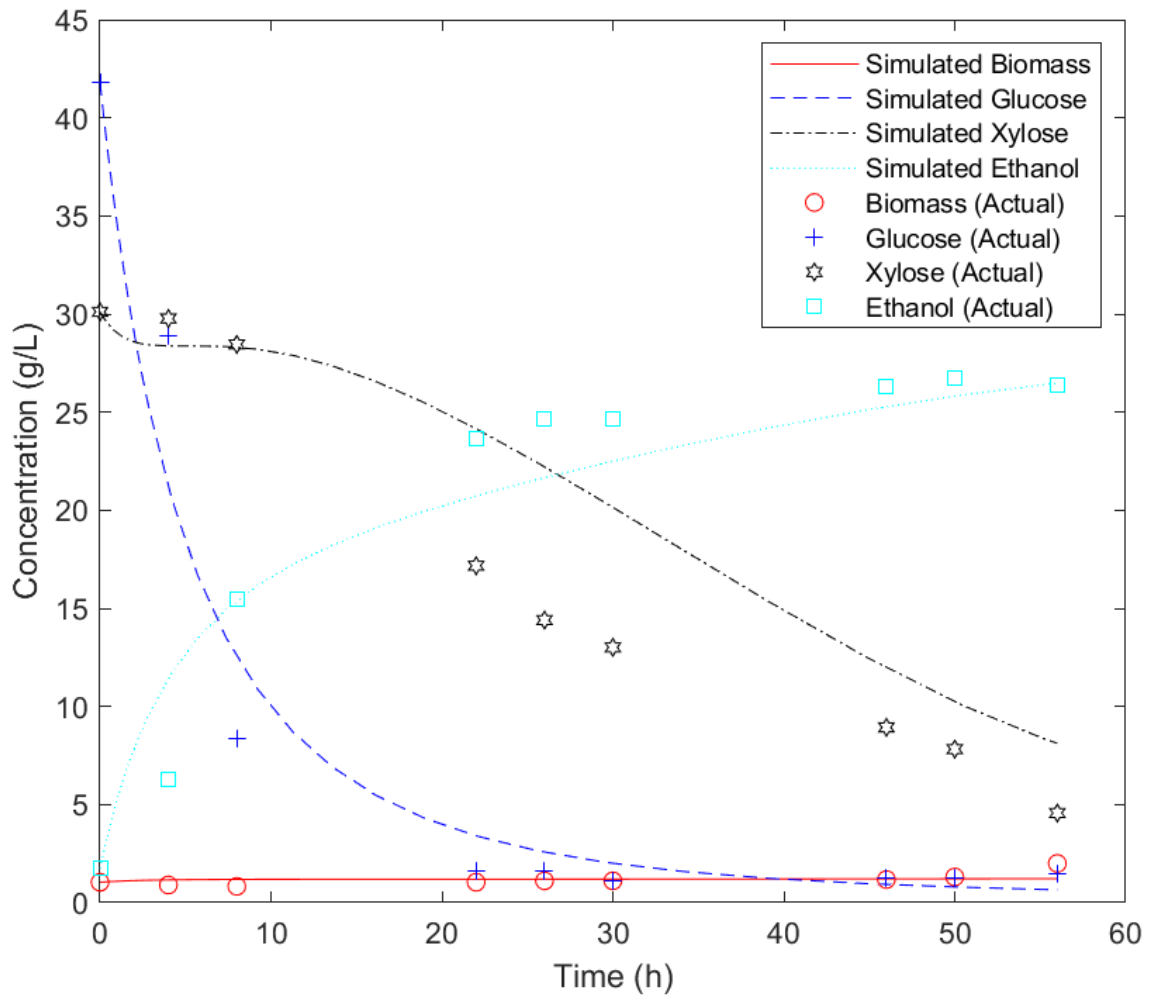
Figure 44. Sensitivity analysis on γ

The ethanol concentration reached when q_{max1}=0.8 instead of 10 is lower. The xylose concentration profile decreases slower at first, then faster towards the end of fermentation to reach 0 g/L. Glucose decreases at a slower pace than the original case and its final concentration is much higher. Biomass concentrations increase slightly.
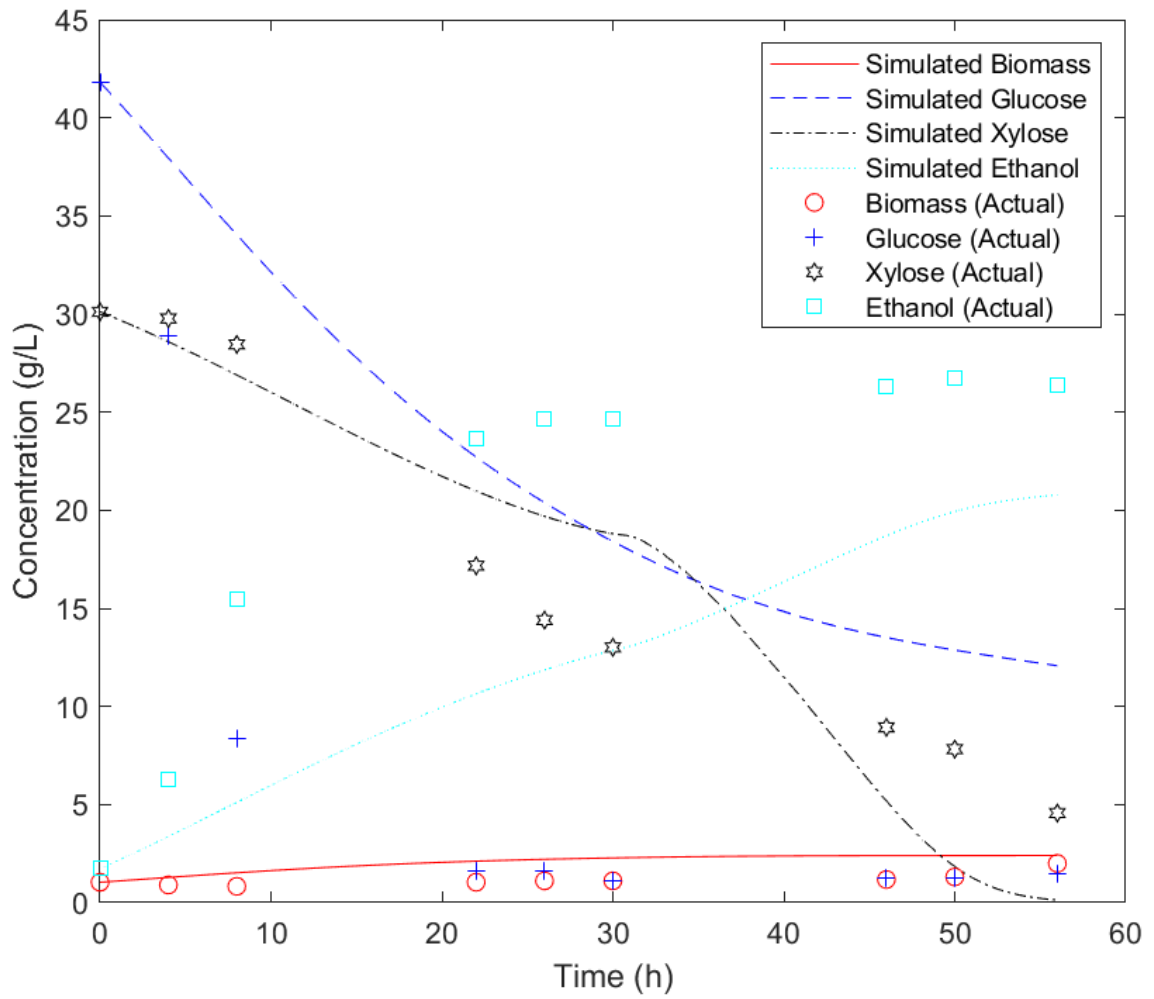
Figure 45. Sensitivity analysis on q_{max1}

K_{S1P}=0.05 instead of 60 causes the ethanol concentration profile to be different than the original case but it eventually reaches the same final concentration. The final concentration of xylose is higher, whereas the glucose concentration reaches 0 g/L at a very early time during fermentation.
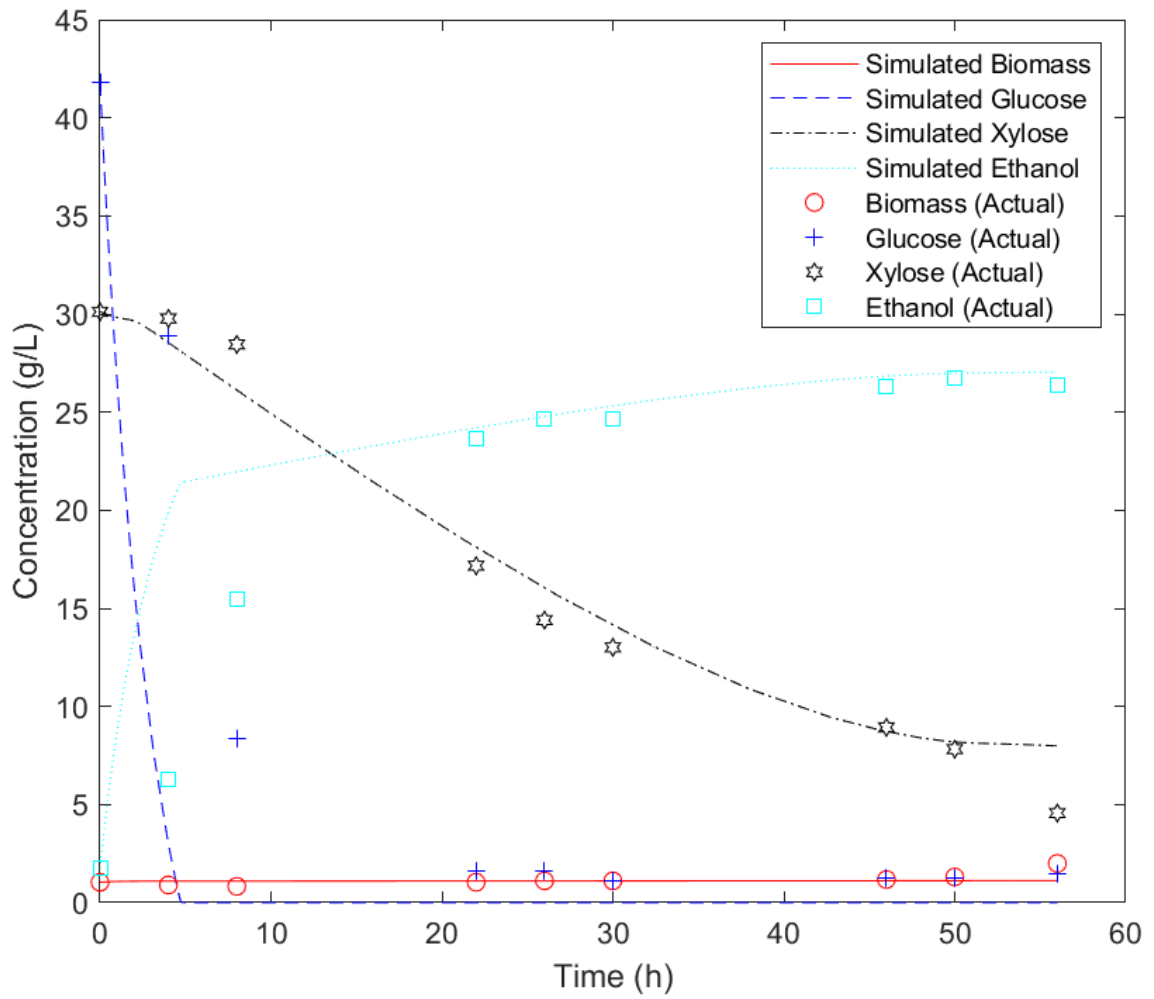
Figure 46. Sensitivity analysis on K_{S1P}

Giving K_{S1Pi} a value of 100 followed by 4890 instead of 300 yield the same results, as seen in the graph below. This parameter has negligeable effects on the differential equations.
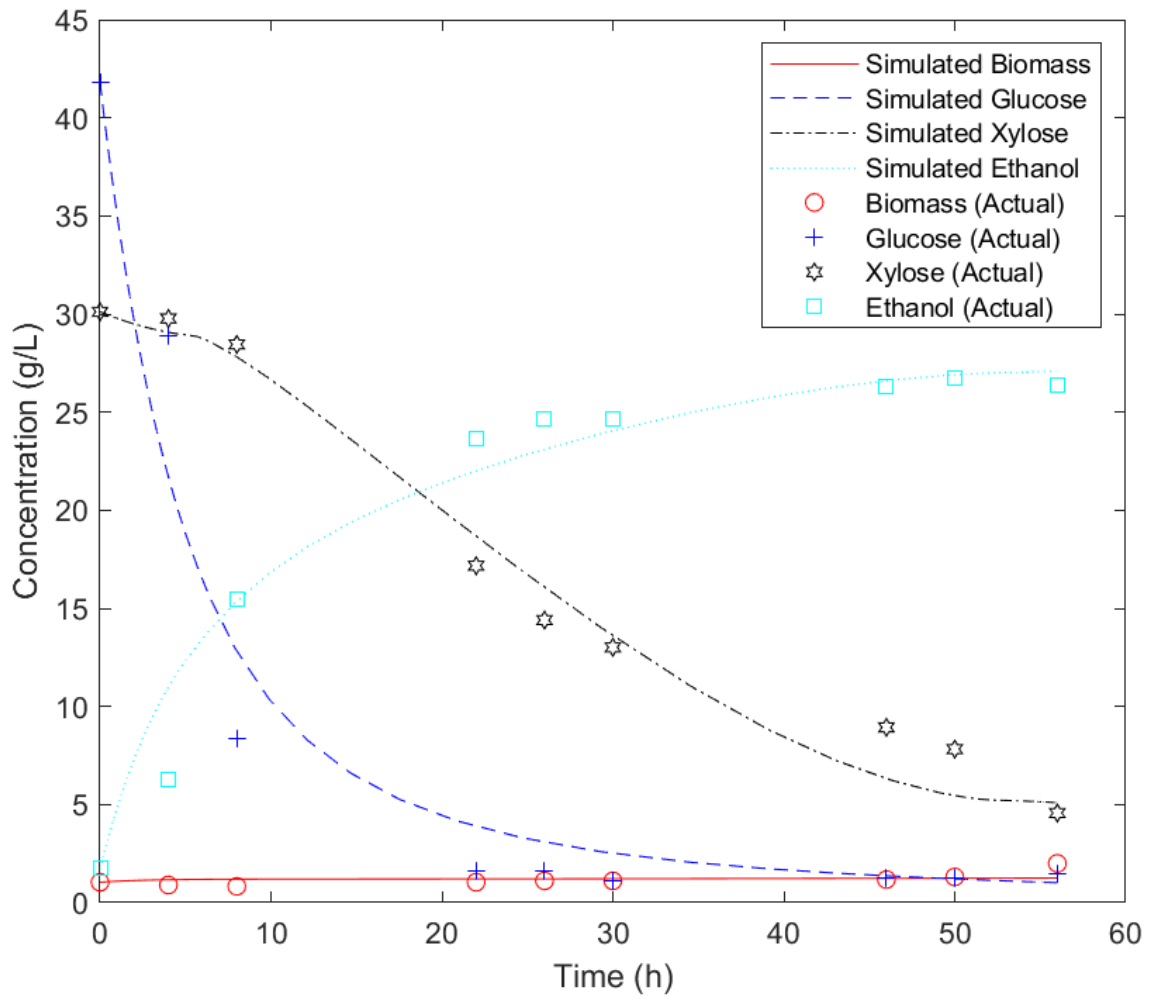
Figure 47. Sensitivity analysis on K_{S1Pi}

$P_{P,max} = 130$ instead of 35 causes the xylose curve to reach higher concentrations than the original case. The ethanol increases at a faster rate, but the same final concentration is reached. The glucose curve decreases slightly faster, and the biomass remains unchanged.
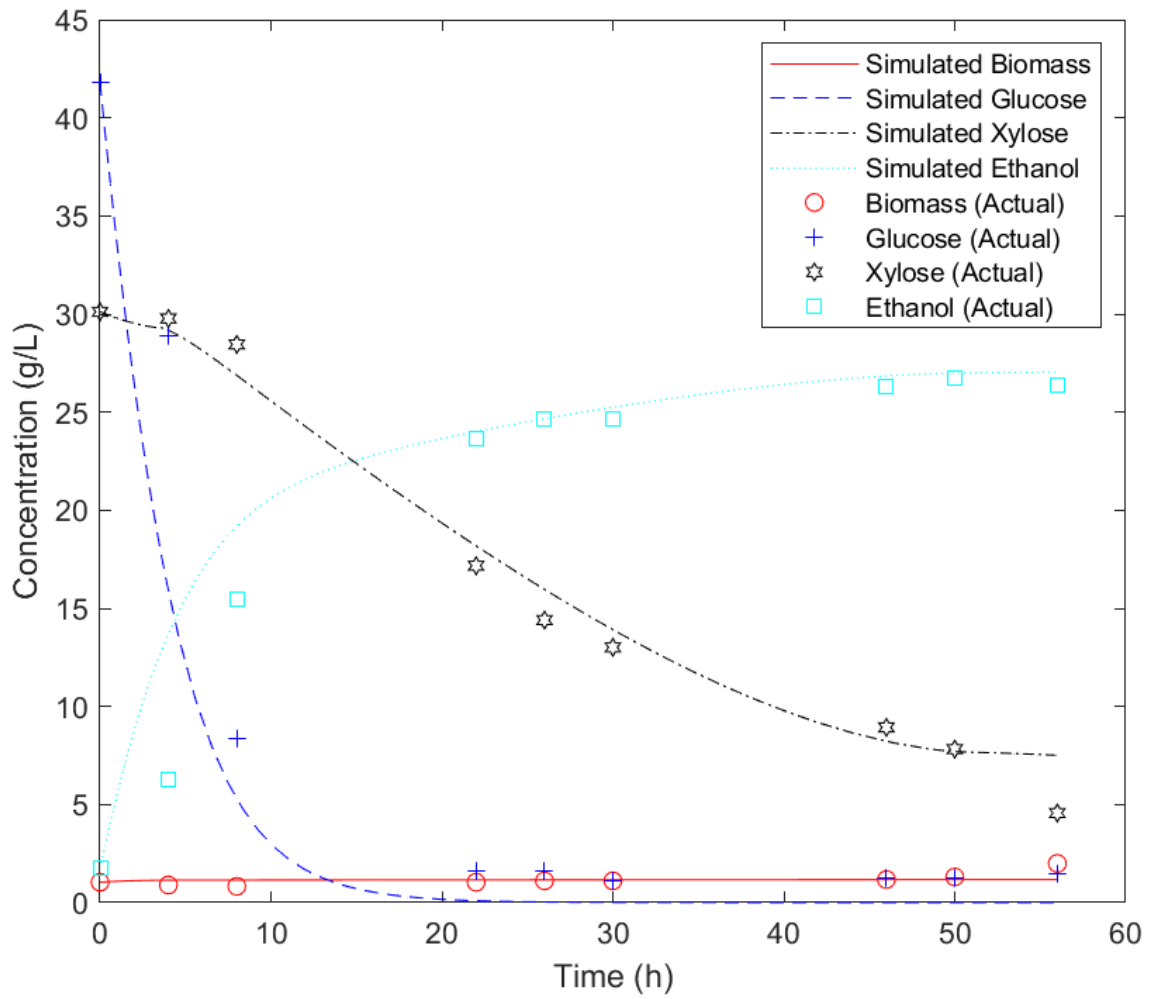
Figure 48. Sensitivity analysis on $P_{P,max}$

K_{S2Pi} affects the ethanol and xylose curves. When a higher value of 81.3 instead of 30 was used, the ethanol concentration slightly increased, and there was a decrease in the xylose curve. No changes were observed on the glucose and biomass curves.
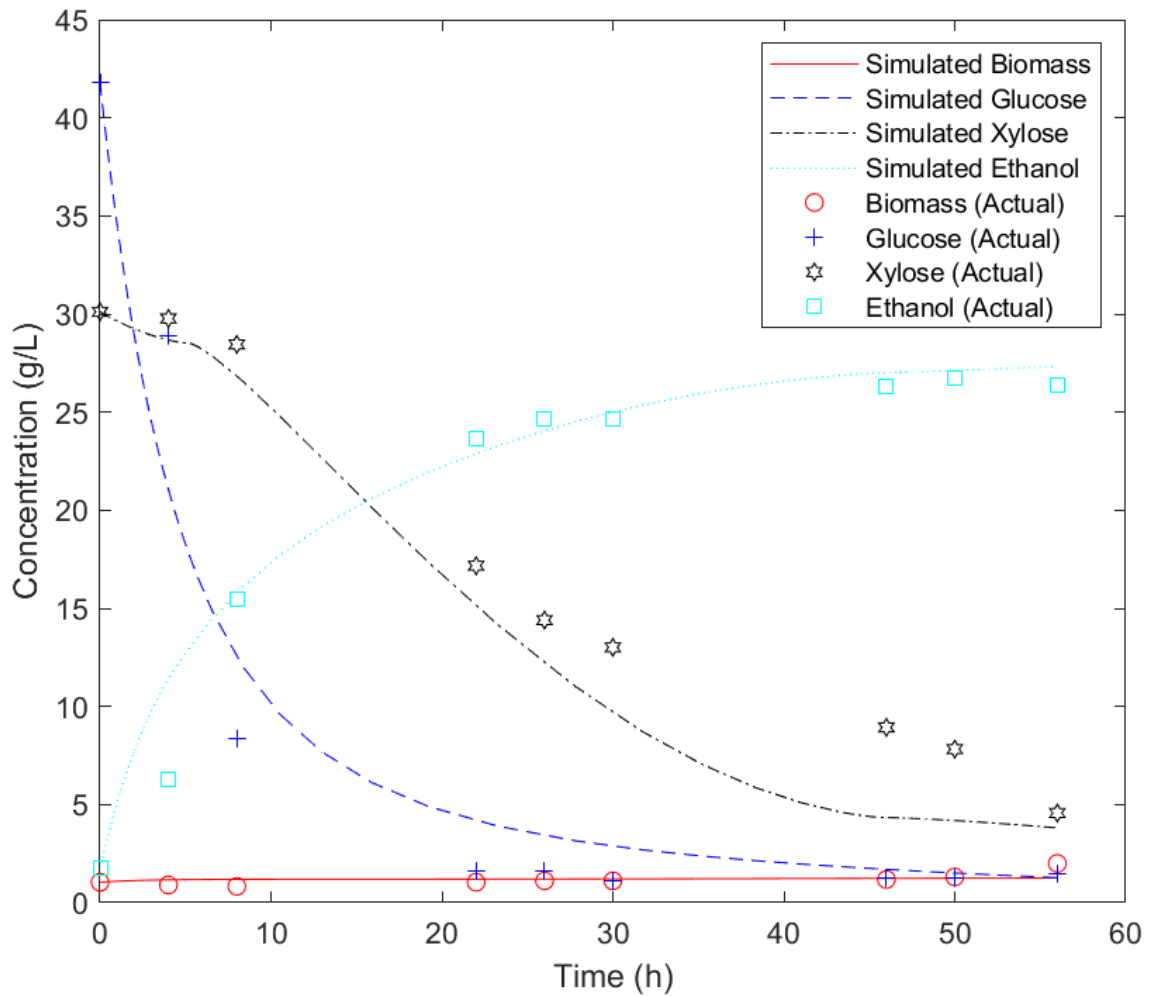
Figure 49. Sensitivity analysis on K_{S2Pi}

A higher ethanol concentration profile was obtained when a higher value for

$P_{P,max2}$ was used (60.2 instead of 27). On the other hand, instead of gradually decreasing,

the xylose profile sharply decreases to reach 0 when t=36 h. No changes were observed

on the glucose and biomass curves.
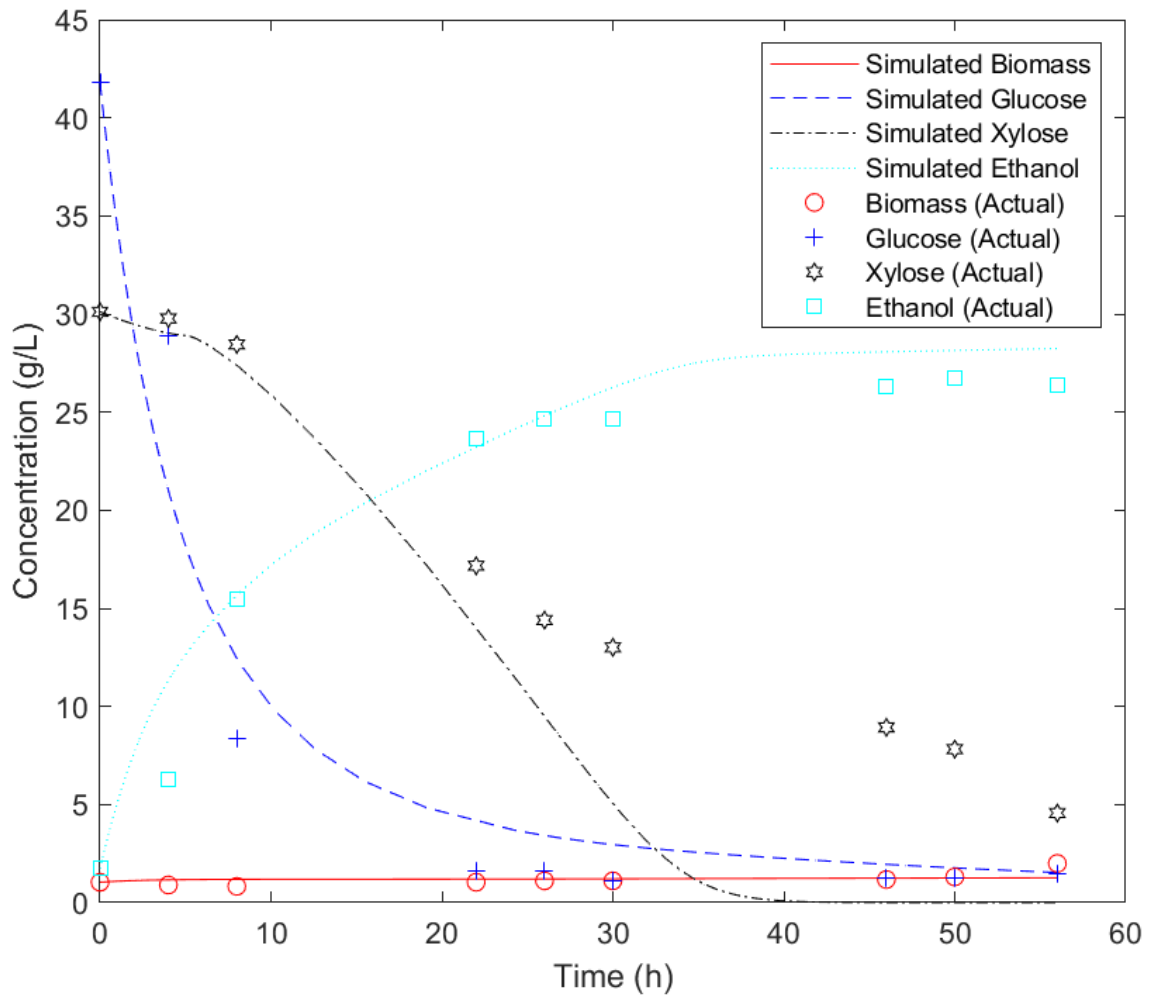
Figure 50. Sensitivity analysis on $P_{P,max2}$

It can be noticed that m influences the glucose and xylose curves. Setting m= 0.1 instead of 0.001 leads to the more gradual decrease of glucose and xylose concentration profiles, with a higher final sugar concentration. No changes in ethanol and biomass.
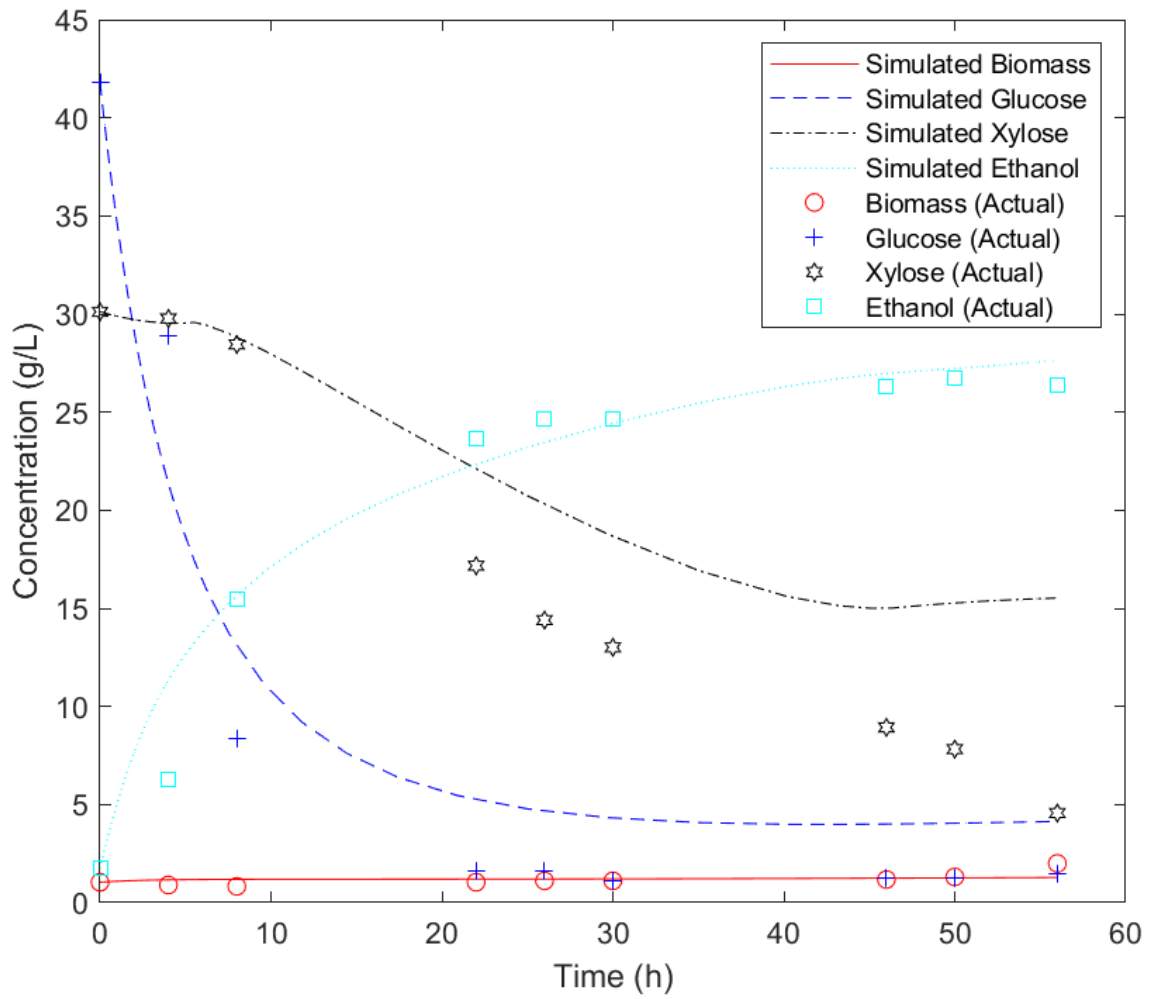
Figure 51. Sensitivity analysis on m

$Y_{X/S1}$=0.005 instead of 0.2 causes the xylose curve to decrease faster and reach 0 when t= 36 h. The glucose curve also decreases faster and reaches 0 at around 10 hours. The ethanol concentration profile increases at a slower rate and the final concentration reached is much lower than the original case.
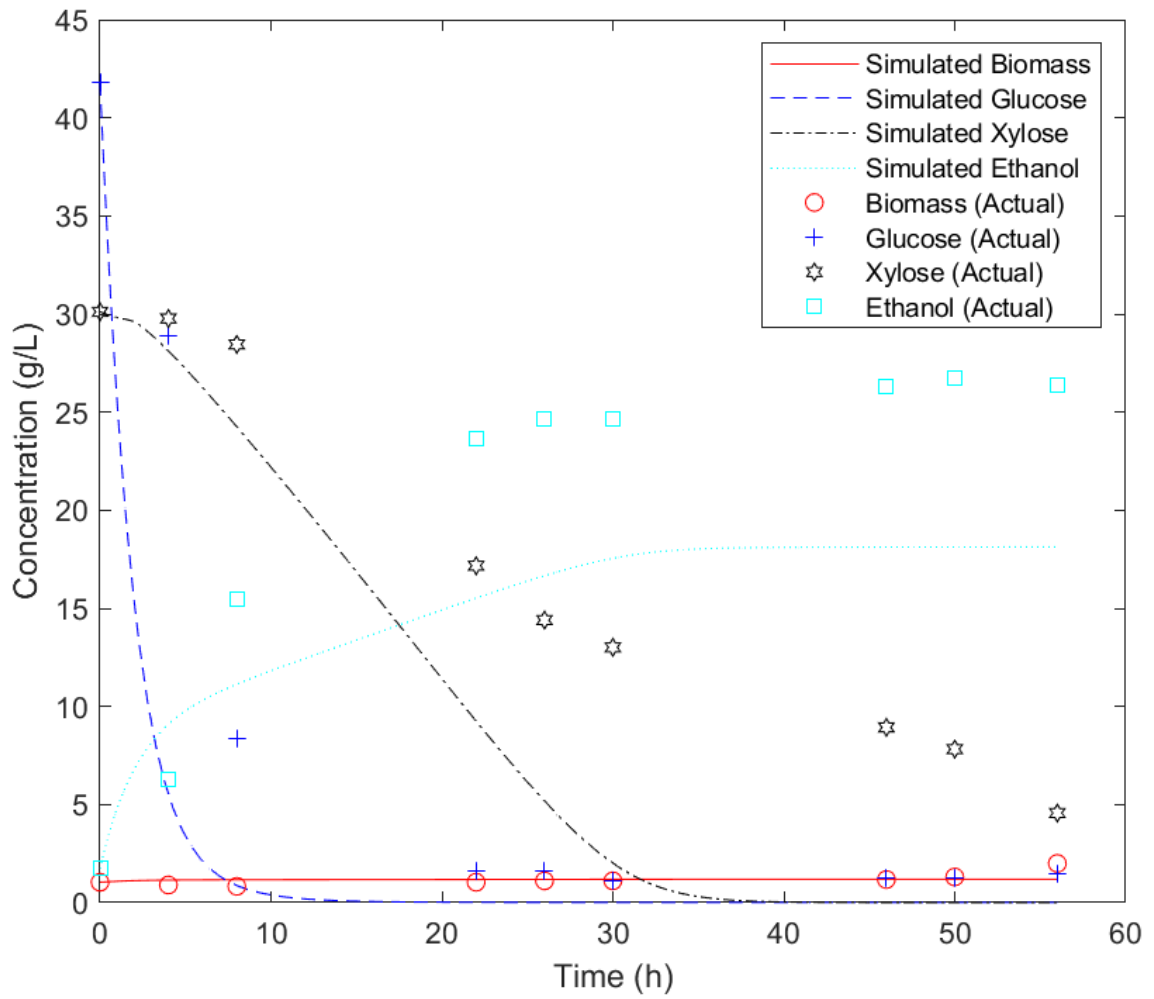
Figure 52. Sensitivity analysis on $Y_{X/S1}$

$Y_{P/S1}=0.1$ instead of 0.46 yields a profile similar to the previous example.
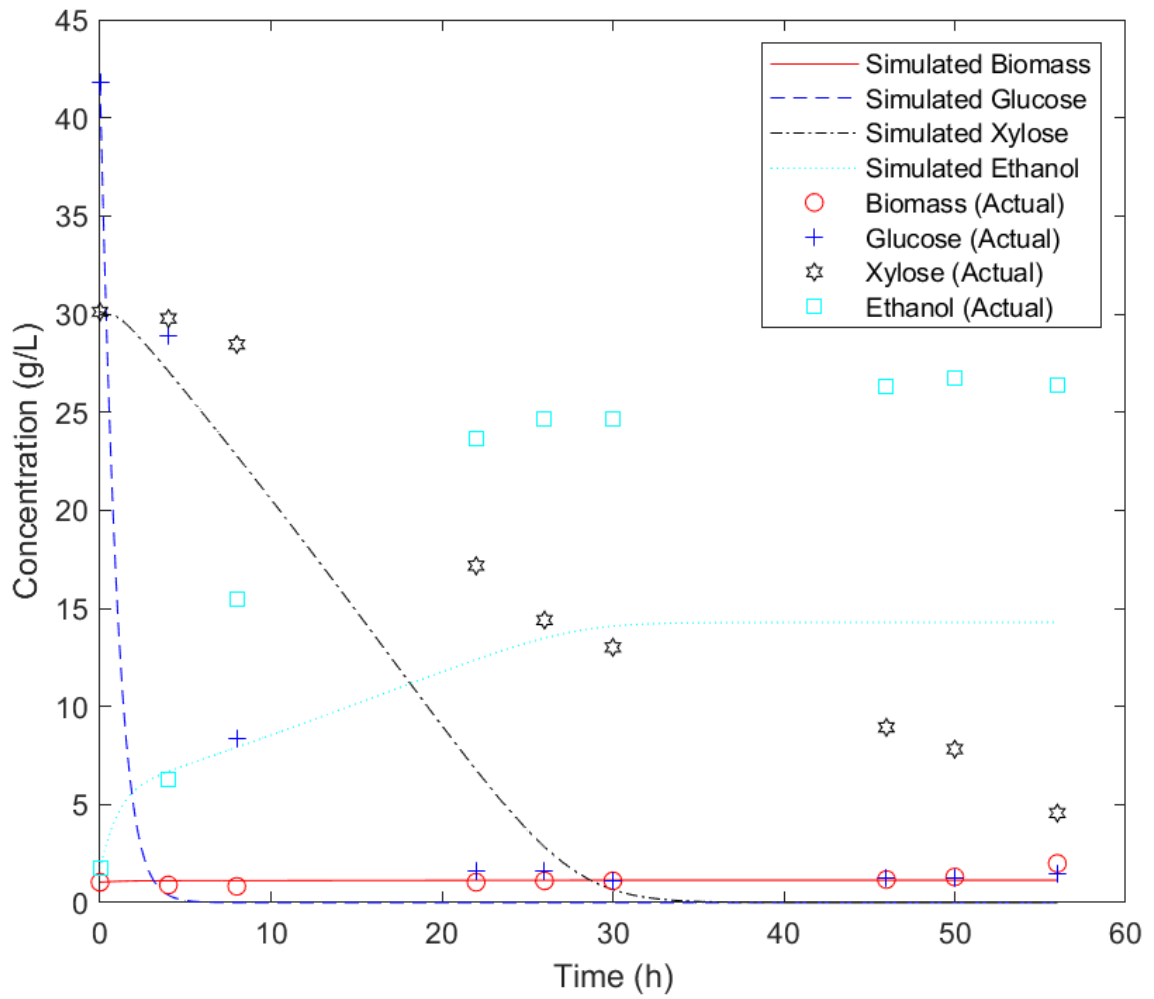
Figure 53. Sensitivity analysis on $Y_{P/S1}$

When varying β_2 and setting it to 0.9 instead of 0.4, the xylose curve decreases more gradually than before and its final concentration is higher than the original case, which causes the ethanol concentration to be less than before (25 g/L). No changes were observed on the glucose and biomass curves.
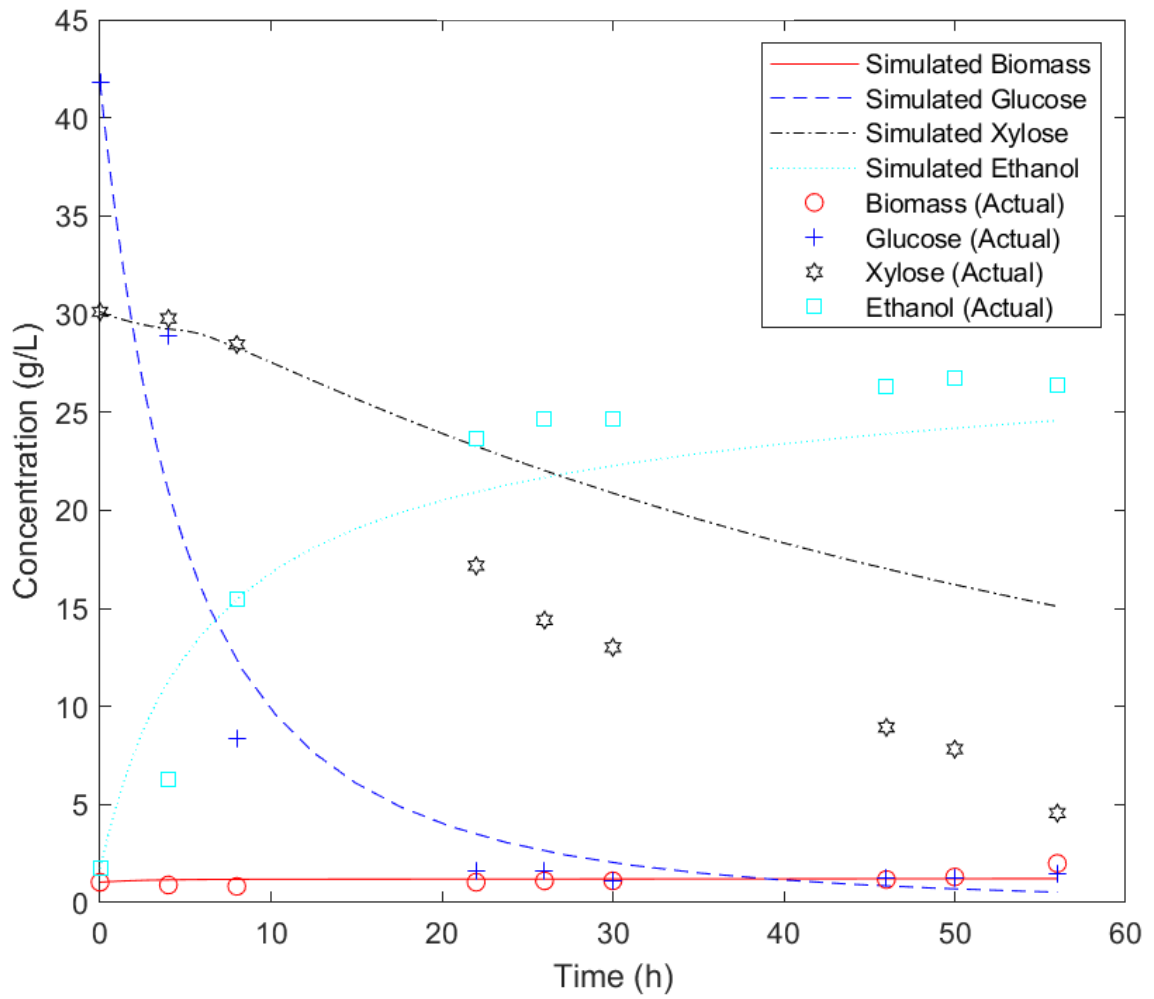
Figure 54. Sensitivity analysis on β_2

$Y_{P/S2}$ only affects the xylose concentration profile. Setting it to 0.7 instead of 0.28 causes the sugar concentration to decrease more gradually, and to reach a high final concentration, around 20 g/L.
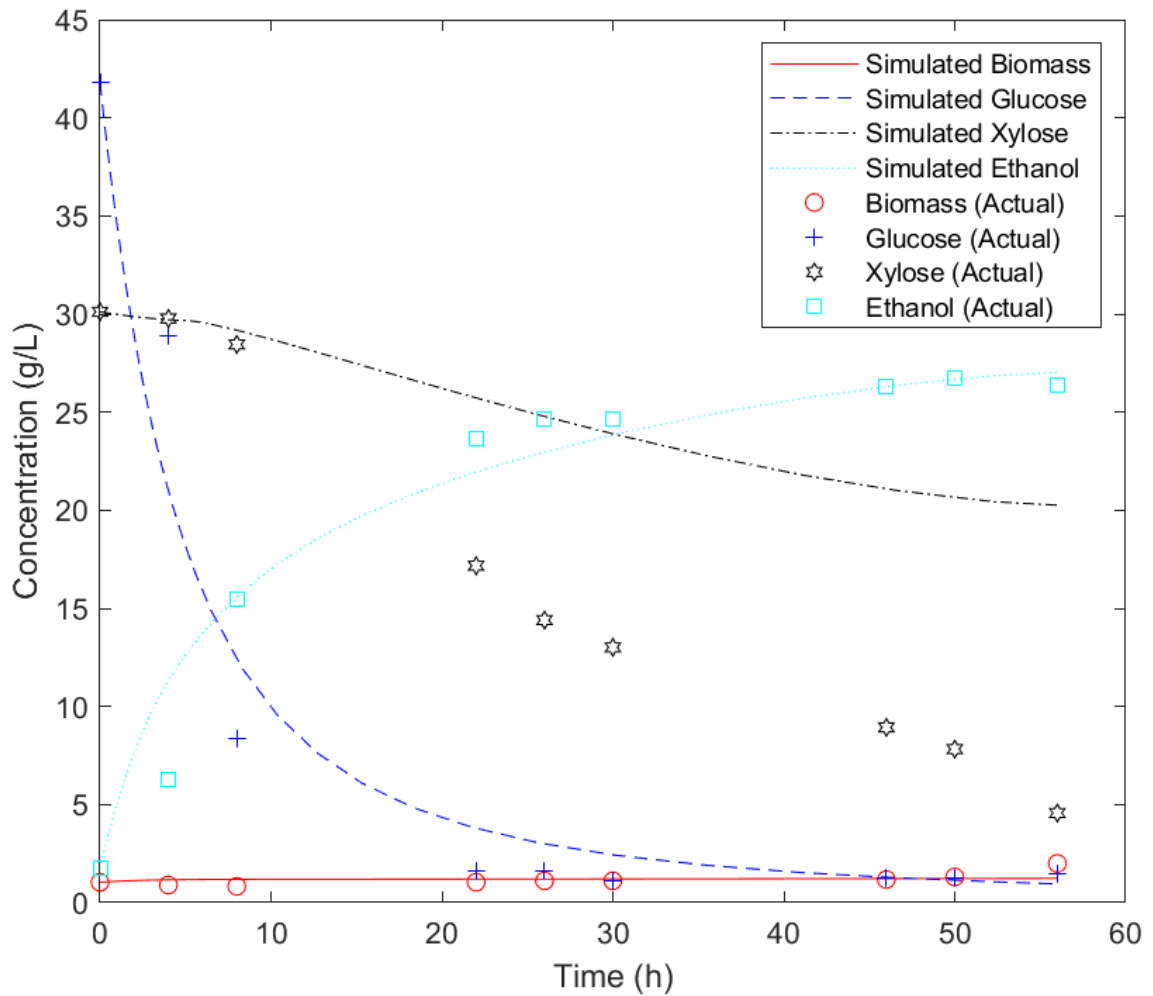
Figure 55. Sensitivity analysis on $Y_{P/S2}$

Several parameters were varied to check which variables affect and influence the results the most. The parameters that were found to have an important influence on xylose are $Y_{P/S2}$, β_2, m, $P_{P,max2}$, μ_{max1}, $P_{X,max}$, $S_{1,max}$, and γ. Ethanol was affected mostly by β_2, $P_{P,max2}$ and γ, and glucose was influenced by m, $P_{X,max}$, K_{S1P}, and P_{Pmax}. Some parameters were found to affect all the curves, like q_{max1} and μ_{max2}. Others have negligible effect, like K_{S1Pi}, and $Y_{X/S1}$ and $Y_{P/S1}$ affect all the results except for biomass.

4.2. Simulation of Arundo donax SHF

The simulation results of the hydrolysis were implemented in the previously developed fermentation model. this was achieved by combining the hydrolysis and fermentation MATLAB codes to mimic the SHF process, as mentioned previously.

It was found that the maximum ethanol concentration, P_{Pmax}, is inhibiting and slowing down ethanol production. In this model, $P_{Pmax}=60$ was used, which is in the range used in the literature, in order to prevent ethanol inhibition. The remaining variables were kept the same as the obtained ones from parameter estimation.

Figure 56. Hydrolysis and Fermentation simulation

An ethanol concentration of around 28 g/L was obtained, similar to results obtained in literature, which proves that the model is accurate and is a good representation of the hydrolysis and fermentation of Arundo donax.

4.3. Arundo donax plantation plan

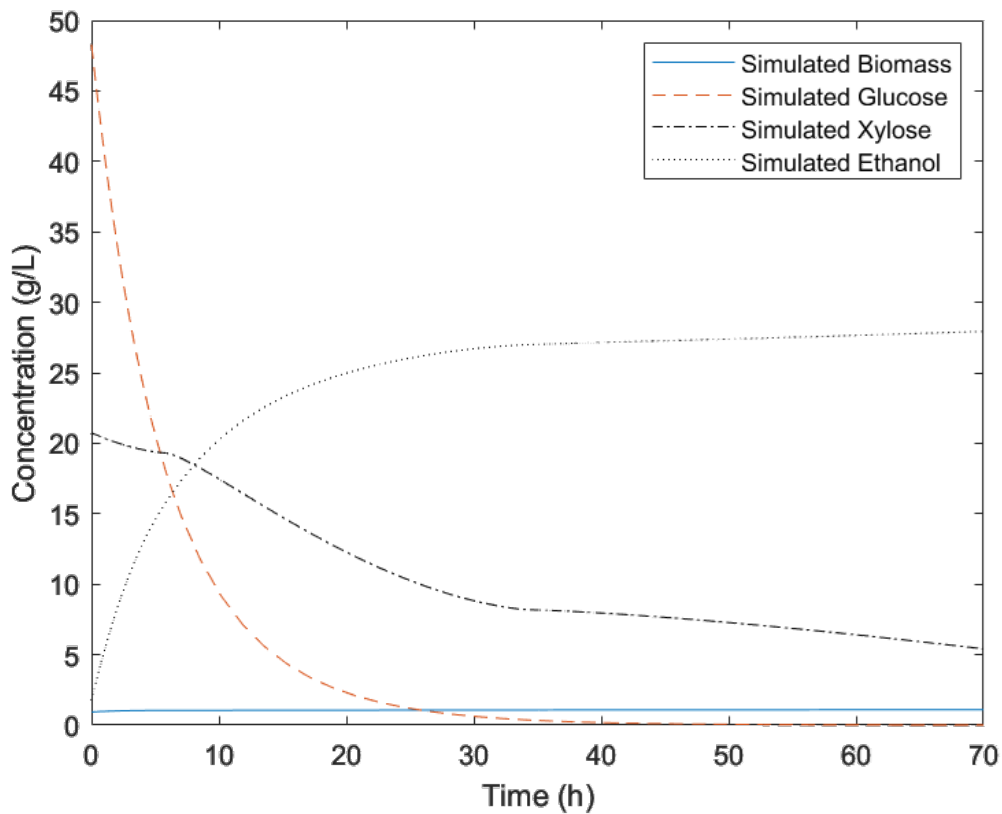Planting usually occurs in Spring, around May [79], and blooming in Fall [80]. Arundo is a perennial plant, which means that it can survive for two growing seasons or more [81]. The growth pattern of the plant is the following. Giant reed shoots develop in March and expand fast in June and July, forming both leaves and stems. Leaves present at a low level begin to dry at the end of July, depending on weather fluctuations. From early October till late November, drying speeds up which causes the moisture content of the plant to dramatically decrease. Winter temperatures cause growth suspension until spring for regrowth. A study obtained, using fertilizers, a crop biomass yield of 27 dry ton/ha, over the course of 6 years (mean value) [82]. Although the use of a fertilizer increased the productivity in the beginning, it was found that with time, using fertilizers yielded the same results as not using them. Harvest timing and crop density were reported to have no effect on the yields of biomass. It was later concluded that Arundo is able to produce around 3 kg of biomass /m^2 yr. Another study conducted in Italy where 39 Arundo donax clones were studied over the period of two years found an average biomass yield of 10.6 t/ha of dry matter in year 1 (highest yield: 14 t/ha) and 22.1 t/ha in year 2 (highest yield: 34.2 t/ha) [83]. Arundo is able to keep growing for 20-25 years without having to replant it, which is very remarkable.

Although Arundo is a perennial plant, the canes grow scruffy throughout the winter and should be trimmed to the floor at the beginning of spring to allow them to regrow. Because new canes formed on a new plant develop flower panicles, trimming the canes during winter helps young plants blossom sooner [84].

To determine the number of Arundo donax plants that should be planted to obtain the amount of ethanol needed, the amount of land will be calculated noting the following:

$$10{,}000 \text{ Arundo rhizomes} \rightarrow 1 \text{ hectare} = 10{,}000 \text{ m}^2 \text{ [85]}$$

$$3 \text{ kg of biomass} \rightarrow \text{m}^2/\text{year}$$

In our simulation, a total working volume of 5 m^3 is used under an optimal feed concentration of 178.52 kg/ m^3. This is equivalent to 894.72 kg of biomass.

The ethanol concentration obtained from the simulation is 28 g/L, which is equivalent to 140.332 kg of ethanol. Dividing by the total mass of lignocellulose biomass fed, an ethanol yield of 15.7% is obtained, as seen in Equation 64.

$$\frac{140.33 \; kg \; ethanol}{894.71 kg \; feed} = 0.157 \; kg \; ethanol \; / \; kg \; lignocellulose \; feed \quad (66)$$

The amount of Arundo donax plants and the land area needed to provide Lebanon with yearly ethanol will be estimated, assuming that up to 10% of ethanol will be mixed with gasoline. According to L'Orient Today, a daily consumption of 281,000 L of fuel was reported in 2022, which is equivalent to 102,565,000 L per year [86]. 10% of this result equates to 10,256,500 L, or 8,092,379 kg of ethanol that should be produced from Arundo donax. Dividing this number by the yield obtained previously, 51,609,560 kg of Arundo biomass will be needed in order to provide Lebanon with the necessary amount of ethanol per year, which would cover around 17,203,187 m^2, if we assume that Arundo produces around 3 kg of biomass /m^2 yr. The previous findings are summarized in the figure below:

8,092,379 kg ethanol
• 10% of the yearly fuel consumption

51,609,560 kg Arundo biomass
• yield obtained = 0.1568 kg ethanol/kg Arundo

17,203,187 m^2
• area of Arundo donax plants needed to provide Lebanon with necessary amount of ethanol/year
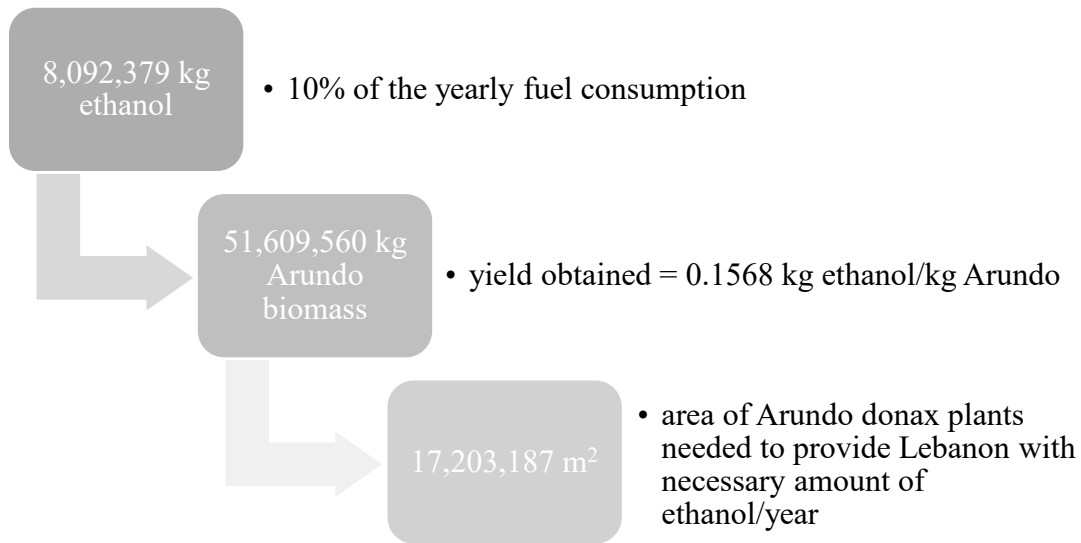
Figure 57. Area of Arundo donax plants needed

As mentioned in Chapter 2, the plan is to plant Arundo donax on landfills. The capital's two infamous coastal landfills, Burj Hammoud (163,000 m^2) and Costa Brava (150,000 m^2), were built as temporary measures during the 2015 waste crisis, when garbage flooded Beirut streets because of the Naameh dump site shutdown and suspended trash collection [87]. The Naameh Landfill (300,000 m^2) was used for inert materials [88]. Other landfills include the Zahle Sanitary Landfill (303,000 m^2) [89], the Saida Landfill (60,000 m^2) [90], the Bsalim Landfill (45,000 m^2), used for the disposal of inert, shredded and bulky waste [91], the Tripoli Landfill (60,000 m^2), the Minyeh, Srar and Al Masnaa Landfills [92]… The locations of the previously mentioned places are shown below.
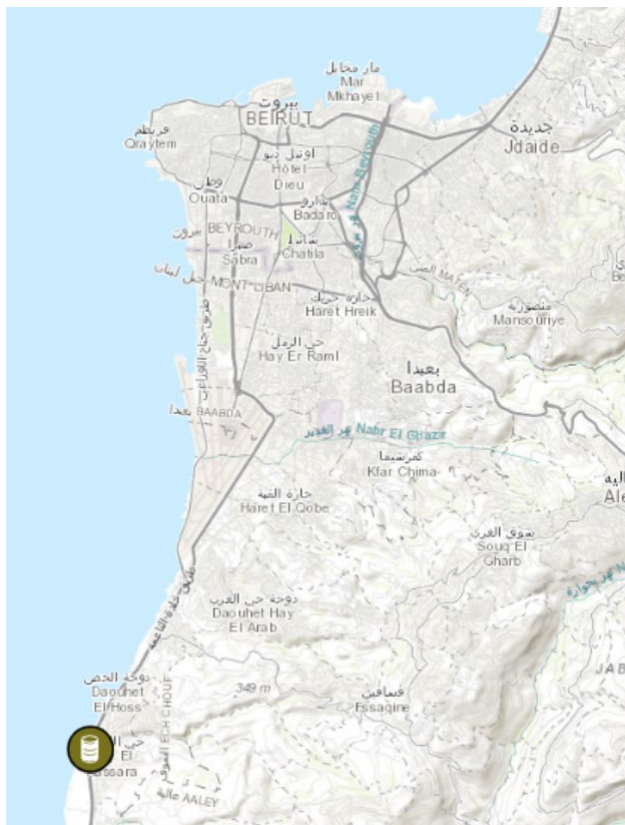
Figure 58. Naameh Landfill, Chouf District [35]

Figure 59. Burj Hammoud, Matn District [93]

Figure 60. Costa Brava, Choueifat [94]

Figure 61. Zahle Sanitary Landfill, Zahleh municipality [89]
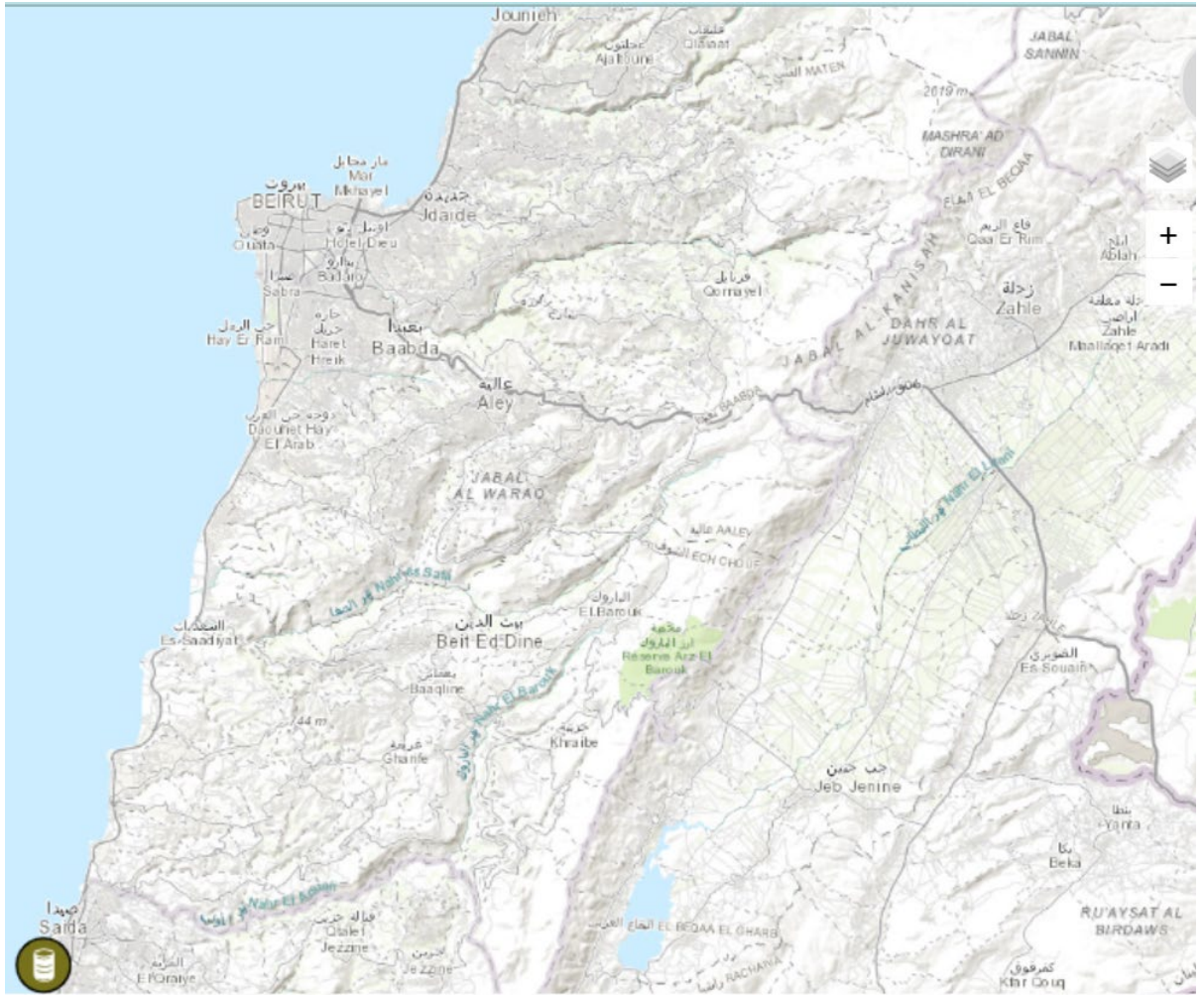
Figure 62. Saida Landfill [90]
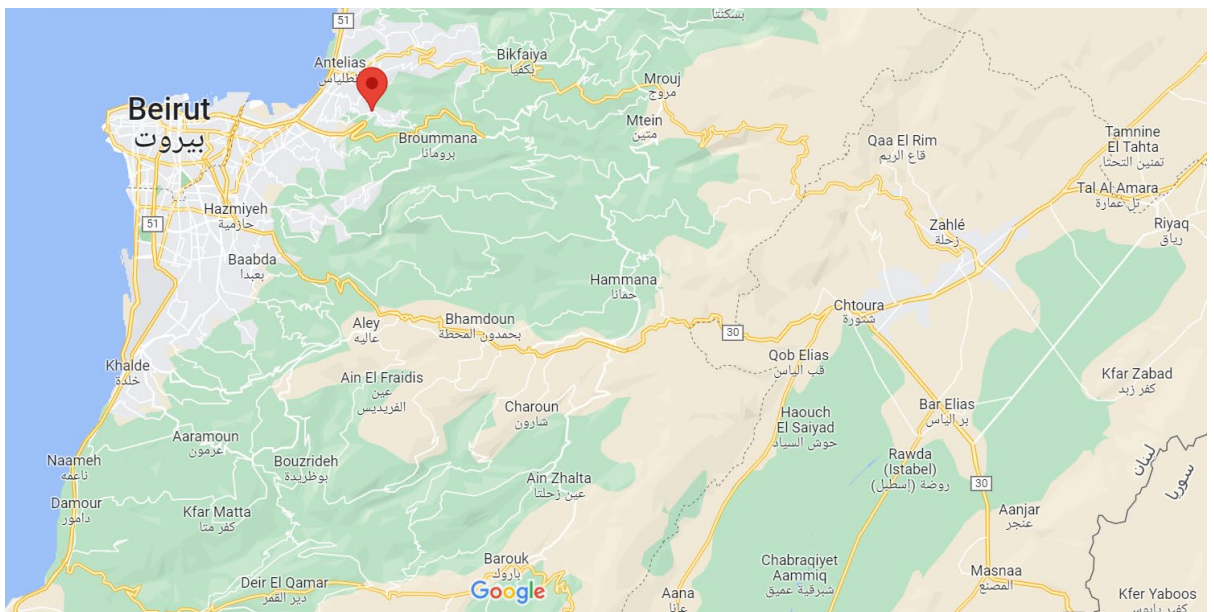
Figure 63. Bsalim Landfill, located in an old quarry in Nahr El Mott valley [91]

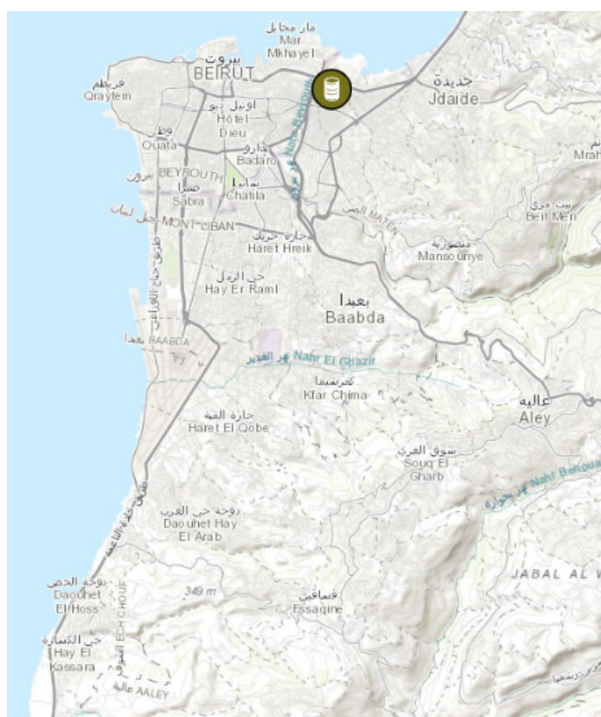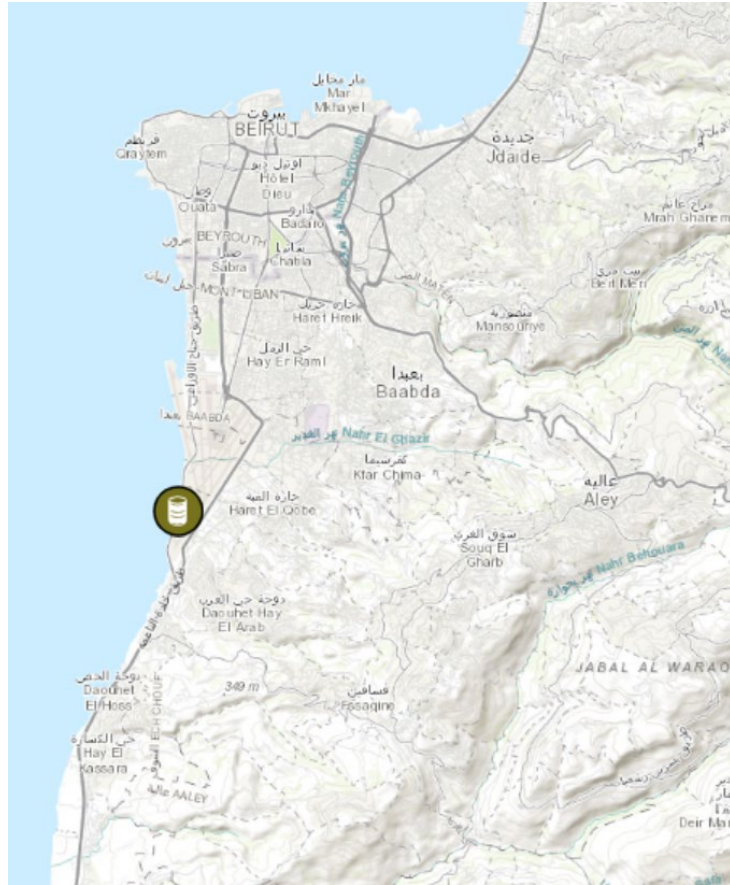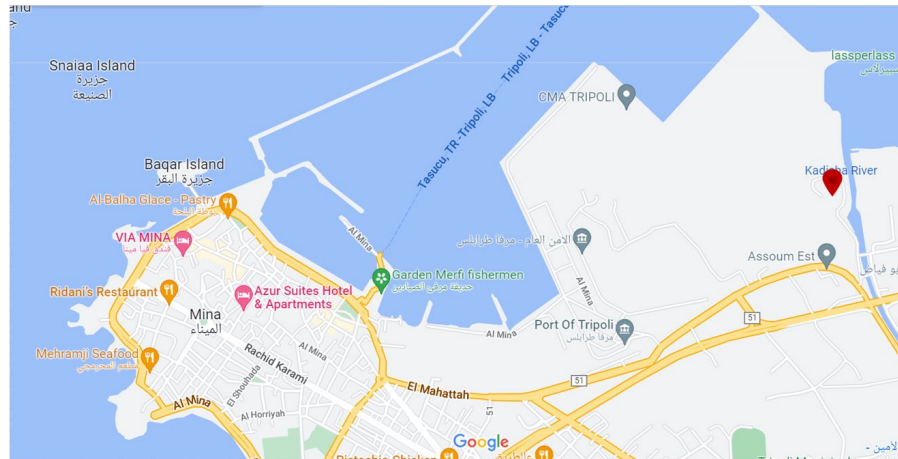Figure 64. Tripoli Landfill, on the Mediterranean coast next to Abu Ali estuary [95]
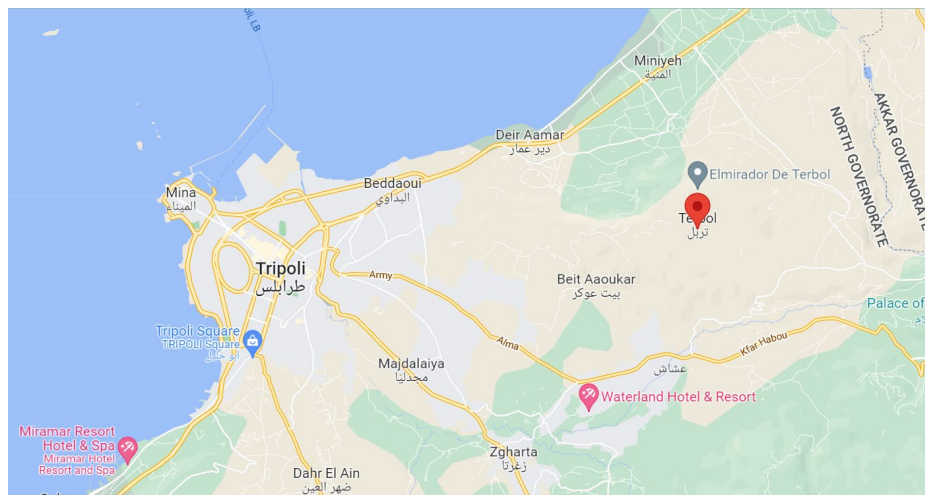
Figure 65. Minyeh, Terbol Landfill
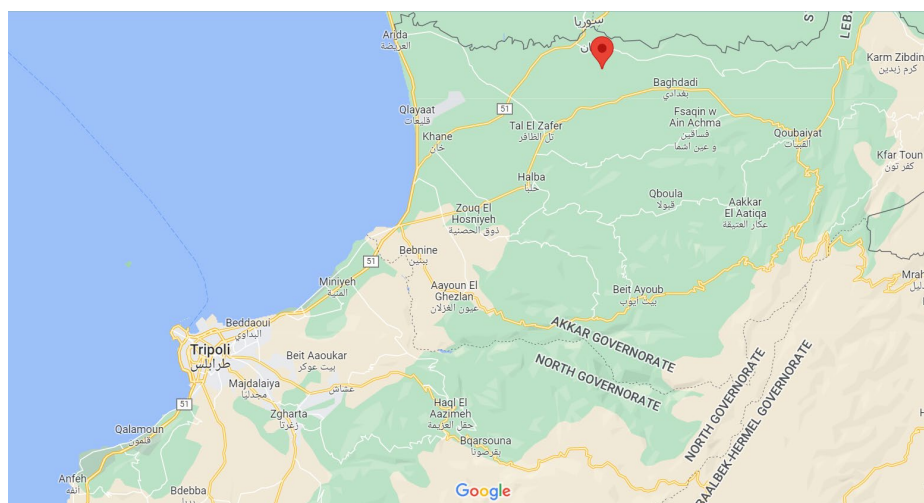
Figure 66. Srar Landfill

The previous agriculture minister proposed back in 2015 the conversion of a couple of dumps in Srar, Akkar (previous figure) and the eastern border of Al Masnaa into sanitary landfills [92]. The east mountain range is a long series of rocky mountains (240 km) [96] situated between Lebanon and the Syrian border, where a stone quarry is present [97]. This could provide an additional area to plant Arundo donax.

The previously listed landfills in Lebanon and their respective areas are summarized in the table below.

Table 15. Lebanese landfills and areas

Landfills	Area (m^2)
Naameh	300,000
Burj Hammoud	163,000
Costa Brava	150,000
Zahle	303,000
Saida	60,000
Bsalim	45,000
Tripoli	60,000
Minyeh	-
Srar	-
Al Masnaa	-
Total	1,081,000

Other than landfills, quarries can also be used as places for Arundo donax plantation sites. There are around 700 quarries (counting operating and abandoned ones) dispersed in Lebanon, as seen in the following map. They generate rock and sand fragments (464 and 246 sites respectively) and provide the need for cement and building stones. Quarries areas range from 5,000 to 1,000,000 m^2 [98].
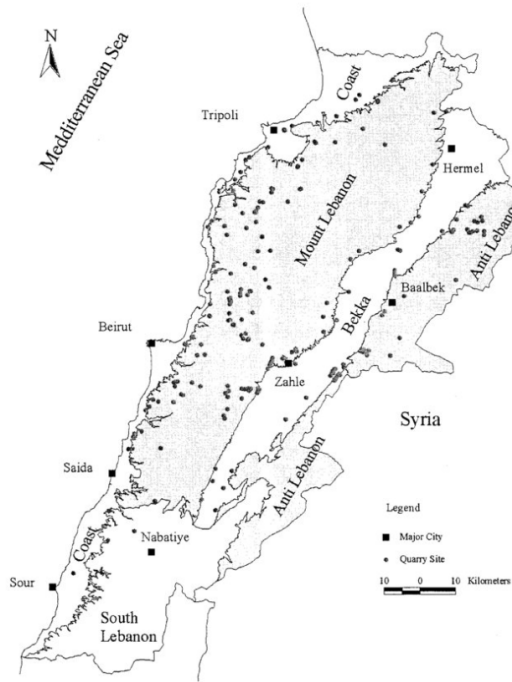
Figure 67. Quarries in Lebanon in 2001 [98]
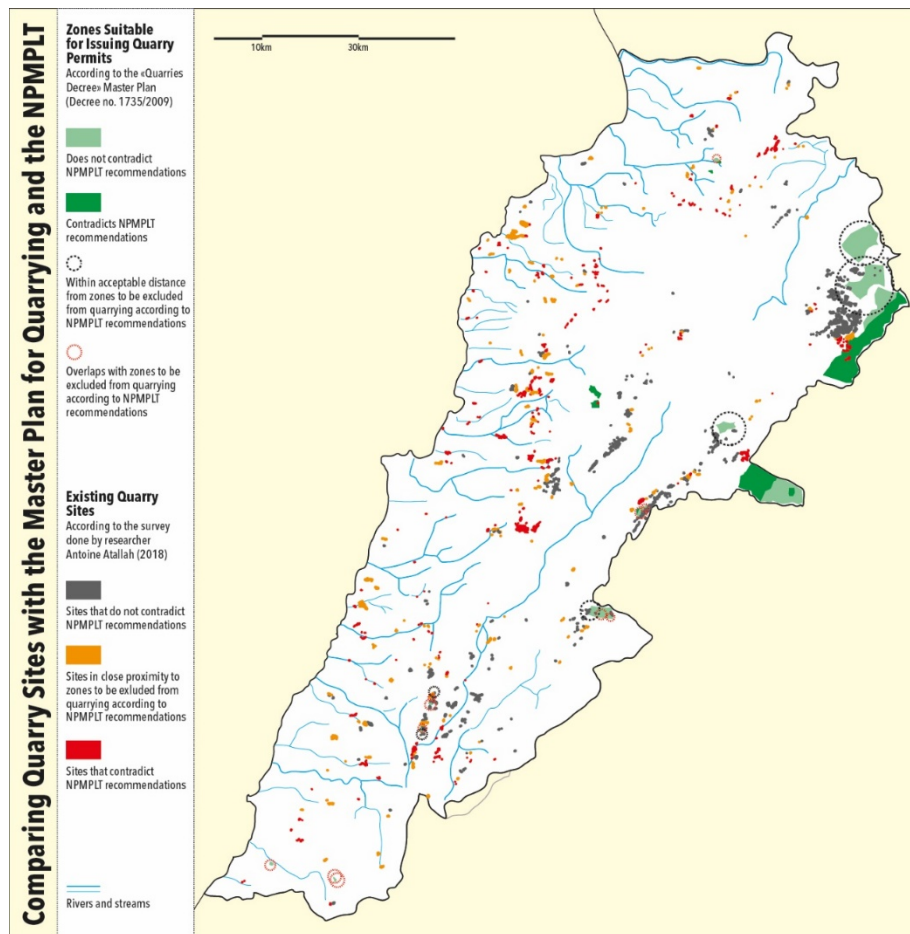
Figure 68. Quarry Planning and Regulation Across Lebanon (2018) [99]

As seen in the previous maps, the majority of quarries are found on sites that contradict the National Master Plan for Quarries and Stone Crushing Sites and the National Physical Master Plan of the Lebanese Territory (NPMPLT). According to the survey reported by architect Antoine Atallah, 52,000,000 m^2 of quarries are distributed in the country, mostly present in Mount Lebanon, in the districts of Metn, Keserwan and Aley [100].

There were plans to turn previous quarry sites into landfills. While quarrying may be done in a sustainable manner, the majority of Lebanon's quarries are illegal, uncontrolled, and are fast destroying the country's mountains [101]. A recent source claims that there are between 700 and 1,300 illegal quarries. An example of an illegal quarry is the Mayrouba Sand Quarry, located in the figure below. Some sand and stone quarries include Mount Lebanon's Majdel Tarshish and Chouf's Ain Darah that will ultimately be converted into a cement factory. Quarries are the primary cause of desertification due to the high pollution and irreversible environmental and economic harm that they cause [102].
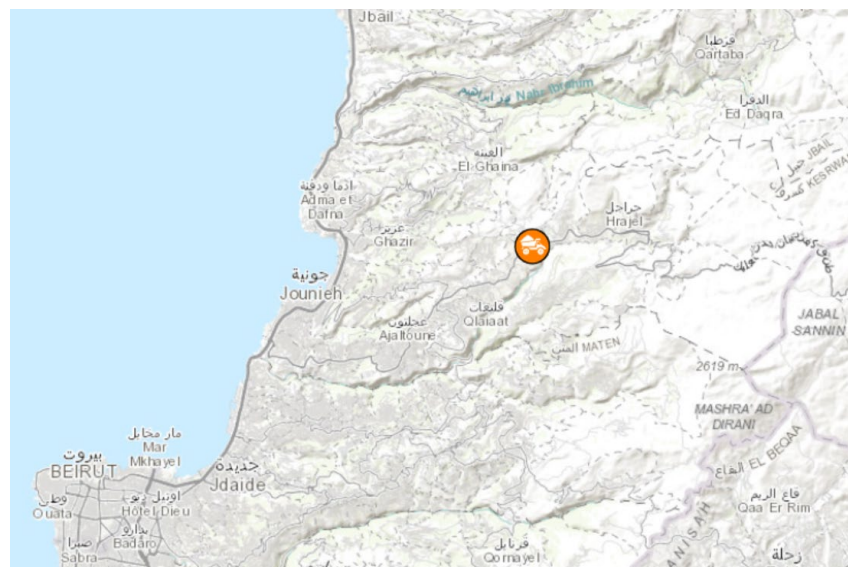
Figure 69. Mayrouba Sand Quarry, Keserwan District [103]

Using quarries as a place to plant Arundo donax would add 52,000,000 m^2 to the 1,081,000 m^2 obtained from the reported landfills. These will easily accommodate the 17,203,187 m^2 of Arundo plants needed to provide Lebanon with the necessary amount of ethanol/year. Studies also proved that Arundo donax can be used for wastewater treatment due to its detoxifying properties, therefore it can be planted next to rivers for water purification [104]. Thus, Arundo can be placed to rehabilitate landfills and quarries across the whole country with a total area of 53,081,000 m^2, which could potentially lead to the production of almost 25 million kg of bioethanol yearly. Ethanol can be produced to serve the local fuel demand with a possibility for exportation (since the total area available exceeds the required area needed for the 10% gasoline blend).

CHAPTER 5

CONCLUSION

The production of ethanol from lignocellulosic biomass is an attractive green alternative to fossil fuel. Various fermentation techniques have been developed in order to increase the amount of ethanol produced and enhance the competition in the renewable energy sector. In this thesis, a hydrolysis kinetic model and a fermentation kinetic model were developed separately to model the production of ethanol from Arundo donax. The hydrolysis model took into consideration the conversion of cellulose and hemicellulose into sugars to be converted into ethanol. The fermentation model simulated the produced ethanol from glucose and xylose with an engineered recombinant yeast able to ferment C5 and C6 sugars simultaneously. Parameter estimation was used to optimize the kinetic variables and the simulations were compared against data in the literature. In addition, a model based on the previously developed hydrolysis and fermentation models was developed to mimic the separate hydrolysis and fermentation process. The results found show that 28 g/L of ethanol was obtained after SHF, with a yield of 0.157 kg ethanol/kg of Arundo donax. The land area required to plant Arundo and to supply one year worth of ethanol, assuming around 10% of the ethanol will be mixed with gasoline, was calculated to be 17,203,187 m^2. Arundo could be planted across landfills and quarries all over the country, with a possibility to export and sell some of the ethanol produced to other countries.

Recommendations for future work include developing an Aspen PLUS flowsheet to analyze the techno-economic feasibility of the process.

APPENDIX

The ODEs used in the hydrolysis model and inserted on MATLAB are listed below. They represent, respectively, the equations of cellulose, cellobiose, glucose, hemicellulose, xylose and biomass.

$$\frac{dS_1}{dt} = -\frac{k_1 * \dfrac{E_{1max}K_{1ad}E_{1F}S_1}{1 + K_{1ad}E_{1F}} * \dfrac{\alpha S_1 V}{\lambda_1 S_F V + S_{1,0}V_0}S_1}{1 + \dfrac{S_2}{K_{1iG_2}} + \dfrac{S_3}{K_{1iG}} + \dfrac{S_5}{K_{1iX}}}$$

$$-\frac{k_2(\dfrac{E_{1max}K_{1ad}E_{1F}S_1}{1 + K_{1ad}E_{1F}} + \dfrac{E_{2max}K_{2ad}E_{2F}S_1}{1 + K_{2ad}E_{2F}})\dfrac{\alpha S_1 V}{\lambda_1 S_F V + S_{1,0}V_0}S_1}{1 + \dfrac{S_2}{K_{2iG_2}} + \dfrac{S_3}{K_{2iG}} + \dfrac{S_5}{K_{2iX}}}$$

$$+\frac{F}{V}(\lambda_1 S_F - S_1)$$

$$\frac{dS_2}{dt} = 1.056 * \frac{k_1 * \dfrac{E_{1max}K_{1ad}E_{1F}S_1}{1 + K_{1ad}E_{1F}} * \dfrac{\alpha S_1 V}{\lambda_1 S_F V + S_{1,0}V_0}S_1}{1 + \dfrac{S_2}{K_{1iG_2}} + \dfrac{S_3}{K_{1iG}} + \dfrac{S_5}{K_{1iX}}}$$

$$-\frac{k_3 E_{2F}S_2}{K_{3M}\left[1 + \dfrac{S_3}{K_{3iG}} + \dfrac{S_5}{K_{3iX}}\right] + S_2} - \frac{F}{V}S_2$$

$$\frac{dS_3}{dt} = 1.111 * \frac{k_2(\dfrac{E_{1max}K_{1ad}E_{1F}S_1}{1 + K_{1ad}E_{1F}} + \dfrac{E_{2max}K_{2ad}E_{2F}S_1}{1 + K_{2ad}E_{2F}})\dfrac{\alpha S_1 V}{\lambda_1 S_F V + S_{1,0}V_0}S_1}{1 + \dfrac{S_2}{K_{2iG_2}} + \dfrac{S_3}{K_{2iG}} + \dfrac{S_5}{K_{2iX}}} + 1.053$$

$$* \frac{k_3 E_{2F}S_2}{K_{3M}\left[1 + \dfrac{S_3}{K_{3iG}} + \dfrac{S_5}{K_{3iX}}\right] + S_2}$$

$$-\frac{\left(\dfrac{v_{mG}S_3}{K'_G + S_3 + \dfrac{S_3^2}{K'_{iG}}} * \left[1 - \left(\dfrac{p_G}{p'_{mG}}\right)^{\varphi'_G}\right]\right)X}{Y_{P/S_3}} - \frac{F}{V}S_3$$

$$\frac{dS_4}{dt} = -k_4 S_4 + \frac{F}{V}(\lambda_2 S_F - S_4)$$

$$\frac{dS_5}{dt} = 1.136 * k_4 S_4 - k_5 S_5 - \frac{\left(\frac{v_{m_X} S_5}{K'_X + S_5 + \frac{S_5^2}{K'_{iX}}} * \left[1 - \left(\frac{p_X}{p'_{mX}}\right)^{\varphi'_X}\right]\right) X}{Y_{P/S_5}} - \frac{F}{V} S_5$$

$$\frac{dX}{dt} = \left(\frac{S_3}{S_3 + S_5}\left(\frac{\mu_{m_G} S_3}{K_G + S_3 + \frac{S_3^2}{K_{iG}}} * \left[1 - \left(\frac{p_G}{p_{mG}}\right)^{\varphi_G}\right]\right)\right.$$

$$\left. + \frac{S_5}{S_3 + S_5}\left(\frac{\mu_{m_X} S_5}{K_X + S_5 + \frac{S_5^2}{K_{iX}}} * \left[1 - \left(\frac{p_X}{p_{mX}}\right)^{\varphi_X}\right]\right)\right) X - \frac{F}{V} X$$

The ODEs used for the fermentation model and inserted on MATLAB are listed below. They represent, respectively, the equations of biomass, ethanol, glucose and xylose.

$$\frac{dX}{dt} = \left[\frac{\mu_{max1} S_1}{K_{S_1 X} + S_1 + \frac{S_1^2}{K_{S_1 Xi}}}\left(1 - \frac{P}{P_{Xmax}}\right)^{\alpha}\right.$$

$$\left. + \frac{\mu_{max2} S_2}{K_{S_2 X} + S_2 + \frac{S_2^2}{K_{S_2 Xi}}}\left(1 - \frac{P}{P_{Xmax_2}}\right)^{\alpha_2}\left(1 - \frac{S_1}{S_{1max}}\right)^{\gamma}\right]$$

$$\frac{dP}{dt} = \left[\frac{q_{max1} S_1}{K_{S_1 P} + S_1 + \frac{S_1^2}{K_{S_1 Pi}}}\left(1 - \frac{P}{P_{Pmax}}\right)^{\beta}\right.$$

$$\left. + \frac{q_{max2} S_2}{K_{S_2 P} + S_2 + \frac{S_2^2}{K_{S_2 Pi}}}\left(1 - \frac{P}{P_{Pmax_2}}\right)^{\beta_2}\left(1 - \frac{S_1}{S_{1max}}\right)^{\gamma}\right]$$

$$\frac{dS_1}{dt} = \left[-\frac{1}{Y_{X/S_1}} \frac{\mu_{max1}S_1}{K_{S_1 x} + S_1 + \frac{S_1^2}{K_{S_1 Xi}}} \left(1 - \frac{P}{P_{Xmax}}\right)^{\alpha} \right.$$

$$\left. -\frac{1}{Y_{P/S_1}} \frac{q_{max1}S_1}{K_{S_1 p} + S_1 + \frac{S_1^2}{K_{S_1 Pi}}} \left(1 - \frac{P}{P_{Pmax}}\right)^{\beta} \right] X + mX$$

$$\frac{dS_2}{dt} = \left[-\frac{1}{Y_{X/S_2}} \frac{\mu_{max2}S_2}{K_{S_2 x} + S_2 + \frac{S_2^2}{K_{S_2 Xi}}} \left(1 - \frac{P}{P_{Xmax_2}}\right)^{\alpha_2} \right.$$

$$\left. -\frac{1}{Y_{P/S_2}} \frac{q_{max2}S_2}{K_{S_2 p} + S_2 + \frac{S_2^2}{K_{S_2 Pi}}} \left(1 - \frac{P}{P_{Pmax_2}}\right)^{\beta_2} \right] \left(1 - \frac{S_1}{S_{1max}}\right)^{\gamma} X + mX$$

The ODEs used for the SHF model and inserted on MATLAB are listed below:

Hydrolysis:

$$\frac{dS_1}{dt} = -\frac{k_1 * \frac{E_{1max}K_{1ad}E_{1F}S_1}{1 + K_{1ad}E_{1F}} * \frac{\alpha S_1 V}{\lambda_1 S_F V + S_{1,0}V_0} S_1}{1 + \frac{S_2}{K_{1iG_2}} + \frac{S_3}{K_{1iG}} + \frac{S_5}{K_{1iX}}}$$

$$-\frac{k_2 \left(\frac{E_{1max}K_{1ad}E_{1F}S_1}{1 + K_{1ad}E_{1F}} + \frac{E_{2max}K_{2ad}E_{2F}S_1}{1 + K_{2ad}E_{2F}}\right) \frac{\alpha S_1 V}{\lambda_1 S_F V + S_{1,0}V_0} S_1}{1 + \frac{S_2}{K_{2iG_2}} + \frac{S_3}{K_{2iG}} + \frac{S_5}{K_{2iX}}}$$

$$+\frac{F}{V}(\lambda_1 S_F - S_1)$$

$$\frac{dS_2}{dt} = 1.056 * \frac{k_1 * \frac{E_{1max}K_{1ad}E_{1F}S_1}{1 + K_{1ad}E_{1F}} * \frac{\alpha S_1 V}{\lambda_1 S_F V + S_{1,0}V_0} S_1}{1 + \frac{S_2}{K_{1iG_2}} + \frac{S_3}{K_{1iG}} + \frac{S_5}{K_{1iX}}}$$

$$-\frac{k_3 E_{2F}S_2}{K_{3M}\left[1 + \frac{S_3}{K_{3iG}} + \frac{S_5}{K_{3iX}}\right] + S_2} - \frac{F}{V}S_2$$

$$\frac{dS_3}{dt} = 1.111 * \frac{k_2 \left(\dfrac{E_{1max}K_{1ad}E_{1F}S_1}{1 + K_{1ad}E_{1F}} + \dfrac{E_{2max}K_{2ad}E_{2F}S_1}{1 + K_{2ad}E_{2F}}\right) \dfrac{\alpha S_1 V}{\lambda_1 S_F V + S_{1,0}V_0} S_1}{1 + \dfrac{S_2}{K_{2iG_2}} + \dfrac{S_3}{K_{2iG}} + \dfrac{S_5}{K_{2iX}}} + 1.053$$

$$* \frac{k_3 E_{2F}S_2}{K_{3M}\left[1 + \dfrac{S_3}{K_{3iG}} + \dfrac{S_5}{K_{3iX}}\right] + S_2} - \frac{F}{V}S_3$$

$$\frac{dS_4}{dt} = -k_4 S_4 + \frac{F}{V}(\lambda_2 S_F - S_4)$$

$$\frac{dS_5}{dt} = 1.136 * k_4 S_4 - k_5 S_5 - \frac{F}{V}S_5$$

Fermentation:

$$\frac{dX}{dt} = \left[\frac{\mu_{max1}S_1}{K_{S_1 X} + S_1 + \dfrac{S_1^2}{K_{S_1 Xi}}} \left(1 - \frac{P}{P_{Xmax}}\right)^{\alpha} \right.$$

$$\left. + \frac{\mu_{max2}S_2}{K_{S_2 X} + S_2 + \dfrac{S_2^2}{K_{S_2 Xi}}} \left(1 - \frac{P}{P_{Xmax_2}}\right)^{\alpha_2} \left(1 - \frac{S_1}{S_{1max}}\right)^{\gamma} \right]$$

$$\frac{dP}{dt} = \left[\frac{q_{max1}S_1}{K_{S_1 P} + S_1 + \dfrac{S_1^2}{K_{S_1 Pi}}} \left(1 - \frac{P}{P_{Pmax}}\right)^{\beta} \right.$$

$$\left. + \frac{q_{max2}S_2}{K_{S_2 P} + S_2 + \dfrac{S_2^2}{K_{S_2 Pi}}} \left(1 - \frac{P}{P_{Pmax_2}}\right)^{\beta_2} \left(1 - \frac{S_1}{S_{1max}}\right)^{\gamma} \right]$$

$$\frac{dS_1}{dt} = \left[-\frac{1}{Y_{X/S_1}} \frac{\mu_{max1}S_1}{K_{S_1 x} + S_1 + \dfrac{S_1^2}{K_{S_1 Xi}}} \left(1 - \frac{P}{P_{Xmax}}\right)^{\alpha} \right.$$

$$\left. - \frac{1}{Y_{P/S_1}} \frac{q_{max1}S_1}{K_{S_1 p} + S_1 + \dfrac{S_1^2}{K_{S_1 Pi}}} \left(1 - \frac{P}{P_{Pmax}}\right)^{\beta} \right] X + mX$$

$$\frac{dS_2}{dt} = \left[-\frac{1}{Y_{X/S_2}} \frac{\mu_{max2} S_2}{K_{S_2 x} + S_2 + \frac{S_2^2}{K_{S_2 Xi}}} \left(1 - \frac{P}{P_{Xmax_2}}\right)^{\alpha_2} \right.$$

$$\left. -\frac{1}{Y_{P/S_2}} \frac{q_{max2} S_2}{K_{S_2 p} + S_2 + \frac{S_2^2}{K_{S_2 Pi}}} \left(1 - \frac{P}{P_{Pmax_2}}\right)^{\beta_2} \right] \left(1 - \frac{S_1}{S_{1max}}\right)^{\gamma} X + mX$$

REFERENCES

[1] H. B. Aditiya, T. M. I. Mahlia, W. T. Chong, H. Nur, and A. H. Sebayang, "Second generation bioethanol production: A critical review," *Renew. Sustain. Energy Rev.*, vol. 66, pp. 631–653, Dec. 2016, doi: 10.1016/j.rser.2016.07.015.

[2] A. Pirolini, "What is Bioethanol?," *AZoCleantech.com*, May 22, 2013. https://www.azocleantech.com/article.aspx?ArticleID=403 (accessed Aug. 05, 2021).

[3] M. Salikandi, "Techno-economic study of bioethanol production from olive wastes cake (OWC) in Iran," p. 12, 2021.

[4] N. Sönnichsen, "Fuel ethanol production in major countries 2020," *Statista*, Feb. 26, 2021. https://www.statista.com/statistics/281606/ethanol-production-in-selected-countries/

[5] M. Torli, *Thermodynamics, Design, Simulation and Benchmarking of Biofuel Processes*. Kgs. Lyngby: Technical University of Denmark, 2019.

[6] J. Hanania, K. Stenhouse, and J. Donev, "Bioethanol - Energy Education," Jan. 08, 2017. https://energyeducation.ca/encyclopedia/Bioethanol (accessed Aug. 05, 2021).

[7] P. Di Donato, I. Finore, A. Poli, B. Nicolaus, and L. Lama, "The production of second generation bioethanol: The biotechnology potential of thermophilic bacteria," *J. Clean. Prod.*, vol. 233, pp. 1410–1417, Oct. 2019, doi: 10.1016/j.jclepro.2019.06.152.

[8] S. H. Mohd Azhar *et al.*, "Yeasts in sustainable bioethanol production: A review," *Biochem. Biophys. Rep.*, vol. 10, pp. 52–61, Jul. 2017, doi: 10.1016/j.bbrep.2017.03.003.

[9] WFP Various, "Hunger Map, World Food Programme," 2019. https://www.wfp.org/publications/2019-hunger-map (accessed Aug. 07, 2021).

[10] R. Sims and M. Taylor, "From 1st to 2nd Generation Biofuel Technologies: An overview of Current Industry and RD&D Activities," *Biofuel Technol.*, p. 124, 2008.

[11] Y. Chen, Y. Wu, B. Zhu, G. Zhang, and N. Wei, "Co-fermentation of cellobiose and xylose by mixed culture of recombinant Saccharomyces cerevisiae and kinetic modeling," *PLOS ONE*, vol. 13, p. e0199104, Jun. 2018, doi: 10.1371/journal.pone.0199104.

[12] D. Kumar and G. S. Murthy, "Chapter 7 - Enzymatic Hydrolysis of Cellulose for Ethanol Production: Fundamentals, Optimal Enzyme Ratio, and Hydrolysis Modeling," in *New and Future Developments in Microbial Biotechnology and Bioengineering*, V. K. Gupta, Ed. Amsterdam: Elsevier, 2016, pp. 65–78. doi: 10.1016/B978-0-444-63507-5.00007-1.

[13] M. Rastogi and S. Shrivastava, "Recent advances in second generation bioethanol production: An insight to pretreatment, saccharification and fermentation processes," *Renew. Sustain. Energy Rev.*, vol. 80, pp. 330–340, Dec. 2017, doi: 10.1016/j.rser.2017.05.225.

[14] M. Melián Rodríguez, *Lignin biomass conversion into chemicals and fuels*. DTU Chemistry, 2016.

[15] Y. Xu, J. Li, M. Zhang, and D. Wang, "Modified simultaneous saccharification and fermentation to enhance bioethanol titers and yields," *Fuel*, vol. 215, pp. 647–654, Mar. 2018, doi: 10.1016/j.fuel.2017.11.072.

[16] S. Mohapatra, R. C. Ray, and S. Ramachandran, "Chapter 1 - Bioethanol From Biorenewable Feedstocks: Technology, Economics, and Challenges," in *Bioethanol Production from Food Crops*, R. C. Ray and S. Ramachandran, Eds. Academic Press, 2019, pp. 3–27. doi: 10.1016/B978-0-12-813766-6.00001-1.

[17] I. Abbas, "Solid Waste Management in Lebanon: Challenges and Recommendations.," *J. Environ. Waste Manag.*, vol. 4, pp. 53–63, Oct. 2017.

[18] A. U. George, "PRODUCTION OF ETHANOL FUEL FROM ORGANIC AND FOOD WASTES," no. 13, p. 11, 2008.

[19] S. W. Mathewson, *The Manual For The Home And Farm Production Of Alcohol Fuels*. 1980. Accessed: Oct. 29, 2021. [Online]. Available: https://www.bestfilebook.com/pdf/manual-for-the-home-and-farm-production-of-alcohol-fuels/

[20] J. H. Kim, J. C. Lee, and D. Pak, "Feasibility of producing ethanol from food waste," *Waste Manag.*, vol. 31, no. 9, pp. 2121–2125, Sep. 2011, doi: 10.1016/j.wasman.2011.04.011.

[21] M. M. Manyuchi, C. Mbohwa, and E. Muzenda, "Bio ethanol Production from the Landfill Organic Waste Fraction," p. 5, 2018.

[22] G. Luo, F. Talebnia, D. Karakashev, L. Xie, Q. Zhou, and I. Angelidaki, "Enhanced bioenergy recovery from rapeseed plant in a biorefinery concept," *Bioresour. Technol.*, vol. 102, no. 2, pp. 1433–1439, Jan. 2011, doi: 10.1016/j.biortech.2010.09.071.

[23] M. Galbe and G. Zacchi, "Simulation of ethanol production processes based on enzymatic hydrolysis of woody biomass," *Comput. Chem. Eng.*, vol. 18, pp. S687–S691, Jan. 1994, doi: 10.1016/0098-1354(94)80112-6.

[24] M. Čihák, *Modeling and simulation of bioethanol production in Aspen Plus*. 2016. doi: 10.13140/RG.2.2.32091.26409.

[25] W. Nabgan, I. Saeh, T. A. T. Abdullah, and B. Nabgan, "Modelling and Thermodynamic Design of Bio-Ethanol Production Plant from Corn via Aspen Plus," *ResearchGate*, 2016, Accessed: Aug. 25, 2021. [Online]. Available: https://www.researchgate.net/publication/302589908_Modelling_and_Thermodynamic_Design_of_Bio-Ethanol_Production_Plant_from_Corn_via_Aspen_Plus

[26] R. Salviano, A. Macedo, L. Pantoja, and A. Santos, "Bioethanol from Jatropha Seed Cakes Produced by Acid Hydrolysis Followed by Fermentation with Baker s Yeast," *Int. J. Appl. Sci. Technol.*, vol. 4, pp. 111–117, Jul. 2014.

[27] M. F. Laborde *et al.*, "SIMULATION OF THE PRODUCTION PROCESS OF BIODIESEL FROM JATROPHA CURCAS OIL," *Lat. Am. Appl. Res.*, p. 7, 2019.

[28] M. Mishra, C. B, T. Chatterjee, and K. Singh, "PRODUCTION OF BIO-ETHANOL FROM JATROPHA OILSEED CAKES VIA DILUTE ACID HYDROLYSIS AND FERMENTATION BY SACCHAROMYCES CEREVISIAE," *Int. J. Biotechnol. Appl.*, vol. 3, pp. 41–47, Apr. 2011, doi: 10.9735/0975-2943.3.1.41-47.

[29] Y. G. Keneni, A. K. (Trine) Hvoslef-Eide, and J. M. Marchetti, "Optimization of the production of biofuel form Jatropha oil using a recyclable anion-exchange resin," *Fuel*, vol. 278, p. 118253, Oct. 2020, doi: 10.1016/j.fuel.2020.118253.

[30] C. F. L. Silva, A. M. Schirmer, N. R. Maeda, A. C. Barcelos, and N. Jr. Pereira, "Potential of giant reed (Arundo donax L.) for second generation ethanol production," *Electronic Journal of Biotechnology*, 2015, doi: 10.1016/j.ejbt.2014.11.002.

[31] R. Bura, S. Ewanick, and R. Gustafson, "Assessment of Arundo donax (Giant reed) as feedstock for conversion to ethanol," *Tappi J.*, vol. 11, pp. 59–65, Apr. 2012, doi: 10.32964/TJ11.4.59.

[32] D. Sharma and A. Saini, "Cellulosic Ethanol Feedstock: Diversity and Potential," in *Lignocellulosic Ethanol Production from a Biorefinery Perspective: Sustainable Valorization of Waste*, D. Sharma and A. Saini, Eds. Singapore: Springer, 2020, pp. 23–63. doi: 10.1007/978-981-15-4573-3_2.

[33] A. Aliberti *et al.*, "Effect of Cellulase, Substrate Concentrations, and Configuration Processes on Cellulosic Ethanol Production from Pretreated Arundo donax," *BioResources*, vol. 12, no. 3, Art. no. 3, Jun. 2017.

[34] R. Sawaya, J. Halwani, I. Bashour, and N. Nehme, "Assessment of the leachate quality from municipal solid waste landfill in Lebanon," *Arab. J. Geosci.*, vol. 14, no. 21, p. 2160, Nov. 2021, doi: 10.1007/s12517-021-08502-4.

[35] C. Moughalian, "Naameh Landfill, Lebanon | EJAtlas," *Environmental Justice Atlas*, 2019. https://ejatlas.org/conflict/naameh-landfill-lebanon (accessed Feb. 08, 2022).

[36] "Arundo BioEnergy," *Arundo BioEnergy*. https://arundobioenergy.com/ (accessed Feb. 08, 2022).

[37] D. Kumar and G. S. Murthy, "Impact of pretreatment and downstream processing technologies on economics and energy in cellulosic ethanol production," *Biotechnol. Biofuels*, vol. 4, no. 1, p. 27, 2011, doi: 10.1186/1754-6834-4-27.

[38] Y. Zheng, Z. Pan, R. Zhang, and B. M. Jenkins, "Kinetic modeling for enzymatic hydrolysis of pretreated creeping wild ryegrass," *Biotechnol. Bioeng.*, vol. 102, no. 6, pp. 1558–1569, Apr. 2009, doi: 10.1002/bit.22197.

[39] F. F. and Y. Shastri, "Optimal control of enzymatic hydrolysis of lignocellulosic biomass," *Resour.-Effic. Technol.*, vol. 2, pp. S96–S104, Dec. 2016, doi: 10.1016/j.reffit.2016.11.006.

[40] K. L. Kadam, E. C. Rydholm, and J. D. McMillan, "Development and Validation of a Kinetic Model for Enzymatic Saccharification of Lignocellulosic Biomass," *Biotechnol. Prog.*, vol. 20, no. 3, pp. 698–705, 2004, doi: 10.1021/bp034316x.

[41] S. Mutturi and G. Lidén, "Model-based estimation of optimal temperature profile during simultaneous saccharification and fermentation of *Arundo donax*: Temperature Optimization During *Arundo* SSF," *Biotechnol. Bioeng.*, vol. 111, no. 5, pp. 866–875, May 2014, doi: 10.1002/bit.25165.

[42] M. Penttilä, "NEMO: 14th International Biotechnology Symposium and Exhibition (IBS2010)," *J. Biotechnol.*, vol. 150, no. Supplement, p. 11, 2010, doi: 10.1016/j.jbiotec.2010.08.043.

[43] M.-L. Chen and F.-S. Wang, "Optimization of a Fed-Batch Simultaneous Saccharification and Cofermentation Process from Lignocellulose to Ethanol," 2010, doi: 10.1021/IE001982.

[44] G. Liu, J. Zhang, and J. Bao, "Cost evaluation of cellulase enzyme for industrial-scale cellulosic ethanol production based on rigorous Aspen Plus modeling," *Bioprocess Biosyst. Eng.*, vol. 39, Jan. 2016, doi: 10.1007/s00449-015-1497-1.

[45] I. De Bari, F. Liuzzi, A. Ambrico, and M. Trupo, "Arundo donax Refining to Second Generation Bioethanol and Furfural," *Processes*, vol. 8, no. 12, Art. no. 12, Dec. 2020, doi: 10.3390/pr8121591.

[46] P.-M. Bondesson and M. Galbe, "Process design of SSCF for ethanol production from steam-pretreated, acetic-acid-impregnated wheat straw," *Biotechnol. Biofuels*, vol. 9, no. 1, p. 222, Oct. 2016, doi: 10.1186/s13068-016-0635-6.

[47] B. Palmqvist and G. Lidén, "Combining the effects of process design and pH for improved xylose conversion in high solid ethanol production from Arundo donax," *AMB Express*, vol. 4, no. 1, p. 41, May 2014, doi: 10.1186/s13568-014-0041-z.

[48] B. Cassells, K. Karhumaa, V. Sànchez i Nogué, and G. Lidén, "Hybrid SSF/SHF Processing of SO2 Pretreated Wheat Straw—Tuning Co-fermentation by Yeast Inoculum Size and Hydrolysis Time," *Appl. Biochem. Biotechnol.*, vol. 181, no. 2, pp. 536–547, Feb. 2017, doi: 10.1007/s12010-016-2229-y.

[49] F. Nielsen, M. Galbe, G. Zacchi, and O. Wallberg, "The effect of mixed agricultural feedstocks on steam pretreatment, enzymatic hydrolysis, and cofermentation in the lignocellulose-to-ethanol process," *Biomass Convers. Biorefinery*, vol. 10, no. 2, pp. 253–266, Jun. 2020, doi: 10.1007/s13399-019-00454-w.

[50] D. Scordia, S. L. Cosentino, and T. W. Jeffries, "Enzymatic hydrolysis, simultaneous saccharification and ethanol fermentation of oxalic acid pretreated giant reed (Arundo donax L.)," *Ind. Crops Prod.*, vol. 49, pp. 392–399, Aug. 2013, doi: 10.1016/j.indcrop.2013.05.031.

[51] I. Petelkov *et al.*, "Encapsulation of brewing yeast in alginate/chitosan matrix: Kinetic characteristics of the fermentation process at a constant fermentation temperature," vol. 69, pp. 1355–1364, Jan. 2016.

[52] P. Ariyajaroenwong, P. Laopaiboon, A. Salakkam, P. Srinophakun, and L. Laopaiboon, "Kinetic models for batch and continuous ethanol fermentation from sweet sorghum juice by yeast immobilized on sweet sorghum stalks," *J. Taiwan Inst. Chem. Eng.*, vol. 66, pp. 210–216, Sep. 2016, doi: 10.1016/j.jtice.2016.06.023.

[53] M. Muloiwa, S. Nyende-Byakika, and M. Dinka, "Comparison of unstructured kinetic bacterial growth models.," *South Afr. J. Chem. Eng.*, vol. 33, pp. 141–150, Jul. 2020, doi: 10.1016/j.sajce.2020.07.006.

[54] J. Monod, "The Growth of Bacterial Cultures," *Annu. Rev. Microbiol.*, vol. 3, no. 1, pp. 371–394, 1949, doi: 10.1146/annurev.mi.03.100149.002103.

[55] F. F. Blackman, "Optima and Limiting Factors," *Ann. Bot.*, vol. os-19, no. 2, pp. 281–296, Apr. 1905, doi: 10.1093/oxfordjournals.aob.a089000.

[56] J. D. Kong, "Modeling Microbial Dynamics: Effects on Environmental and Human Health," 2017. doi: 10.7939/R3FT8DZ73.

[57] J. B. S. Haldane, "Enzymes," *MIT Press*, 1930, Accessed: Sep. 25, 2022. [Online]. Available: https://mitpress.mit.edu/9780262580038/enzymes/

[58] G. Teissier, "Growth of bacterial populations and the available substrate concentration," *Rev Sci Instrum*, vol. 3208, no. 3208, pp. 209–214, 1942.

[59] H. Moser, "The dynamics of bacterial populations maintained in the chemostat.," *Dyn. Bact. Popul. Maint. Chemostat*, 1958.

[60] D. E. Contois, "Kinetics of bacterial growth: relationship between population density and specific growth rate of continuous cultures," *J. Gen. Microbiol.*, vol. 21, no. Journal Article, p. 40, 1959.

[61] H. V. Westerhoff, J. S. Lolkema, R. Otto, and K. J. Hellingwerf, "Thermodynamics of growth. Non-equilibrium thermodynamics of bacterial

growth. The phenomenological and the mosaic approach," *Biochim. Biophys. Acta*, vol. 683, no. 3–4, pp. 181–220, Dec. 1982, doi: 10.1016/0304-4173(82)90001-5.

[62] S. Aiba, M. Shoda, and M. Nagatani, "Kinetics of product inhibition in alcohol fermentation," *Biotechnol. Bioeng.*, vol. 10, no. 6, pp. 845–864, 1968, doi: 10.1002/bit.260100610.

[63] T. Yano and S. Koga, "Dynamic behavior of the chemostat subject to substrate inhibition," *Biotechnol. Bioeng.*, vol. 11, no. 2, pp. 139–153, 1969, doi: 10.1002/bit.260110204.

[64] K. Han and O. Levenspiel, "Extended monod kinetics for substrate, product, and cell inhibition," *Biotechnol. Bioeng.*, vol. 32, no. 4, pp. 430–447, 1988, doi: 10.1002/bit.260320404.

[65] E. O. Powell, "The growth rate of microorganisms as a function of substrate concentration," *Microb. Physiol. Contin. Cult.*, 1967, Accessed: Sep. 25, 2022. [Online]. Available: https://scholar.google.com/scholar_lookup?&title=The%20growth%20rate%20of %20microorganisms%20as%20a%20function%20of%20substrate%20concentratio n&pages=34-55&publication_year=1967&author=Powell%2CEO

[66] PF. Verhulst, "Notice sur la loi que la population suit dans son accroissement," *Corresp Math Phys*, vol. 10, pp. 113–126, 1838.

[67] J. H. T. Luong, "Generalization of monod kinetics for analysis of growth data with substrate inhibition," *Biotechnol. Bioeng.*, vol. 29, no. 2, pp. 242–248, 1987, doi: 10.1002/bit.260290215.

[68] J. Leyden. Webb, *Enzyme and metabolic inhibitors*. New York: Academic Press, 1963, pp. 1–984. doi: 10.5962/bhl.title.7320.

[69] J. F. Andrews, "A mathematical model for the continuous culture of microorganisms utilizing inhibitory substrates," *Biotechnol. Bioeng.*, vol. 10, no. 6, pp. 707–723, Nov. 1968, doi: 10.1002/bit.260100602.

[70] V. Shopska, R. Denkova, V. Lyubenova, and G. Kostov, "13 - Kinetic Characteristics of Alcohol Fermentation in Brewing: State of Art and Control of the Fermentation Process," in *Fermented Beverages*, A. M. Grumezescu and A. M. Holban, Eds. Woodhead Publishing, 2019, pp. 529–575. doi: 10.1016/B978-0-12-815271-3.00013-0.

[71] M. D. Putra and A. E. Abasaeed, "A more generalized kinetic model for binary substrates fermentations," *Process Biochem.*, vol. 75, pp. 31–38, Dec. 2018, doi: 10.1016/j.procbio.2018.09.017.

[72] M. S. Krishnan, N. W. Ho, and G. T. Tsao, "Fermentation kinetics of ethanol production from glucose and xylose by recombinant Saccharomyces 1400(pLNH33)," *Appl. Biochem. Biotechnol.*, vol. 77–79, pp. 373–388, 1999, doi: 10.1385/abab:78:1-3:373.

[73] T. Liu, S. Huang, and A. Geng, "Recombinant Diploid Saccharomyces cerevisiae Strain Development for Rapid Glucose and Xylose Co," *Fermentation*, vol. 4, no. 3, Art. no. 3, Sep. 2018, doi: 10.3390/fermentation4030059.

[74] D. N. Moysés, V. C. B. Reis, J. R. M. de Almeida, L. M. P. de Moraes, and F. A. G. Torres, "Xylose Fermentation by Saccharomyces cerevisiae: Challenges and Prospects," *Int. J. Mol. Sci.*, vol. 17, no. 3, p. 207, Feb. 2016, doi: 10.3390/ijms17030207.

[75] N. Nosrati-Ghods, S. T. L. Harrison, A. J. Isafiade, and S. L. Tai, "Ethanol from Biomass Hydrolysates by Efficient Fermentation of Glucose and Xylose – A

Review," *ChemBioEng Rev.*, vol. 5, no. 5, pp. 294–311, 2018, doi: 10.1002/cben.201800009.

[76] Y. Chen, "Development and application of co-culture for ethanol production by co-fermentation of glucose and xylose: a systematic review," *J. Ind. Microbiol. Biotechnol.*, vol. 38, no. 5, pp. 581–597, May 2011, doi: 10.1007/s10295-010-0894-3.

[77] MathWorks, "Parameter Estimation." https://www.mathworks.com/discovery/parameter-estimation.html (accessed Apr. 09, 2022).

[78] P. M. Doran, "5 - Energy Balances," in *Bioprocess Engineering Principles*, P. M. Doran, Ed. London: Academic Press, 1995, pp. 86–109. doi: 10.1016/B978-012220855-3/50005-5.

[79] "Planting reeds - when, where and how are reeds planted?," *magicgardening.net*. //magicgardening.net/2951-planting-reeds-this-is-how-its-done (accessed Oct. 03, 2022).

[80] D. Ravenscroft, "Arundo Donax - How to Grow Spanish Cane," *Gardeners HQ*. https://www.gardenershq.com/Arundo-donax.php (accessed Nov. 02, 2022).

[81] "Arundo donax (Giant Reed, Giant Reed Grass) | North Carolina Extension Gardener Plant Toolbox." https://plants.ces.ncsu.edu/plants/arundo-donax/ (accessed Nov. 02, 2022).

[82] L. G. Angelini, L. Ceccarini, and E. Bonari, "Biomass yield and energy balance of giant reed (Arundo donax L.) cropped in central Italy as related to different management practices," *Eur. J. Agron.*, vol. 22, no. 4, pp. 375–389, May 2005, doi: 10.1016/j.eja.2004.05.004.

[83] S. L. Cosentino, V. Copani, G. M. D'Agosta, E. Sanzone, and M. Mantineo, "First results on evaluation of Arundo donax L. clones collected in Southern Italy," *Ind. Crops Prod.*, vol. 23, no. 2, pp. 212–222, Mar. 2006, doi: 10.1016/j.indcrop.2005.06.004.

[84] "Arundo donax - Growing Guide - Burncoose Nurseries." https://www.burncoose.co.uk/site/content.cfm?ref=Arundo+donax+-+Growing+Guide (accessed Nov. 02, 2022).

[85] R. Pilu, A. Manca, and M. Landoni, "Arundo donax as an energy crop: Pros and cons of the utilization of this perennial plant," *Maydica*, vol. 58, Jan. 2013.

[86] "Lebanon's daily fuel consumption drops by 14 percent in first seven months of 2022," *L'Orient Today*, Aug. 24, 2022. https://today.lorientlejour.com/article/1309350/lebanons-daily-fuel-consumption-down-by-14-percent-in-the-first-seven-months-of-2022.html (accessed Nov. 20, 2022).

[87] Emily Lewis, "Out of sight, out of mind: Lebanon expands landfill to clear garbage from streets," *Al Arabiya English*, May 09, 2020. Accessed: Nov. 23, 2022. [Online]. Available: https://english.alarabiya.net/features/2020/05/09/Out-of-sight-out-of-mind-Lebanon-expands-landfill-to-clear-garbage-from-streets

[88] R. Sawaya, H. Kourani, J. Halwani, and N. Nehme, "Landfills in greater Beirut area: A protracted part of municipal solid waste management," pp. 184–185, Oct. 2022.

[89] Laceco, "Zahleh Sanitary Landfill," *Laceco*. https://www.laceco.me/work/zahleh-sanitary-landfill/ (accessed Nov. 23, 2022).

[90] Christophe Elias Maroun, "Saida Garbage Mountain, Lebanon | EJAtlas," *Environmental Justice Atlas*, 2019. https://ejatlas.org/conflict/garbage-mountain-saida (accessed Nov. 24, 2022).

[91] F. Montes, "SOLID WASTE MANAGEMENT," *Solid Waste Manag.*, p. 21.

[92] Civil Society Knowledge Center, "Akkar residents hold sit-in to denounce new garbage plan," *Civil Society Knowledge Centre*, Sep. 14, 2015. https://civilsociety-centre.org/sir/akkar-residents-hold-sit-denounce-new-garbage-plan (accessed Nov. 24, 2022).

[93] C. Moughalian, "Bourj Hammoud Garbage Mountain, Lebanon | EJAtlas," *Environmental Justice Atlas*, 2019. https://ejatlas.org/conflict/bourj-hammoud-garbage-mountain (accessed Nov. 24, 2022).

[94] T. Meraaby, "Costa Brava Landfill, Lebanon | EJAtlas," *Environmental Justice Atlas*, 2019. https://ejatlas.org/conflict/costa-brava-landfill-lebanon (accessed Nov. 24, 2022).

[95] A. Moustafa, M. Hamzeh, M. Baroudi, B. Ouddane, and S. Net, "55 xenobiotic organic compounds in Tripoli landfill-Lebanon leachate and their fluxes to the Abou Ali River and Mediterranean Sea," *Environ. Monit. Assess.*, vol. 194, no. 12, p. 856, Oct. 2022, doi: 10.1007/s10661-022-10522-w.

[96] L. Etheredge, "Lebanon Mountains." Accessed: Nov. 25, 2022. [Online]. Available: https://www.britannica.com/place/Lebanon-Mountains

[97] N. Bulos, "Lebanon's Hezbollah group insists: We're not the 'menace' Trump says we are," *Los Angeles Times*, Jul. 31, 2017. https://www.latimes.com/world/middleeast/la-fg-hezbollah-20170731-story.html (accessed Nov. 25, 2022).

[98] M. El-Fadel, S. Sadek, and W. Chahine, "Environmental Management of Quarries as Waste Disposal Facilities," *Environ. Manage.*, vol. 27, pp. 515–31, May 2001, doi: 10.1007/s002670010167.

[99] M. Basbous, "Reading the Quarries' Map in Lebanon," *Jadaliyya - جدلية*, Apr. 17, 2019. https://www.jadaliyya.com/Details/38569 (accessed Nov. 24, 2022).

[100] Najib, "A Map of Every Quarry in Lebanon," *Blog Baladi*, Jul. 10, 2018. https://blogbaladi.com/a-map-of-every-quarry-in-lebanon/ (accessed Nov. 24, 2022).

[101] L. Diab, "Illegal quarries in Lebanon," 2016, Accessed: Nov. 24, 2022. [Online]. Available: https://www.academia.edu/31389343/Illegal_quarries_in_Lebanon

[102] N. Mazloum, "Sand and stone quarries: One of Lebanon's leading causes of desertification – Newsroom Nomad," 2016. Accessed: Nov. 24, 2022. [Online]. Available: https://newsroomnomad.com/2016/06/18/sand-and-stone-quarries-one-of-lebanons-leading-causes-of-desertification/

[103] Christophe Maroun, "Mayrouba Sand Quarries, Lebanon | EJAtlas," *Environmental Justice Atlas*, 2019. https://ejatlas.org/conflict/mayrouba-sand-quarries-lebanon (accessed Nov. 24, 2022).

[104] M. K. Fidele and P. Audra, "Residual Wastewater Treatment by an Aquatic Plant System in Tropical Area: Assessment of Arundo Donax and Pennisetum Purpureum Schumach," *Int. J. Water Wastewater Treat.*, vol. 7, no. 1, 2020, doi: 10.16966/2381-5299.177.